R-07-63

Hydrogeological flux scenarios at Forsmark

Generic numerical flow simulations and compilation of climatic information for use in the safety analysis SFR1 SAR-08

Patrik Vidstrand, Bergab

Jens-Ove Näslund, Svensk Kärnbränslehantering AB

Juha Hartikainen, Helsinki University of Technology

Urban Svensson, CFE AB

November 2007

Svensk Kärnbränslehantering AB
Swedish Nuclear Fuel
and Waste Management Co
Box 5864
SE-102 40 Stockholm Sweden
Tel 08-459 84 00
+46 8 459 84 00
Fax 08-661 57 19
+46 8 661 57 19

ISSN 1402-3091
SKB Rapport R-07-63

Hydrogeological flux scenarios at Forsmark

Generic numerical flow simulations and compilation of climatic information for use in the safety analysis SFR1 SAR-08

Patrik Vidstrand, Bergab

Jens-Ove Näslund, Svensk Kärnbränslehantering AB

Juha Hartikainen, Helsinki University of Technology

Urban Svensson, CFE AB

November 2007

Keywords: dokID 1090114, SFR 1 SAR-08, Hydrogeology, Climate, Permafrost.

Preface

This document describes the climate evolution, including ice sheet and permafrost development, at SFR 1 and resulting effects on groundwater flow in a long-time perspective. The document constitutes one of the references used in the safety analysis SFR 1 SAR-08.

Patrik Vidstrand, Bergab, Jens-Ove Näslund, SKB, Juha Hartikainen, Helsinki University of Technology and Urban Svensson, CFE AB have conducted the modelling work and compiled the report.

This document has been reviewed and all comments have been documented in accordance with SKIFS 2004:1.

Stockholm, November 2007

Anna Gordon
Project leader, SFR 1 SAR-08

Foreword

The compilation of climatic information and modelling results on ice sheet and permafrost development was conducted by Jens-Ove Näslund at SKB and Juha Hartikainen at Helsinki University of Technology. Together they produced all of Chapter 2. Jens-Ove Näslund also provided input to the discussion section.

The numerical modelling of groundwater flow was conducted by a modelling team with expertise from Bergab – Berggeologiska Undersökningar AB and Computer-aided Fluid Engineering (CFE). Urban Svensson at CFE produced a first set-up of the numerical base code and reviewed all additional set-ups produced by Patrik Vidstrand at Bergab. Patrik Vidstrand specified the conceptual framework for the groundwater modelling and conducted all the numerical simulations and post-processing. He is the author of all chapters except Chapter 2.

Contents

1 Introduction

1.1 Background

Over the life-span of relevance for a nuclear waste geological repository, climate models predict future climatic situations that result in permafrost development as well as glacial conditions, but also changes in shoreline elevation with possibilities for both elevated and submerged situations.

Subsequent to the modelling work by /Holmén and Stigsson 2001/, SKB decided to carry out additional hydrogeological modelling studies in order to investigate the effects on the groundwater flow at the SFR due to different surface conditions imposed by climate changes.

As a background for the safety analysis, SFR1 SAR-08, this modelling study of different generic upper boundary conditions, as influenced by climate change and landform development, has been conducted.

1.1.1 Earlier modelling

During work on the SFR-SAFE assessment, a hydrogeological study was conducted incorporating scenarios of shore-level change and associated flow changes /Holmén and Stigsson 2001/. The study was conducted as a nested model with a local model within a larger regional model. The regional model had the primary purpose of providing boundary conditions for the local model in which the flow system within and surrounding the SFR was investigated by means of numerical flow simulations.

The simulations were conducted in a fresh water model, since an even earlier study /Stigsson et al. 1998/ had concluded that density effects have little importance to the flow situation at the SFR.

The simulations were representative of present-day hydrogeological conditions, but accounted for a changing shoreline, meaning that the SFR locality, today approximately at the shoreline, with time became located inland.

The study did not account for any long-term changes in the upper boundary conditions due to climatic impacts such as permafrost or large-scale glaciations.

Since the study by /Holmén and Stigsson 2001/, further relevant groundwater flow information has been derived during the site investigation programme for a deep geological repository for spent fuel at Forsmark. In addition, a significant number of numerical groundwater flow simulations have addressed flow issues for the candidate deep repository site at Forsmark e.g. /Hartley et al. 2006/. SFR fringes this area.

1.1.2 SKI and SSI commentary

A review by SKI and SSI identified a number of important issues not fully addressed by the SFR-SAFE assessment. Among these the two most relevant for this study are briefly noted below.

The hydrogeological flow modelling was found to be too constrained by the calibration and the treatment of property variations was also found, in part, to be too limited.

The review further found that the omission of climate scenarios with significantly different upper boundary conditions was not justified over the time frame the reviewers found important.

1.1.3 Strategy

This study mainly addresses the possible effects of different upper boundary conditions. The different scenarios considered are based on the SR-Can climate scenarios for the Forsmark site.

Even though the study is a hydrogeological flow study, it was not intended to create a realistic representation of the "true" groundwater flow situation at the SFR. The purpose was instead to provide the safety analysis with quantification of, and uncertainty indicators for, the possible effects of different upper boundary conditions.

In order to address some of the SKI and SSI review comments, a wide range of uncertainty analyses have been conducted.

Overall, the strategy was to use simplified models in the simulation of scenario cases to provide the safety analysis with relative flux values and uncertainty ranges.

1.1.4 Deliverables

The deliverables of the study are the relative values of mass fluxes through the hypothetical repository volumes for the different surface conditions associated with the climate scenarios described in Chapter 2.

1.2 Scope and objectives

The purpose of this study is to support the safety analysis of the SFR repository, both in terms of hydrogeological issues related to climate-imposed changes of the surface conditions, and in terms of climate and climate-related changes in general that will be used in other studies within the safety assessment of the SFR repository.

One aspect of this study is to summarise the climate scenarios for the Forsmark area compiled for the SR-Can safety assessment. SR-Can simulations of ice sheets, shore-level changes and permafrost-produced indications of permafrost conditions for different climate scenarios were assessed. For the present study, three climate scenarios were selected and defined as *climate variants*. These climate variants provided a set of different surface conditions (climate domains); that were translated into a number of different upper boundary cases used in the generic hydrogeological simulations presented in this report.

The main objective of the hydrogeological modelling is to provide scaling factors for flow velocities, derived in previous studies, relevant for the different top boundary cases. These scaling factors will be used in subsequent modelling for the SFR1 SAR-08.

1.3 Site description

Due to the generic character of this study only a brief introduction to the site is presented herein. For details on hydrogeological characteristics, as well as information on the SFR, see /Holmén and Forsman 2004, SKB 2005, 2006c/, respectively.

SFR is located in Forsmark in the northern part of Uppland, close to the Forsmark nuclear power plant.

SFR is a geological repository for low and intermediate level operational and spent nuclear waste. SFR comprises an above-ground surface part and a second part located underground.

The underground part comprises rock caverns for the disposal of the waste along with a tunnel system. The underground part is approximately 60 metres below ground surface.

Figure 1-1. *Overview of the region that surrounds the SFR.*

1.4 Settings and limitations

The geometrical description used is a simplification, being both two-dimensional and generic, and the boundary conditions are adapted to the two-dimensional problem. Therefore, this study has the limitations and sensitivities of a typical generic two-dimensional hydrogeological model. Also, the simulations are all steady-state.

The intent of this study was to assess hydrogeological properties, boundary conditions, and conditions of the surface associated with different climate scenarios. The results, in part, depend on input from simplified numerical models in dimensions from 1D to 3D. The physical processes associated with permafrost and ice sheet growth are rather well understood. However, since the knowledge is not complete, a consequence is that the degree of conservatism in the assumptions used and boundary conditions adopted cannot be quantified; however, these uncertainties are handled by the adopted scenario approach.

The groundwater study is restricted to 2D advective-diffusive flow processes in steady-state and within a freshwater model. Thus, density driven flow is not included and the only driving force in the model simulations is the imposed topographical differences in the upper boundary conditions.

1.5 Layout of report

This report presents a number of simulations using generic climate-determined upper boundary conditions. These simulations were conducted in order to investigate the potential impact of the different surface conditions in the geosphere, specifically for a hypothetical repository specified to represent the SFR. In Chapter 2, climate information relevant for building climate variants (Base, Greenhouse, and Permafrost) for SFR1 SAR-08 is compiled. Chapter 3 presents the overall groundwater flow model methodology, model specifications and deliverables. Chapter 3 further presents the results of the numerical groundwater flow simulations. Chapter 4 contains a summary of results and a discussion of their relevance and implications. Chapter 5 and Chapter 6 present recommendations and conclusions drawn from the investigation and scaling factors adopted for assessment purposes.

2 Climate

2.1 Introduction

This section describes information and results on ice sheet and permafrost development at Forsmark compiled from the SR-Can project /SKB 2006a/. In order to use the information from the SR-Can analyses for the safety assessment of the SFR repository, a number of factors need to be taken into consideration. The SR-Can studies on permafrost development were made with a 1D permafrost model employing site-specific data from the site investigations. This means that the results cannot be used for the SFR1 SAR-08 assessment without further consideration. For example, since the analyses for SR-Can were made with a 1D model, the results do not describe lateral variations in the development of permafrost as affected by variations in surface topography, nor do they address lateral variations in bedrock and groundwater characteristics. The selected groundwater modelling approach, and the analysis and discussion of the results, have been adopted to take account of these restrictions. The results from SR-Can are used mainly to discuss the appropriate timing of the time slices for groundwater flow modelling adopted in the present study. Concerning the effect time has on repository safety, see further Chapter 4.

The following sections on vertical permafrost development at Forsmark under various climate scenarios are extracts from /SKB 2006a/ and were presented as part of the SR-Can safety assessment /SKB 2006b/. The selected results are relevant also for the SFR repository, even though this repository is loctated at a significantly shallower depth, 40–110 m, than would be the case for a KBS-3 repository for high-level waste.

2.2 Strategy for providing estimates of the long-term evolution of climate and climate-related conditions

2.2.1 Definition of climate domains

Climate-related changes, such as changes in shoreline elevation and development of permafrost and ice sheets, are the most important naturally occurring external factors affecting a repository for nuclear waste in a time perspective from tens to hundreds of thousands of years.

It is not possible to predict the evolution of the climate in a 100,000-year time perspective with enough confidence for a safety assessment. However, the extremes within which the climate of Sweden may vary can be estimated with reasonable confidence. Within these limits, characteristic climate-related conditions of importance for repository safety can be identified. The conceivable climate-related conditions can be represented as *climate-driven process domains* /Boulton et al. 2001/ where such a domain is defined as *a climatically determined environment in which a set of characteristic processes of importance for repository safety appear.* In the following, these climate-driven process domains are referred to as *climate domains*.

The identified relevant climate domains are named:

- The temperate domain.
- The permafrost domain.
- The glacial domain.

The purpose of identifying climate domains is to create a framework for the assessment of issues of importance for repository safety associated with particular climatically determined environments that may occur in Sweden. If it can be shown that a repository fulfils the safety requirements independent of the prevailing climate domain, and the possible transitions between them, then the uncertainty regarding their exact timing in the future is of less importance.

The temperate domain is defined as regions without permafrost or ice sheets. It is dominated by a temperate climate in a broad sense, with cold winters and either cold or warm summers. Precipitation may fall at any time of the year, i.e. there is no dry season. The precipitation falls either as rain or snow. The temperate domain has the warmest climate of the three climate domains. Within the temperate domain, a site may also at times be submerged by the sea or by ice-dammed lakes.

The permafrost domain is defined as periglacial regions that contain permafrost. It is a cold region, but without the presence of an ice sheet. The permafrost occurs either in sporadic-, discontinuous-, or continuous form. Regions belonging to the permafrost domain are not necessarily the same as regions with a climate that *supports* permafrost. In the permafrost domain, climate may be warmer with diminishing permafrost. However, as long as permafrost is present, the region is defined as belonging to the permafrost domain, regardless of the prevailing temperature at the ground surface. This way of defining the domain is used because the presence of permafrost is more important for the safety function of the repository than the actual temperature at the ground surface. In general, the permafrost domain has a climate colder than the temperate domain and warmer than the glacial domain. Precipitation may fall either as snow or rain.

The glacial domain is defined as regions that are covered by ice sheets. Within the glacial domain, the ice sheet may, in some cases, be underlain by subglacial permafrost. In line with the definition of the permafrost domain, areas belonging to the glacial domain may not necessarily at all times have a climate that supports the presence of ice sheets. However, in general, the glacial domain has the coldest climate of the three climate domains. Precipitation normally falls as snow in this domain. In the present study, it is assumed that no subglacial channels form along the 2D transect that is used for groundwater simulations.

It is currently not possible to make confident predictions of future long-term climate, particularly taking into account the potential long-term significance of inferred current human-induced perturbations of the natural climate system. It is, however, likely that the three climate domains will appear repeatedly during the 100,000 year assessment period, i.e. any reasonable evolution will have to address them, and transitions between them.

2.2.2 Safety assessment scenarios

In SR-Can, a main scenario, additional scenarios, and scenario variants were selected and analysed /SKB 2006b/. For the present study, the three most relevant of these have been selected, spanning the full range of environmental conditions of interest. For the sake of clarity a somewhat different nomenclature for these scenarios and variants is used in the present study. The so-called Base variant and Greenhouse variant of the SR-Can Main scenario are, in the present study, referred to as the *Base variant* and *Greenhouse variant*. The climate information from the Buffer-freezing scenario of SR-Can is, in the present study, referred to as the *Permafrost variant*. The latter name is chosen in order to signify that this variant describes a climate development exceptionally favourable for permafrost growth, in contrast to the Base- and Greenhouse variants, in which permafrost development also occurs, but to a much more limited degree.

The Base variant comprises a reconstruction of climate and climate-related processes during the last glacial cycle, the Weichselian. This serves as *one example* of climate evolution during a glacial cycle. In SR-Can, the Base variant was used as a well-founded basis for the selection of other complementary scenarios describing more extreme climate developments than during the last glacial cycle. As a complement to this, the climate domains are also analysed in the Greenhouse variant, in which the inferred current human influence on climate is taken into account, a human influence not included in the Base variant.

The selected variants are summarised in Table 2-1.

2.3 Permafrost development – overview

2.3.1 General description

Permafrost is defined as ground in which the temperature remains at or below 0°C for at least two years /French 1996/. This definition is based exclusively on temperature, and disregards the texture, degree of compaction, water content, and lithologic character of the material. As a result, the term *permafrost* does not always equate to *perennially frozen ground*, since, depending on pressure and composition of groundwater, and on adsorptive and capillary properties of the ground, water in the ground freezes at temperatures below 0°C. Therefore, permafrost encompasses the perennially frozen ground surrounded by a *cryopeg*, i.e. a ground layer in which water remains unfrozen at sub-zero temperatures.

Freezing of water within permafrost is based on the thermodynamics of interdependent thermal, hydraulic, mechanical and chemical processes in the ground. In turn, freezing of water influences the thermal, hydraulic, mechanical, and chemical properties of the ground. Thermal properties change from those of unfrozen ground to those of frozen ground, affecting the heat transfer process. Ice formation in pores of the ground confines groundwater, by restricting flow through the almost impermeable frozen ground. Hence the overall groundwater circulation is altered. Frost weathering and degradation of the ground surface and patterned ground are further consequences of cyclic freezing and thawing processes. Moreover, exclusion of salts in the process of freezing saline groundwater can lead to increased salinity concentrations in the unfrozen cryopeg.

For information on the theoretical background to heat exchange and associated permafrost development see /SKB 2006a/.

Table 2-1 Selected climate-development scenarios.

Name in present study	Name in SR-Can	Description
Base variant	Base variant of Main scenario	Repetition of conditions during last glacial cycle, including the Weichselian glaciation.
Greenhouse variant	Greenhouse variant of Main scenario	Climate development including anthropogenic warming.
Permafrost variant	Buffer-freezing scenario	Climate development exceptionally favourable for permafrost growth.

2.3.2 Model studies

The purpose of the permafrost model studies was to analyse the main factors of importance for the development of permafrost and perennially frozen ground. The permafrost model includes mathematical expressions for freezing and thawing of saline groundwater-saturated bedrock. The bedrock was treated as an elastic porous medium and the groundwater as an ideal solution of water and ionic solvents. The model is based on the principles of continuum mechanics, macroscopic thermodynamics and the theory of mixtures. It is capable of describing heat transfer, freezing of saline water, groundwater flow and deformations of bedrock. The transport of solutes, however, was excluded from the model. In addition to the common thermal, hydraulic and mechanical couplings in the balance laws, relevant thermo-hydro-mechanical effects associated with freezing and thawing ground are treated through the constitutive relations for groundwater flow, stresses, water/ice phase change and internal energy. A description of the model can be found in /Hartikainen 2004/.

To capture the most important factors and parameters affecting the development of permafrost, sensitivity analyses have been performed considering

1) Surface conditions; and

2) subsurface (bedrock) conditions.

The permafrost calculations were originally made for a KBS-3 repository for high-level waste /SKB 2006ab/, in which the presence of the repository constituted an additional source of heat. For the SFR repository, this heat contribution is not relevant. Therefore, the presented results were selected so as to exclude this heat source. However, in a few cases no such results were available, and these cases are specifically indicated in the text.

Annual mean temperatures at the surface, together with the influence of various types of surface cover such as snow, vegetation and water bodies, have been included as factors of importance in determining the surface conditions. The investigated subsurface conditions are thermal properties of the bedrock and conditions deep in the Earth affecting geothermal heat flow. A 1D subsurface model based on present-day reference data for Forsmark was used, see Table 2-2.

The reduction of permeability due to freezing was calculated as a function of the unfrozen groundwater content:

$$k = k_u \times X^a$$

where k is permeability, k_u is unfrozen permeability, X is unfrozen water fraction ($0 \leq X \leq 1$), and a is a constant ($4 \leq a \leq 6$). Based on experimental observations, the range of a from 4 to 6 has been proposed for soils /Hartikainen and Mikkola 1997/. Experimental data on a is not available for rocks, therefore the mean soil value of 5 has been used in the simulations.

The calculations were carried out in two steps; 1) by using constant surface temperatures for studies of permafrost development rates, and subsequently 2) using surface temperatures based on site-specific climate scenarios for studies of permafrost development, including permafrost depths and growth rates. Surface geothermal heat flow data have been corrected to take account of persistent palaeoclimatic effects, mainly due to the warm period of the Holocene, based on /Balling 1995/.

Table 2-2. Site-specific reference physical properties and conditions of rock mass and groundwater at Forsmark, mainly from the site descriptive model Forsmark 1.2 /SKB 2005/.

Rock mass

Thermal properties

Parameter	Unit	Reference	Min	Max	Temperature dependency
Thermal conductivity	W/(m·K)	3.6	3.2	4.0	11.0% decrease/100°C increase
Heat capacity	MJ/(m³·K)	2.3	2.1	2.5	27.5% increase/100°C increase
Thermal diffusivity	mm²/s	1.57	1.28	1.90	30.2% decrease/100°C increase

Interior Earth conditions by depth

		0 m			10,000 m		
Parameter	Unit	Reference	Min	Max	Reference	Min	Max
Geothermal heat flow	mW/m²	59.0	48.0	65.0	43.2	41.7	46.0
Radiogenic heat prod.	μW/m³	2.5	1.0	3.0	0.92	0.37	1.10

Reference temperature conditions by depth

Parameter	Unit	400 m	500 m	600 m
Temperature	°C	10.6	11.7	12.8
Temperature gradient	°C/km		11.0	

Reference hydro-mechanical properties by depth

Parameter	Unit	100 m	200 m	300 m	≥ 400 m
Bulk density	kg/m³	2,700	2,700	2,700	2,700
Young's modulus	GPa	74	74	74	74
Poisson's ratio	–	0.26	0.26	0.26	0.26
Kinematic porosity	–	0.00001	0.00001	0.00001	0.00001
Total porosity	–	0.0001	0.0001	0.0001	0.0001
Permeability	m²	$1.0 \cdot 10^{-13}$	$1.0 \cdot 10^{-15}$	$1.0 \cdot 10^{-17}$	$1.0 \cdot 10^{-18}$

Groundwater

Reference ionic concentrations by depth

Ionic solvent	Unit	10 m	100 m	300 m	500 m	≥ 1,000 m
Na^+	g/m³	65	500	2,000	2,000	2,000
Ca^{2+}	g/m³	60	250	1,200	1,000	3,500
Cl^-	g/m³	15	1,300	5,500	5,500	10,000
SO_4^{2-}	g/m³	20	170	500	400	50

The permafrost development rates (aggradation rates) for constant ground-surface temperatures under these reference conditions at Forsmark are shown in Figure 2-1.

Permafrost development was then modelled for time-varying site-specific surface conditions in order to construct the various climate variants. First, data from ice sheet model simulations were extracted for use in the permafrost simulations. To this end, site-specific time series of ground-level annual air temperatures and basal ice sheet temperatures, as well as information on site-specific ice thickness variations were extracted /SKB 2006a/. In addition, data from a Glacial Isostatic Model were used to describe the development of the shoreline /SKB 2006a/. Three variants were analysed:

- The *Base variant* employing the "Reference surface conditions".
- The *Greenhouse variant*, employing the same "Reference surface conditions" as in the Base variant, but with a prolonged initial period of temperate conditions.
- *The Permafrost variant* favouring permafrost development by employing "Extreme surface conditions".

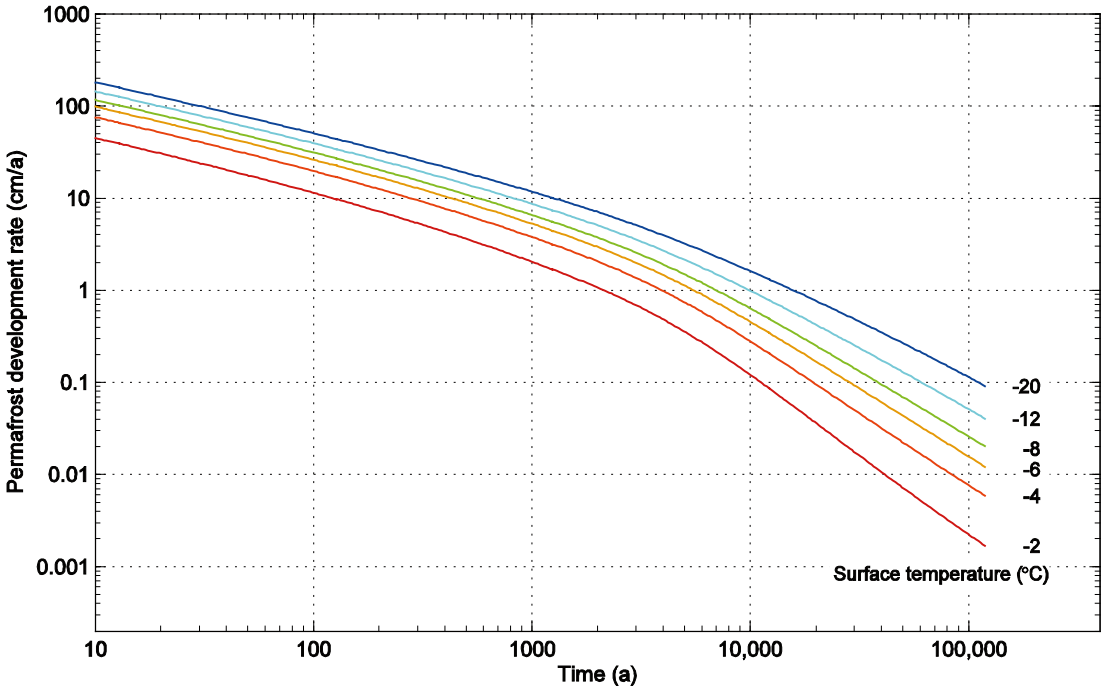

Figure 2-1. *Evolution of permafrost development rate for constant ground surface temperatures of –2, –4, –6, –8, –12 and –20°C at Forsmark when site-specific subsurface properties are assigned.*

In addition, simulations with talik formation were also made; taliks being unfrozen areas within a region with continuous permafrost that can occur, for example, under lakes. Inputs for the time-varying permafrost simulations are shown in Figure 2-2 and Figure 2-3.

The Base variant (Figure 2-2) describes a situation with ice-sheet development and shoreline migration occurring as reconstructed for the last glacial cycle. The Permafrost variant (Figure 2-3) describes a situation with cooling air temperatures as reconstructed for the last glacial cycle, but in an extremely dry climate with no ice sheet formation. In the Permafrost variant, the site remains above sea level during the entire period and there is no seasonal snow or vegetation cover. All in all, this produces climatic conditions exceptionally favourable for permafrost development. When the site is covered by an ice sheet, surface temperatures, shown in Figure 2-2, are equal to the basal temperatures as calculated by the ice sheet model. When the site is submerged, the surface temperature was set to +4°C. In the Permafrost variant (Figure 2-3) the site-specific air temperature was calculated from ice sheet model data on air temperatures (Figure 2-2) by making a lapse-rate correction for the difference in elevation between the height of the ice sheet and that of the ground surface.

The following sections of Chapter 2 describe the permafrost development at Forsmark for the variants of future climate development, based on the above assumptions on ground surface temperatures (Figure 2-2 and Figure 2-3) and subsurface properties (Table 2-1).

2.4 Base variant

The rationale for, and general approach to, compiling the evolution of climate-related conditions is found in the /SKB 2006a/. One thing of importance to remember is that the Base variant and Greenhouse variant are not attempts to *predict* probable future evolutions. Instead, they are *relevant examples* of possible future evolutions that, in a realistic and consistent way, cover all relevant climate-related changes that can be expected in a 100,000-year time perspective. In the original SR-Can analyses, they formed a well-founded basis for the selection of additional scenarios in which repository safety was also assessed, for example the variant exceptionally favourable for permafrost growth.

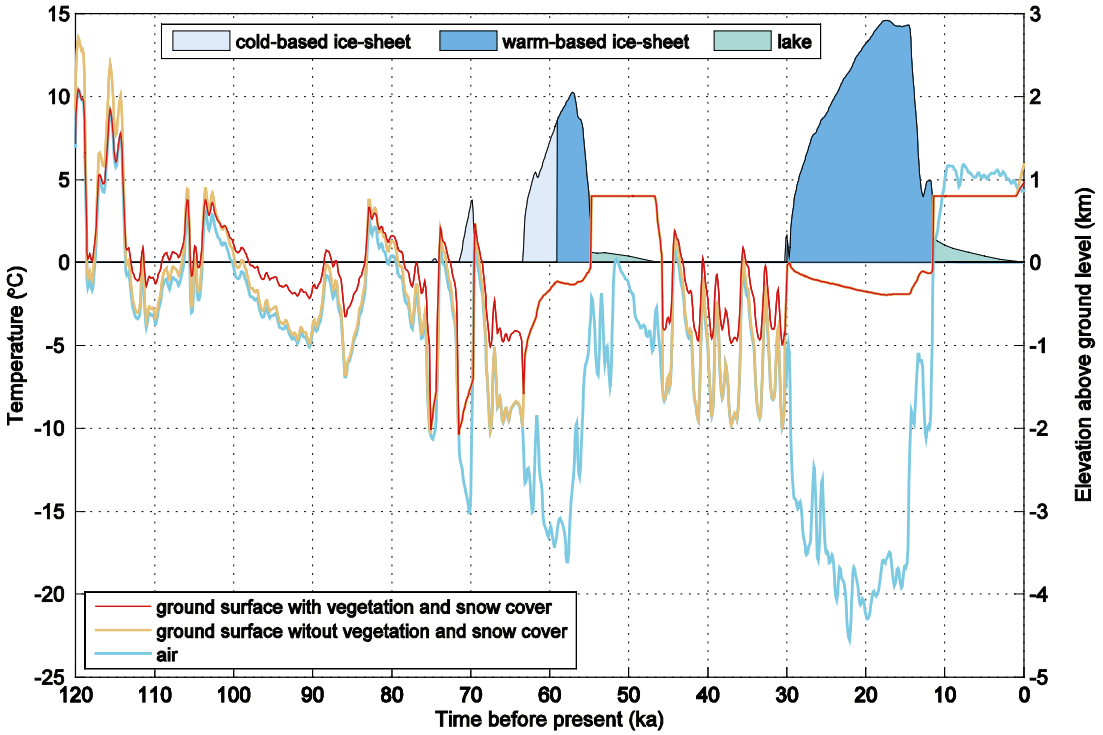

Figure 2-2. *Reconstruction of the evolution of air temperature, ice sheet thickness, lake depth and modelled ground surface temperature with and without vegetation and snow cover for the last glacial cycle. Time scale runs from 120 ka before present to 0 (present) since this is a reconstruction of climate conditions for the last glacial cycle. For details on the results, see /SKB 2006a/.*

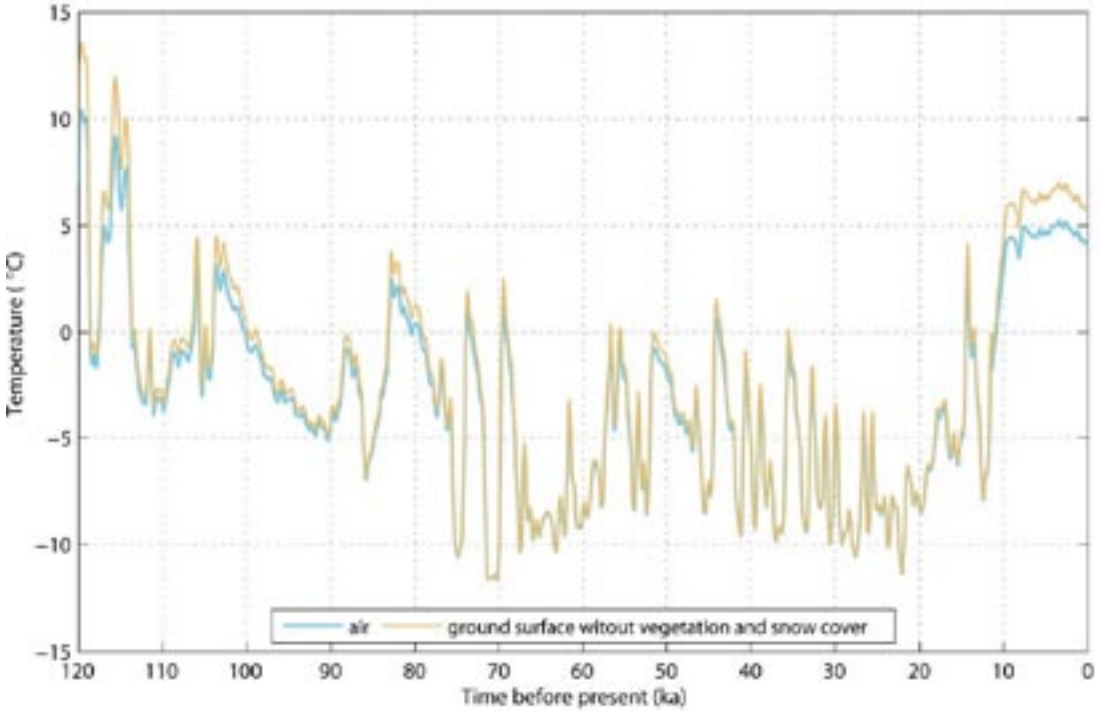

Figure 2-3. *Reconstructed evolution of air temperature and modelled ground surface temperature without vegetation and snow cover at Forsmark to use as input to the Permafrost variant. Temperature variation is as during the reconstruction of the last glacial cycle, but no ice sheet development takes place and the site remains above sea level. Furthermore, there is no seasonal snow or vegetation cover. Time scale runs from 120 ka before present to 0 (present) since this is a reconstruction of climate conditions for the last glacial cycle. For details on results, see /SKB 2006a/.*

2.4.1 Evolution of bedrock temperature and permafrost at Forsmark

In the Base variant, i.e. the repetition of the last glacial cycle, permafrost develops during the progressively colder phases of the glacial cycle. When the ice sheet advances to cover the permafrost, the permafrost typically stops developing and starts to diminish. When the ground is re-exposed to a cold climate, such as during the ice-free stage between the two major ice advances (Figure 2-2), permafrost starts to grow again.

The development of permafrost at Forsmark for the Base variant is shown in Figure 2-4.

The evolution of subsurface temperatures at Forsmark for reference surface conditions, with vegetation and snow cover, down to a depth of 160 m is shown in Figure 2-5. For the Base variant, sensitivity tests were made on the impact of varying geothermal bedrock characteristics. Selected results are shown in Figure 2-6 and Figure 2-7.

The results from the sensitivity tests can be used to estimate bedrock temperatures that can be expected for the specific bedrock thermal characteristics of the SFR site.

In the Base variant, the development of permafrost at Forsmark starts about 8,000 years into the scenario. The permafrost and frozen ground depth reach a maximum at Forsmark prior to the first major glacial advance, at about 50 ka after repository closure. At that time, the modelled permafrost depth reaches approximately 250 metres at Forsmark. The frozen depth is, at the same time, a few tens of metres shallower. When the ice sheet advances over the region, the permafrost stops developing and instead starts to diminish, for example around 60,000 years into the scenario. Subsequently, permafrost again develops during the ice-free period between the two major ice advances, but at that time to a somewhat shallower depth, about 180 metres.

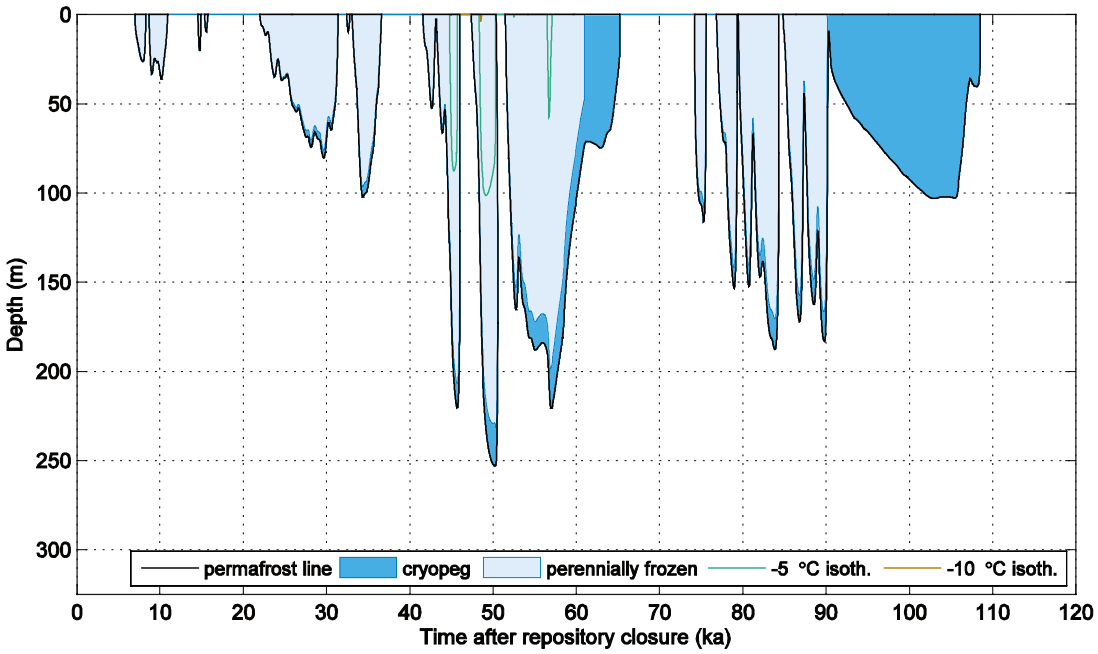

Figure 2-4. *Evolution of permafrost, perennially frozen bedrock and unfrozen cryopeg at Forsmark in the Base variant, i.e. a reconstruction of conditions during the last glacial cycle. The figure shows a future scenario, based on a repetition of reconstructed last glacial cycle conditions, with a time scale running from 0 (present) to 120,000 years into the future. In this plot, the heat from spent fuel from a KBS-3 repository at 400 depth is included. For a more applicable permafrost development curve, without this heat contribution, see Figure 2-6 and Figure 2-7.*

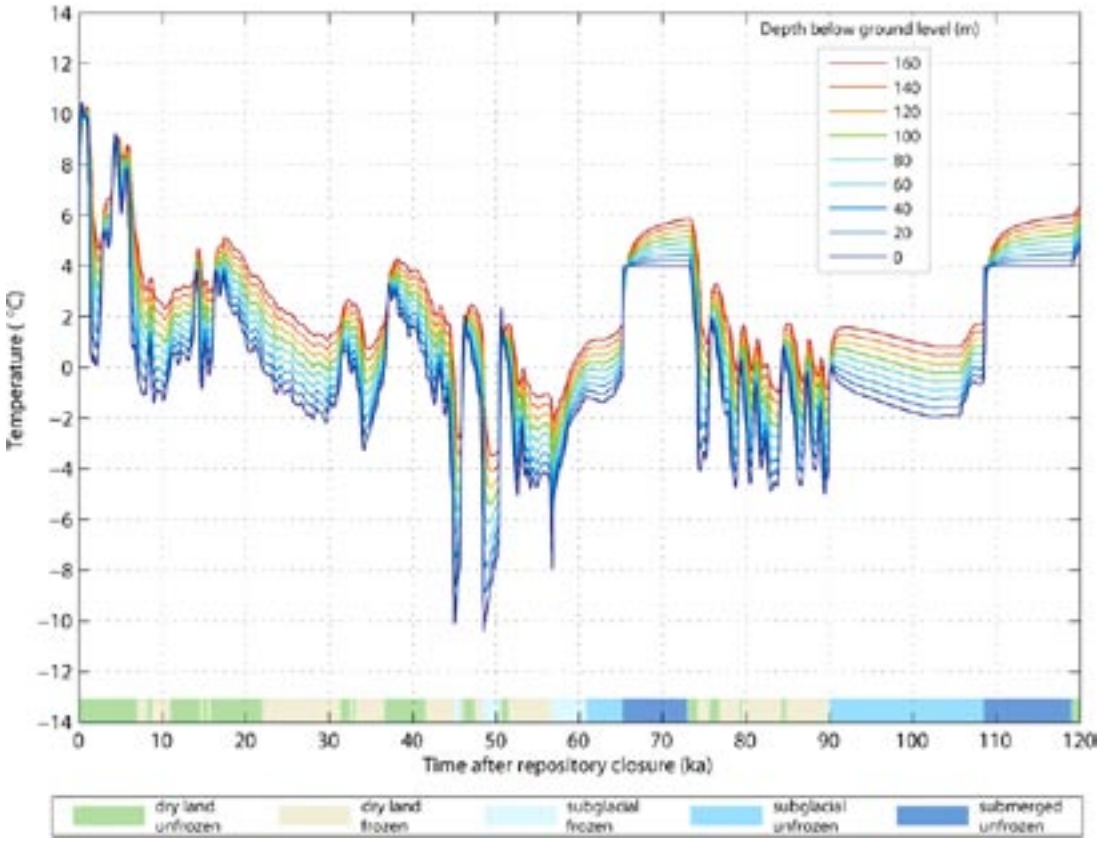

Figure 2-5. *Evolution of bedrock temperatures at Forsmark down to a depth of 150 m for the Base variant, i.e. repetition of last glacial cycle conditions under reference surface conditions with vegetation and snow cover, and reference subsurface properties as in Table 2-2. The figure also shows the physical state of the ground surface.*

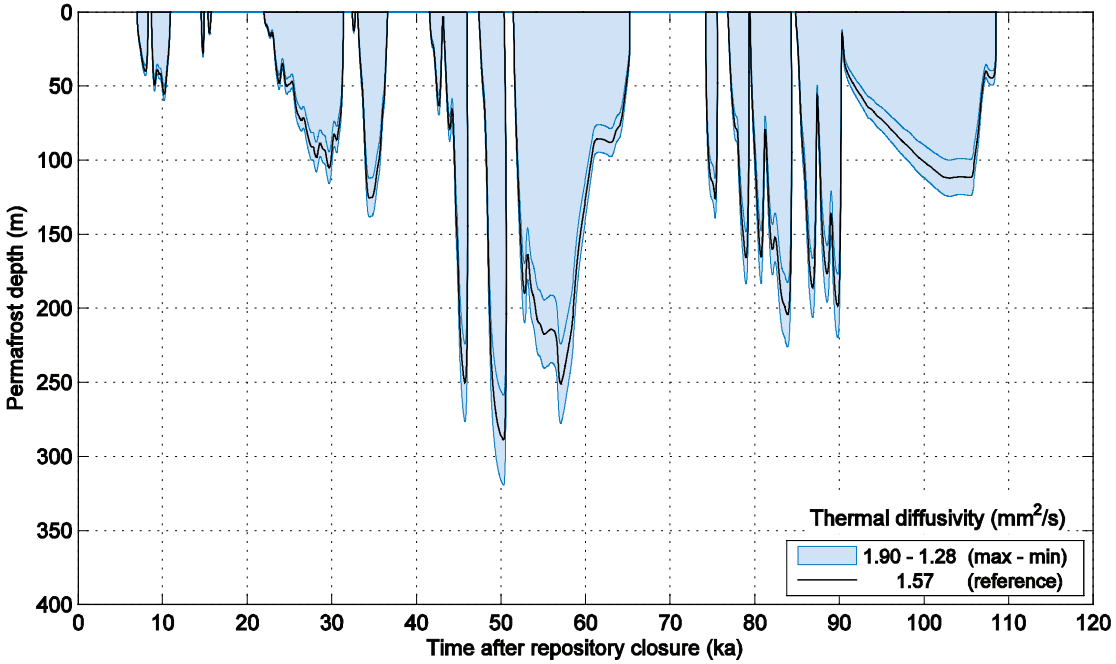

Figure 2-6. *Sensitivity tests on variations in thermal diffusivity for the Base variant. The upper edge of the shadowed area is associated with the minimum, and the lower edge with the maximum, value of thermal diffusivity. Calculations were made without the additional heat contribution from a KBS-3 repository.*

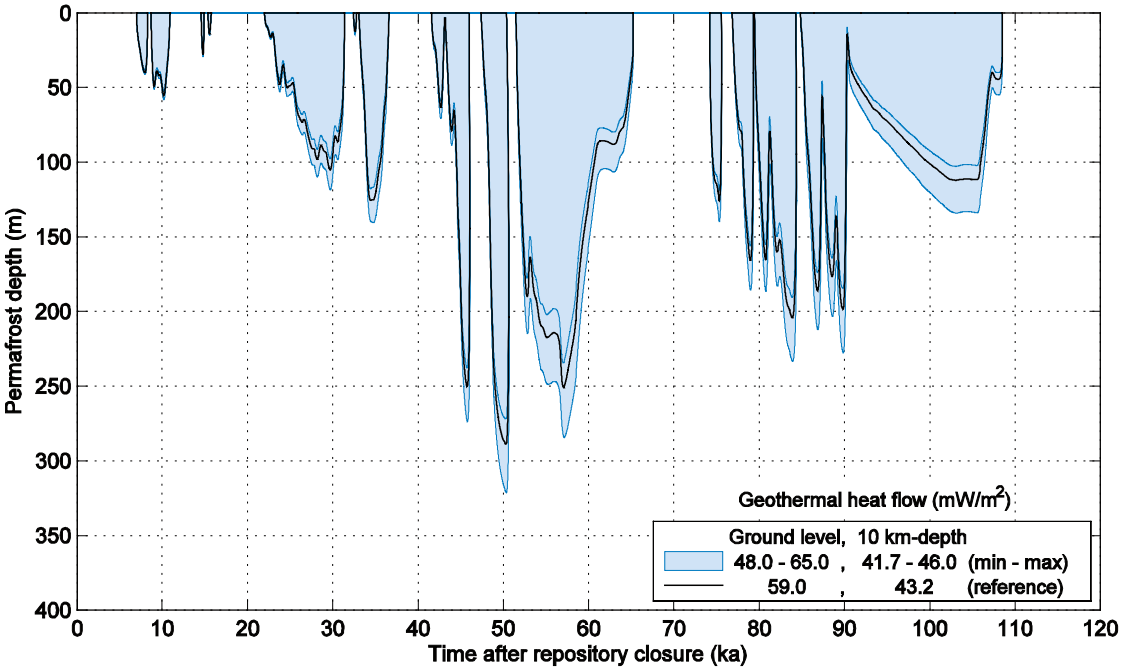

Figure 2-7. *Sensitivity tests on variations in geothermal heat flow for the Base variant. The upper edge of the shadowed area is associated with the maximum, and the lower edge with the minimum value of geothermal heat flow. Calculations were made without the additional heat contribution from a KBS-3 repository.*

During the major phase of ice coverage, including the ice-sheet maximum at more than 100,000 years into the scenario, the maximum permafrost depth is around 100 metres. Note that, at that time, the frozen depth is zero due to the high water pressure induced by ice load, and hence all bedrock is at this time at the pressure melting point temperature.

The rates of permafrost growth and degradation in the Base variant are shown in Figure 2-8.

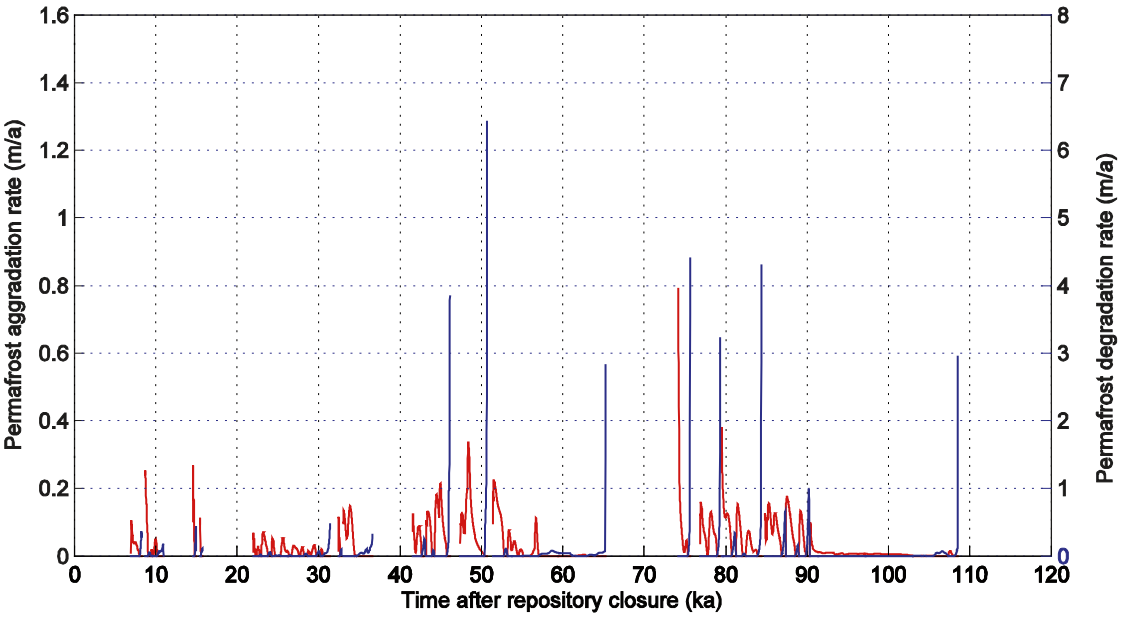

Figure 2-8. *Permafrost growth and degradation rates at Forsmark for the Base variant of the main scenario. Calculations were made without the heat contribution from a KBS-3 repository.*

2.4.2 Evolution of climate domains at Forsmark in the Base variant

Based on the reconstructions of ice sheet, shoreline and permafrost for the last glacial cycle (results above and in /SKB 2006a/ the Base variant development at Forsmark can be described as a succession of climate domains and submerged periods (Figure 2-9). The evolution of all relevant climate-related variables in the Base variant is presented in Figure 2-10.

The climate succession bars (Figure 2-9) show that the Forsmark site is dominated by temperate conditions for the first approximately 25,000 years, although short periods of permafrost domain occur around 10,000 years after repository closure. Then, through the ice-sheet-free period, temperate conditions are gradually replaced by permafrost conditions. The ice-free period around 80–90 ka into the scenario is clearly dominated by permafrost conditions. The trend with gradually more dominating permafrost conditions is a natural result of the progressively colder climate during the glacial cycle. An exception to this trend is the short period after the submerged phase that follows the final deglaciation, at the very end of the scenario. At that time, ice-free conditions again are dominated by temperate conditions in a warm interglacial climate. Another effect of the progressively colder climate during the glacial cycle is the increasing length of the periods with glacial domain.

Periods of temperate domain occupy about 31,000 years of the Base variant at Forsmark. These occur in the early phase of the glacial cycle, during the interstadial between the two major ice advances, and during the interglacial period following the glacial maximum. The periods of temperate domain during the initial interglacial and early phases of the reference glacial cycle are generally warmer and longer than those occurring during interstadials in the later part of the glacial.

During the first 50,000 years of the evolution, and in the period between the two ice advances, the increasingly colder climate results in progressively longer periods of permafrost. The total duration of the permafrost domain is about 41,000 years at Forsmark. In this Base variant, the permafrost develops to quite great depths during the most severe permafrost periods. The maximum calculated permafrost depth is approximately 250 metres at Forsmark (see Figure 2-10).

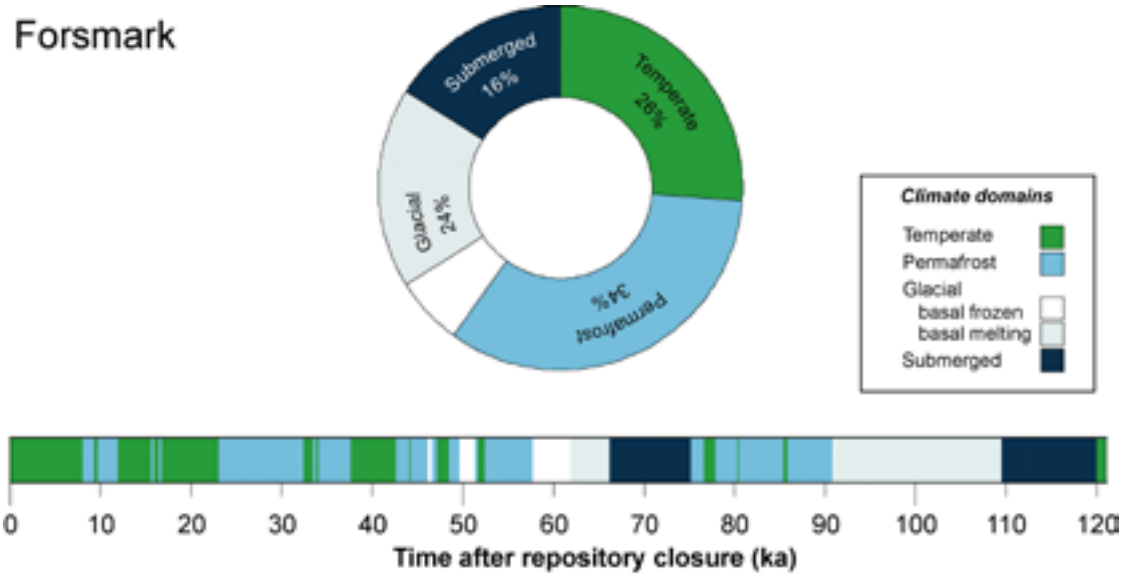

Figure 2-9. *Duration of climate domains at Forsmark, expressed as percentage of the total time of the Base variant. The bar below the pie chart shows the development of climate-related conditions for the Base variant as a time series of climate domains and submerged periods.*

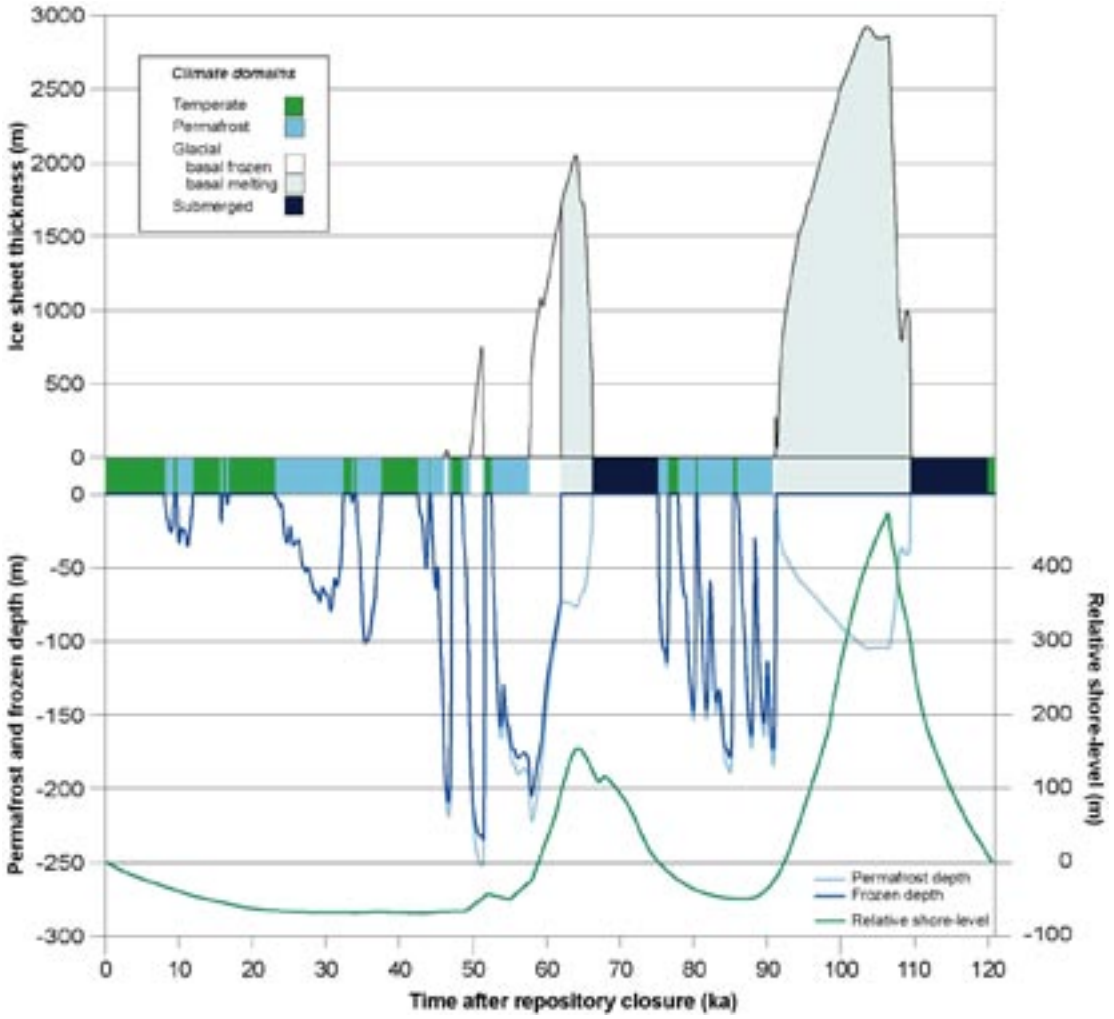

Figure 2-10. *Evolution of important climate-related variables at Forsmark for the Base variant. Heat from a KBS-3 repository is included in the calculation of permafrost depths.*

Forsmark is exposed to two major ice advances and retreats during the Base variant glacial cycle, the first around 60,000 years into the scenario and the second after about 90,000 years (Figure 2-10). Prior to both of these glaciated periods, the site is situated above sea level with prevailing permafrost conditions when the ice sheet advances towards and over the site.

A period of basal frozen ice sheet conditions initiates the first major phase of glacial domain (i.e. ice-sheet coverage). The period of basal frozen conditions, and hence no groundwater recharge, is approximately 4,000 years long. During this period the permafrost, which is now subglacial, reaches its maximum depth of about 250 metres.

When the ice sheet grows over the site, it insulates the subsurface from the cold climate and, in time, induces ice sheet basal melting conditions. During periods of ice sheet coverage, the development of subglacial permafrost is much more restricted than permafrost development during ice-free conditions prior to ice sheet coverage. The total length of periods of ice sheet coverage at Forsmark is, in the Base variant, approximately 30,000 years. During this time, basal melting conditions, with associated groundwater recharge, dominate.

For a description of the evolution of hydrological conditions, groundwater and mechanical conditions in the Base variant of the main scenario in SR-Can, see /SKB 2006a/.

2.5 Greenhouse variant

A variant with an increased greenhouse effect has been investigated. There are two main reasons for doing this; 1) modelling studies of the climate response to increased greenhouse gas emissions, mainly CO_2, indicate that global temperatures will rise in the future under such CO_2 scenarios /e.g. IPCC 2001, 2007/, and 2) climate cycles are believed to be driven by changes in insolation, which are projected to be smaller in the future than they have been over the last glacial cycle. The coming 100,000 year period is initially characterised by exceptionally small amplitudes of insolation variations /Berger 1978/, possibly making the present interglacial exceptionally long. /Berger and Loutre 2002/ and others suggest it may end approximately 50,000 years from now. Furthermore, the combination of small amplitude variations in insolation and anthropogenically enhanced greenhouse warming may lead to an even longer interglacial /BIOCLIM 2003/.

For the purpose of a safety assessment, the impact of greenhouse warming on climate-related conditions in Sweden can be regarded as being expressed through a long and, at least part of the time, very warm period of temperate domain. In the Greenhouse variant, it is assumed that the temperate domain will prevail for another 50,000 years until the first, restricted, ice advance in Fennoscandia takes place. After that, the first 70,000 years of the Base variant evolution is assumed to follow. The first major ice advance will thus occur after approximately 100,000 years in the Greenhouse variant. This scenario is in broad agreement with results of the BIOCLIM project. For two greenhouse-warming cases, a warm Eurasian climate and restricted ice coverage were simulated for up to about 100,000 years into the future /BIOCLIM 2003/.

For a description of the treatment of sea-level and shoreline migration in the Greenhouse variant, see /SKB 2006a/.

Figure 2-11 presents the duration of climate domains at Forsmark for the Greenhouse variant. Naturally, the temperate domain dominates in this scenario, with temperate conditions prevailing for 65% of the time (78,000 years). Permafrost conditions prevail for 23% of the time (28,000 years), whereas glacial conditions are met with for 9% of the time (11,000 years). The resulting evolution of important climate-related variables at Forsmark for the Greenhouse variant is shown in Figure 2-12.

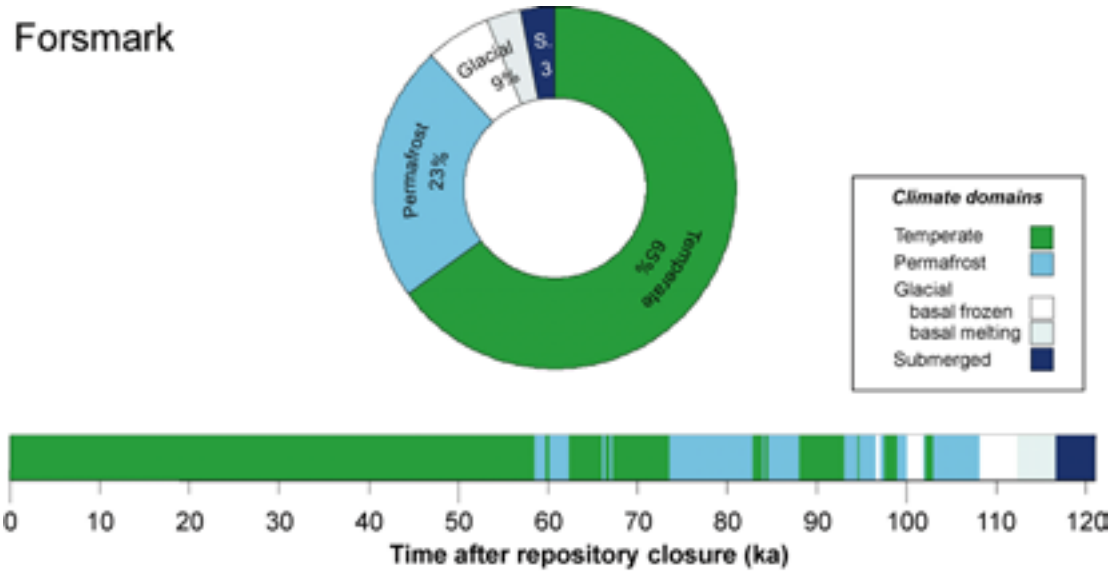

Figure 2-11. *Duration of climate domains at Forsmark, expressed as percentage of the total time of the Greenhouse variant. The bar below the pie chart shows the Greenhouse variant development of climate-related conditions as a time series of climate domains and submerged periods.*

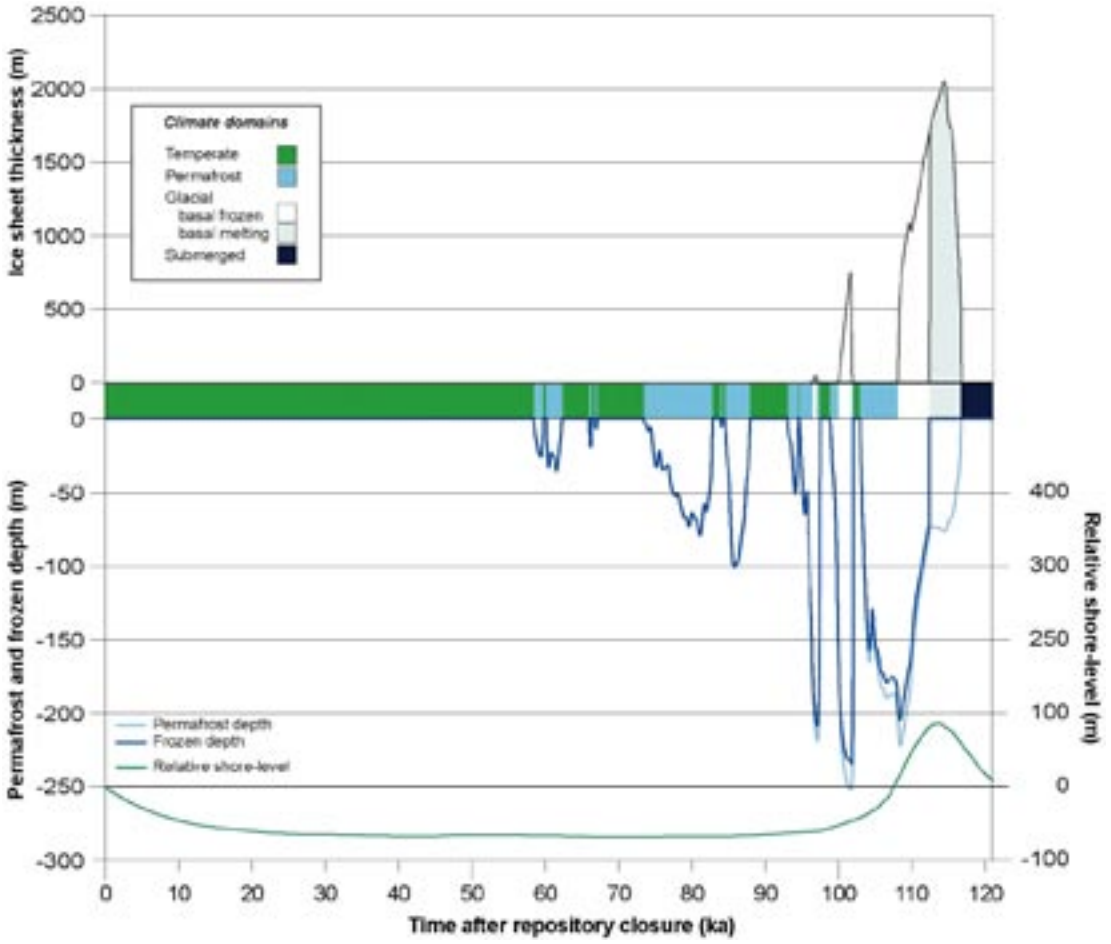

Figure 2-12. *Evolution of important climate-related variables at Forsmark for the Greenhouse variant of the main scenario. The permafrost curve includes heat contribution from a KBS-3 repository.*

2.5.1 Climate conditions

The climate is dominated by an initial approximately 100,000 year long warm period without ice sheet coverage; a period that gets colder towards the end. During a large part of this warm period, mean annual air temperatures at the site may be as warm as, or warmer than, present. During this initial long warm period, it is likely that climate within the temperate domain may vary significantly, with a range that may be larger than that during the Holocene.

The length of the initial period of temperate domain in the Greenhouse variant should not be taken as a prediction of future greenhouse climate change. Under a future warming climate, this period could be shorter or longer than that described in the scenario.

During the second half of the Greenhouse variant, climate varies within the same range as the first part of the Base variant, and consequently the climate-related processes will act in the same way as in the Base variant.

2.5.2 Permafrost development in the Greenhouse variant

The first periods of permafrost appears approximately 60,000 years into the Greenhouse variant (Figure 2-12). After the initial temperate period, the pattern of permafrost development in the Greenhouse variant follows that in the Base variant. Therefore, the maximum permafrost depth at Forsmark is the same in the Greenhouse variant as in the Base variant of the main scenario, i.e. 250 metres, but it occurs considerably later in the scenario, after approximately

100,000 years. The first and only major ice advance during the 120,000 years of the Greenhouse variant occurs after more than 110,000 years. After the glacial advance, Forsmark is submerged for about 4,000 years before the end of the scenario. For more details of the SR-Can Greenhouse variant, see /SKB 2006a/.

2.6 Permafrost variant

Investigations of permafrost development under exceptionally favourable conditions were undertaken. In this variant, air temperatures were assumed to fall according to the glacial cycle temperature curve of the reference evolution, but in an extremely dry climate not supporting any ice sheet growth. To favour permafrost growth further, the mitigating effects of snow cover and vegetation were excluded from consideration, and the site was assumed to always remain above sea level. For a discussion and motivation for the selection of the SR-Can scenario exceptionally favourable for permafrost growth, see /SKB 2006a/. The evolution of permafrost at Forsmark in the Permafrost variant is shown in Figure 2-13. Subsurface temperatures at Forsmark for this variant, down to a depth of 160 m, are shown in Figure 2-14.

As in the Base variant, sensitivity tests were made for the Permafrost variant on the impact of varying geothermal bedrock characteristics (Figure 2-15 and Figure 2-16).

The results from the sensitivity tests can be used to estimate bedrock temperatures that can be expected for the specific bedrock thermal characteristics of the SFR site.

In the case of development of permafrost under exceptionally favourable conditions, without an ice sheet forming during cooling of the glacial cycle and without snow and vegetation cover, the maximum permafrost depth at Forsmark is 400 m. The −5 and −10°C isotherms reach maximum depths of 200 m and 40 m, respectively (Figure 2-13).

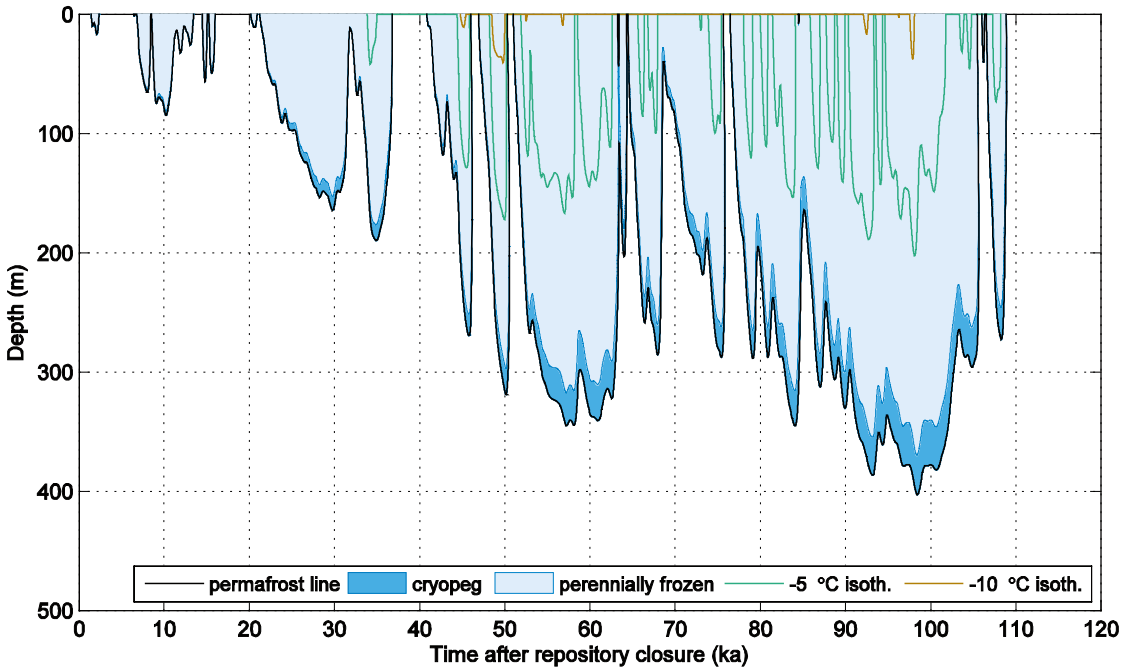

Figure 2-13. *Evolution of permafrost, perennially frozen bedrock and unfrozen cryopeg at Forsmark in the Permafrost variant, i.e. conditions exceptionally favourable for permafrost growth. The time scale runs from 0 (present) to 120,000 years into the future. Heat from spent fuel from a KBS-3 repository was not included in the calculation.*

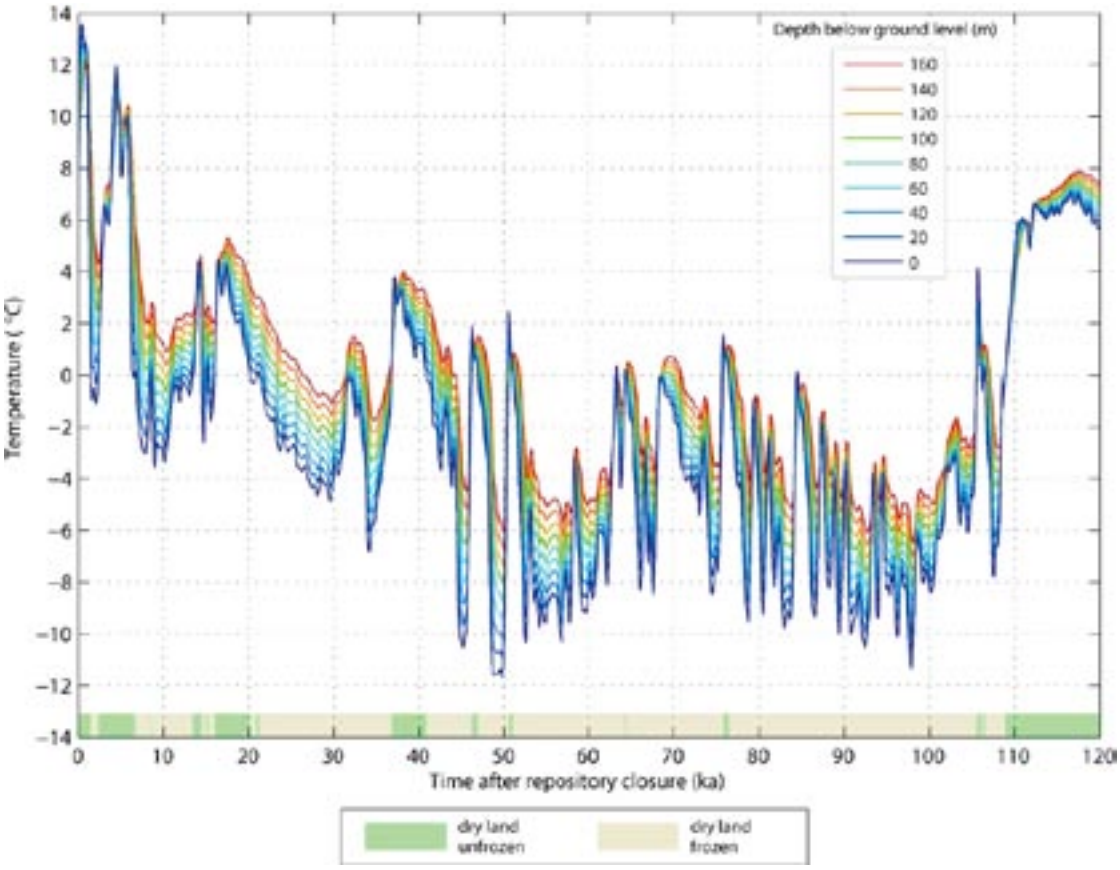

Figure 2-14. *Evolution of subsurface temperature at Forsmark down to a depth of 160 m for the Permafrost variant, i.e. considering surface conditions without ice sheets or submergence, and without snow or vegetation cover. Reference subsurface properties and no heat from a KBS-3 repository were used. The figure also shows the physical state of the ground surface.*

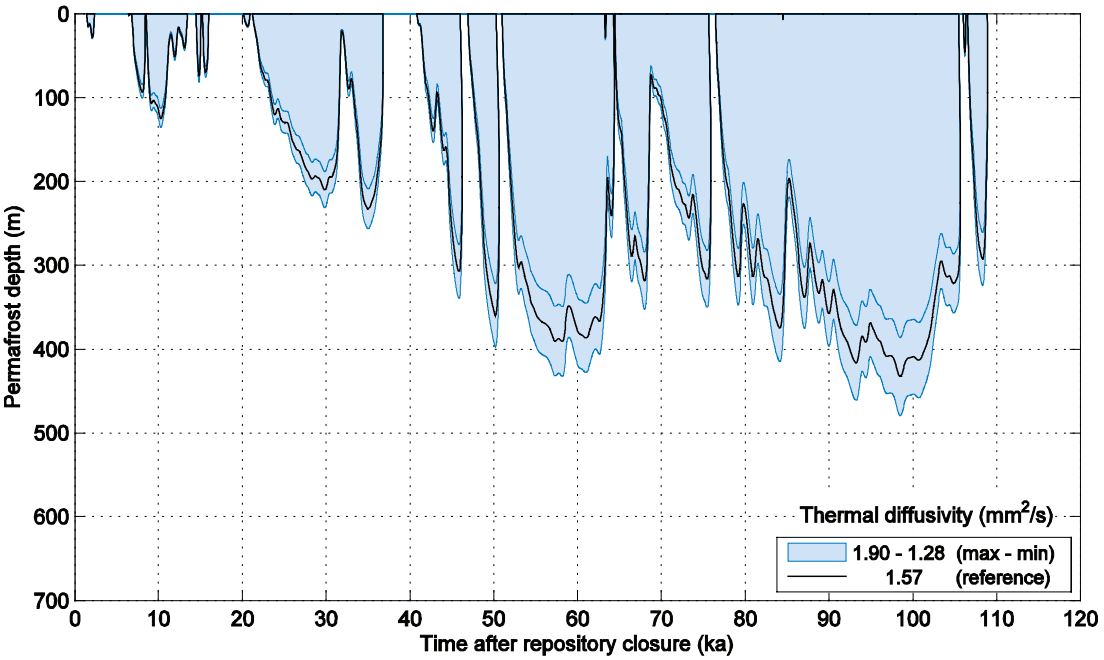

Figure 2-15. *Sensitivity tests on variations in thermal diffusivity for the Permafrost variant. The upper edge of the shadowed area is associated with the minimum, and the lower edge with the maximum, value of thermal diffusivity. Calculations were made without the additional heat contribution from a KBS-3 repository.*

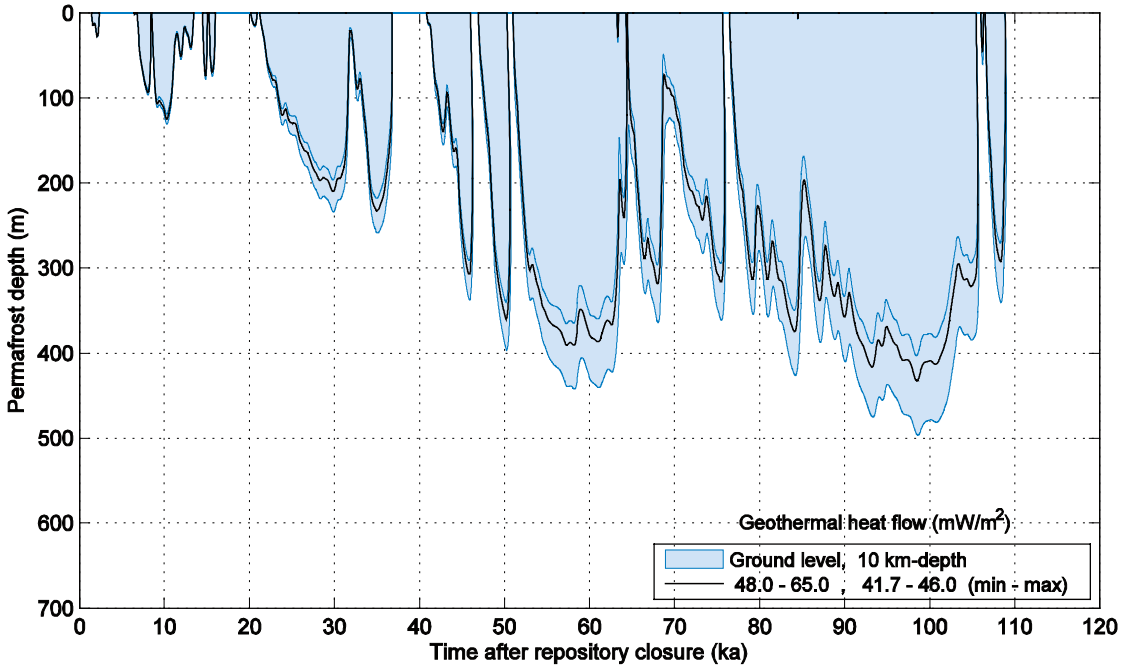

Figure 2-16. *Sensitivity tests on variations in geothermal heat flow for the Permafrost variant. The upper edge of the shadowed area is associated with the maximum and, the lower edge with the minimum, value of geothermal heat flow. Calculations were made without the additional heat contribution from a KBS-3 repository.*

The rates of permafrost growth and degradation in the Permafrost variant are seen in Figure 2-17. Figure 2-18 presents a comparison of permafrost depths at Forsmark for the Permafrost variant with and without a heat contribution from a KBS-3 repository.

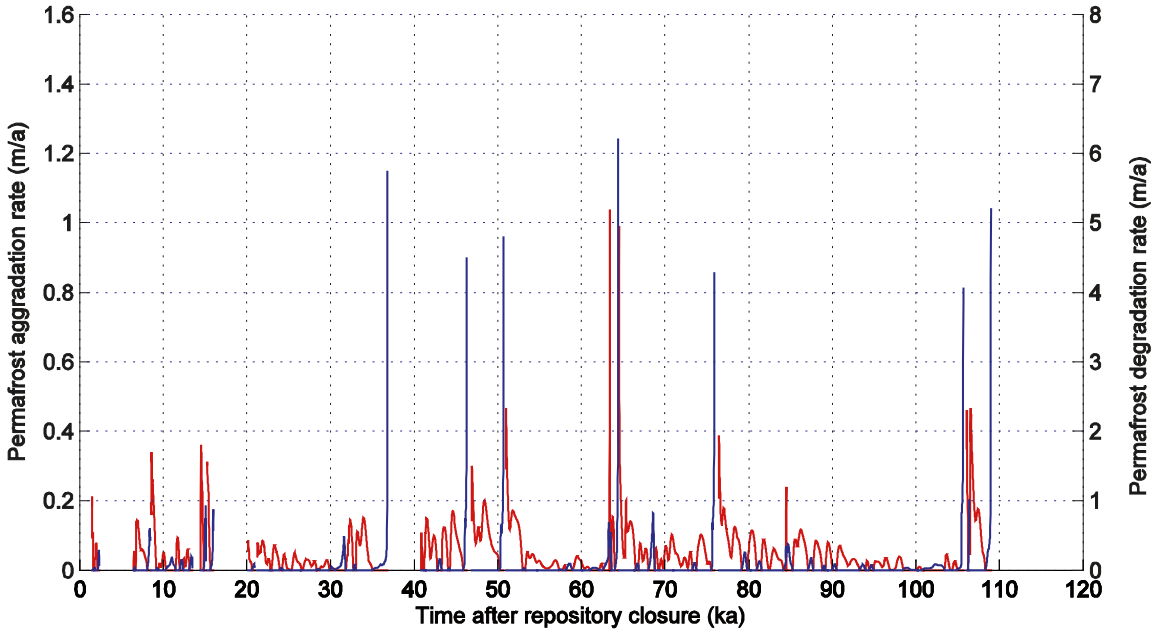

Figure 2-17. *Permafrost growth and degradation rates for the permafrost variant at Forsmark. Calculations were made without the heat contribution from a KBS-3 repository.*

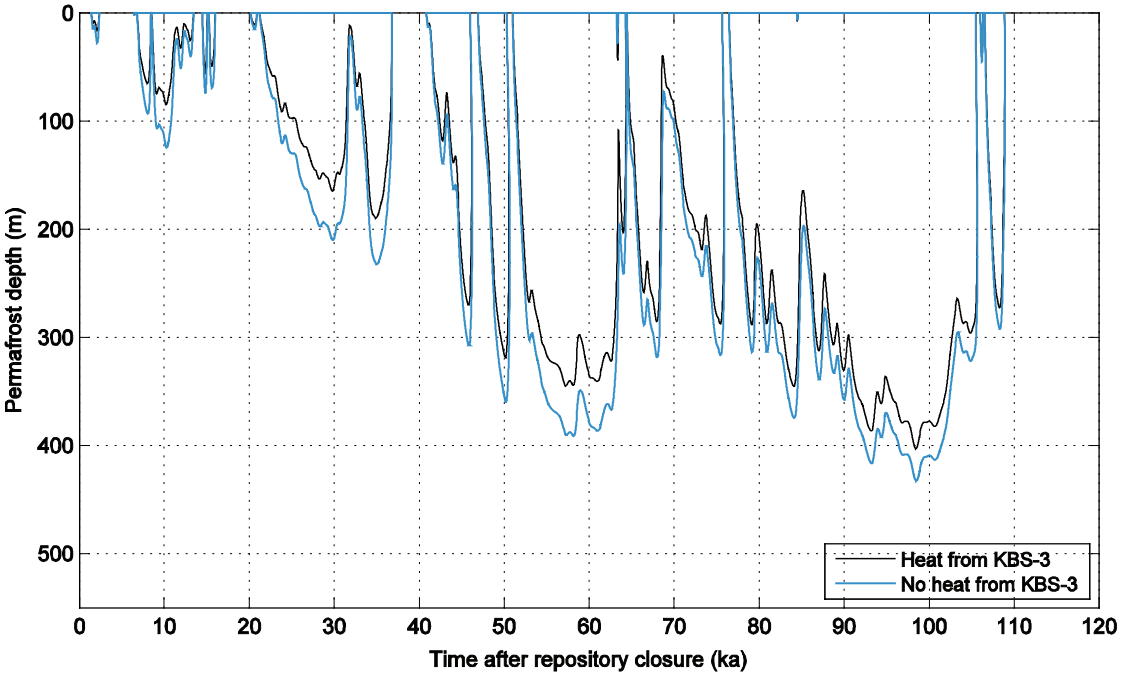

Figure 2-18. *Comparison of permafrost development at Forsmark, for the Permafrost variant, with and without a heat contribution from a KBS-3 repository at 400 m depth.*

2.7 Simulations of talik formation

Water bodies like lakes or rivers affect permafrost depth and can give rise to the presence of taliks, i.e. unfrozen areas within regions of continuous permafrost. A talik can exist beneath a water body when the water bottom temperature remains above the freezing point. Based on /Yershov 1998, Burn 2002/ and modelling results obtained with favourable conditions for lake ice development, it has been determined that a two metre deep water body maintains its bottom temperature above 0°C and that a water body deeper than 8 metres has a bottom temperature around +4°C. The size of the water body required to maintain a talik was investigated by permafrost modelling. To this end, permafrost development was simulated in the vicinity of circular lakes with constant positive lake bottom temperatures and constant negative lake bottom level subsurface temperatures. The results shown in Figure 2-19 indicate that an open talik can survive beneath a circular shallow lake, if the radius of the lake is greater than the thickness of surrounding undisturbed permafrost. Furthermore, the results in Figure 2-20 demonstrate that a lake radius greater than 0.6 times the thickness of surrounding undisturbed permafrost is big enough for a deep circular lake to maintain an open talik. The same results were obtained with two sets of different subsurface properties. It is notable that these results seem to be independent of the site. Moreover, the results apply for different lake bottom level subsurface temperatures.

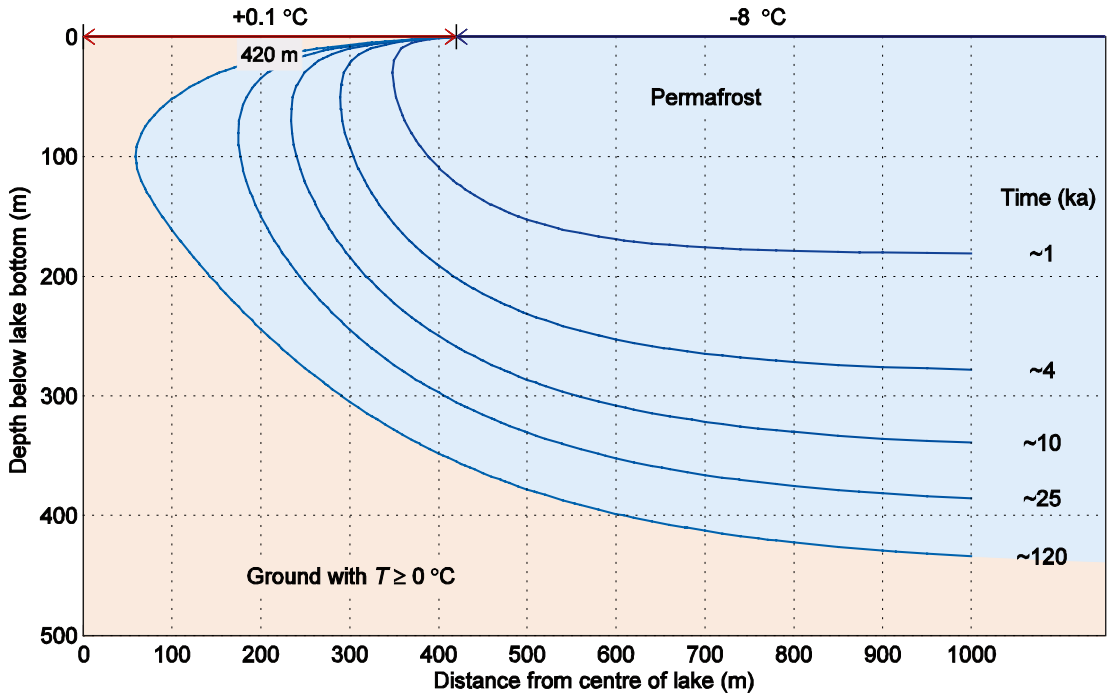

Figure 2-19. *Evolution of permafrost in the vicinity of a circular lake (red colour) of radius of 420 m at Forsmark when a constant lake bottom temperature of +0.1°C, and a constant ground temperature of –8°C at lake bottom level prevail and reference subsurface properties are assigned.*

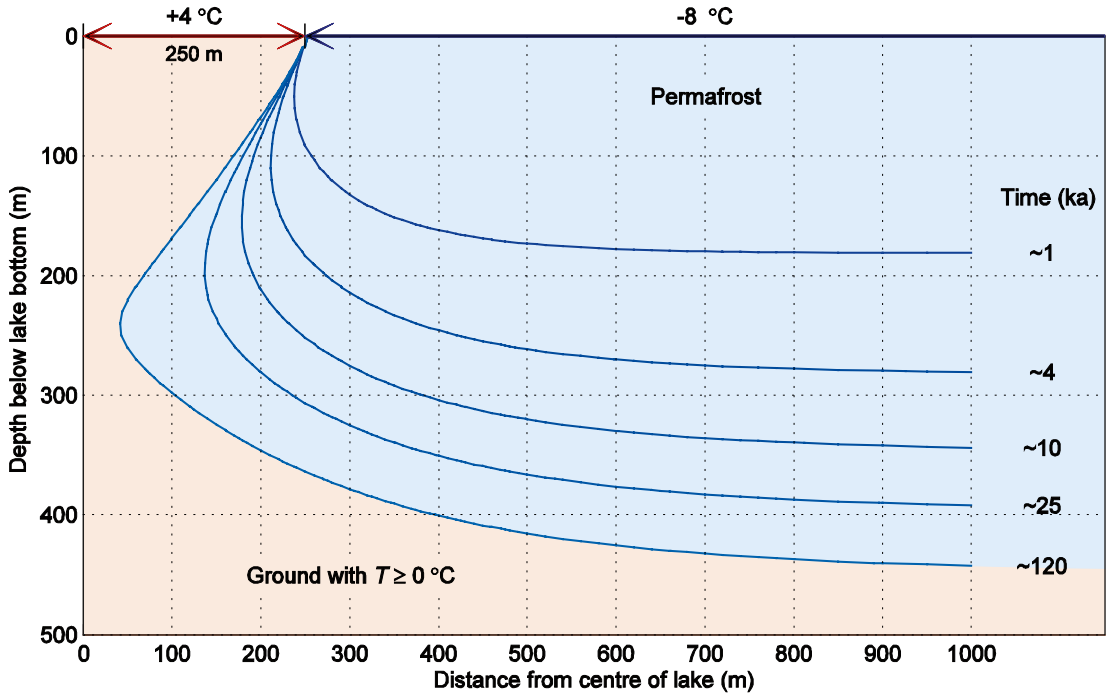

Figure 2-20. *Evolution of permafrost in the vicinity of a circular lake (red colour) of radius of 250 m at Forsmark when a constant lake bottom temperature of +4°C, and a constant ground temperature of –8°C at lake bottom level prevail and reference subsurface properties are assigned.*

2.8 Modelling uncertainty

2.8.1 Permafrost model simplification and uncertainty

The major model simplification is to carry out the studies in 1D, thus excluding implications from lateral variations in physical properties, boundary conditions and geometry. For example, full consideration of the anisotropy of thermal conductivity and heat capacity and the features of water bodies and topography requires 3D modelling. The 1D modelling approach could, in certain situations, result in somewhat higher temperatures than would be calculated using a full 3D approach. Lateral groundwater flow is the most important factor that would need 3D modelling instead of 1D in the context of permafrost development. However, groundwater flow only has a minor role in permafrost development, compared with heat conduction. Furthermore, the anisotropy of thermal properties is not a problem in 1D, since one can choose a combination of thermal properties that would give the lowest temperatures, or at least very close to the lowest temperatures that would be estimated through full 3D modelling.

Additional model simplifications are the continuum approach for the modelling of groundwater flow and neglect of salinity transport. However, the Forsmark site is largely composed of relatively low-porosity and low-permeable bedrock, in which case the groundwater flow and salinity of groundwater have minor effects on permafrost development. If salt transport were to have been included, some calculated permafrost depths would have been slightly shallower.

2.8.2 Input data and data uncertainty

Some data uncertainty exists when it comes to effective thermal conductivity and heat capacity of rock at the site. In the calculation of ground temperature and the rate of freezing, thermal conductivity is the most important input parameter in terms of physical properties of the ground. The predominant rock type in Forsmark has a mean thermal conductivity of 3.56–3.71 W/m·K depending on the method used for the determination /SKB 2005/, whereas subordinate rock types have values between 2.96 and 3.54 W/m·K.

Uncertainty also exists in determination of hydraulic and mechanical properties of bedrock and salinity concentrations of groundwater versus depth at the repository site /SKB 2005/.

The in situ ground temperature has been measured in boreholes to a depth between 500 and 1,400 metres. Between different boreholes the temperature varies over a range of 2°C /SKB 2005, 2006c/. A considerable uncertainty is associated with determination of the ground-surface temperature from the air temperature as well as with estimation of the in situ temperature and geothermal heat flow in the depth range of 1,000–10,000 metres for the thermal boundary and initial conditions of the model.

2.9 Treatment of climate in groundwater flow simulations

From the three climate scenarios described above (e.g. Base variant, Greenhouse variant, and Permafrost variant), five relevant cases can be defined for further steady-state analysis of groundwater flow; i) Temperate climate conditions, ii) Sporadic permafrost conditions, iii) Continous permafrost conditions, iv) Ice sheet presence without permafrost, and v) Ice sheet overriding permafrost. For each of these cases, groundwater modelling simulations can be made under representative hydrogeological steady-state conditions.

3 Numerical flow simulations

3.1 Hydrogeological modelling tool

The code version used in this study was DarcyTools V3.0. The computer code DarcyTools has been developed for simulations of groundwater flow and mass transport in porous and fractured media; the code uses continuum equations.

The DarcyTools code is further based on a finite volume formulation of the governing differential equations for flow and mass transport. This means that the hydraulic properties of the computational grid cells are volumetric functions of:

- The chosen grid resolution.
- Assigned characteristics and properties of large-scale deformation zones.
- Assigned characteristics and properties of small-scale fractures.
- Assigned characteristics and properties of "background" fractures (on a scale too small to be discretised).

DarcyTools calculates the mass flux in kg/s. For a fresh water model this equals the flow in l/s across a surface. In order to derive a Darcy velocity, the mass flux is divided by the surface area and the density of the flowing fluid, an operation that yields results in the unit m/s.

Detailed descriptions of the code concepts, calculation methods, and equations of DarcyTools are documented in /Svensson et al. 2004/.

3.2 Model setup and specifications

This study assessed situations based on simplified geometrical descriptions, took no account of salinity variations, and was based on steady-state simulations. Furthermore, it did not include general assessments of geometrical alternatives, or address uncertainties of side and bottom boundary conditions with one exception (cf Section 3.3.6), or time-step dependences.

Brief descriptions of the geometrical model used and boundary conditions of the model are presented below.

3.2.1 Modelling methodology

The modelling methodology used in this study followed SKB's system approach for hydrogeological modelling /Rhén et al. 2003/, however herein much simplified. This approach divides the geosphere into three types of Hydraulic Domains, representing the Quaternary deposits, or Hydraulic Soil Domain (HSD), the fracture zones (HCD), and the rock mass between the fracture zones (HRD), see Figure 3-1.

This study was conducted in two dimensions, even though such an approach is not necessarily well suited to the representation of fracture systems. Also, the study did not concentrate on a surface hydrology and hence did not include any soil cover (soil domain). The bedrock is in principle assumed to be a homogeneous porous medium with isotropic characteristics. For one sensitivity case, a situation similar to a soil domain on top of a bedrock domain was simulated.

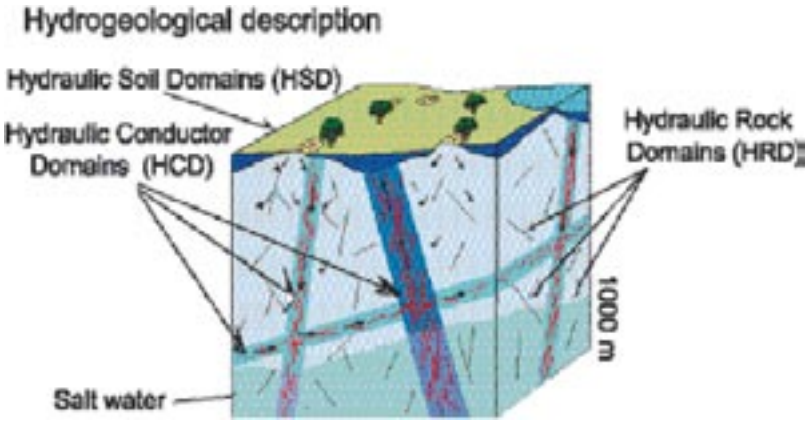

Figure 3-1. *The Quaternary deposits and the crystalline bedrock are divided into separate hydraulic domains named the Hydraulic Soil Domains (HSD), Hydraulic Rock Mass Domains (HRD), and Hydraulic Conductor Domains (HCD). Within each domain, the hydraulic properties are represented by mean values or by spatially distributed statistical distributions. After /Rhén et al. 2003/.*

3.2.2 Climate and surface processes

A fresh water model was adopted, with zero salinity throughout the model domain.

The corrected precipitation in Forsmark for the measurement period August 1 2003 to July 31 2004 was 630 mm. This value indicates a 5–10% higher precipitation rate as compared with the weather station at Örskär (SMHI). The total "potential evapotranspiration" as reported in /Lindborg 2005/ was 472 mm for the same period. This indicates enough water to validate the herein used prescribed pressure boundary at the surface.

The local topography of the SFR region and the high-confidence large-scale deformation zones as defined in the site investigation programme is presented in Figure 3-2.

In the 2D approach adopted, surface processes were mimicked by specified pressure situations. In this process, the underlying hypothesis is that the specified pressures are cautious representations of the most plausible situations in each of the simulated climate domains.

Based on the climate domains described in Chapter 2, a set of the top boundary cases have been established, which have been used as boundary conditions in hydrogeological groundwater flow simulations that have been conducted. For the temperate situation (reference case), the different permafrost situations, and for the situation in front of an ice sheet, the pressure was specified at ground surface. Beneath the ice sheet the pressure was specified using an empirical relationship /Paterson 1994/. This approach has been used in different earlier numerical flow simulations and is believed to over-estimate the impact of an ice sheet /e.g. Chan et al. 2005/.

For detailed descriptions of the surface processes during the different climate variants and their domains see /SKB 2006a/ and Chapter 2.

3.2.3 Boundary conditions

Within a 2D flow model, the most realistic boundary condition at the top is a specified pressure which is what was adopted in this study. Also, all elevations at zero altitudes or lower were specified as sea with a fresh water head of zero.

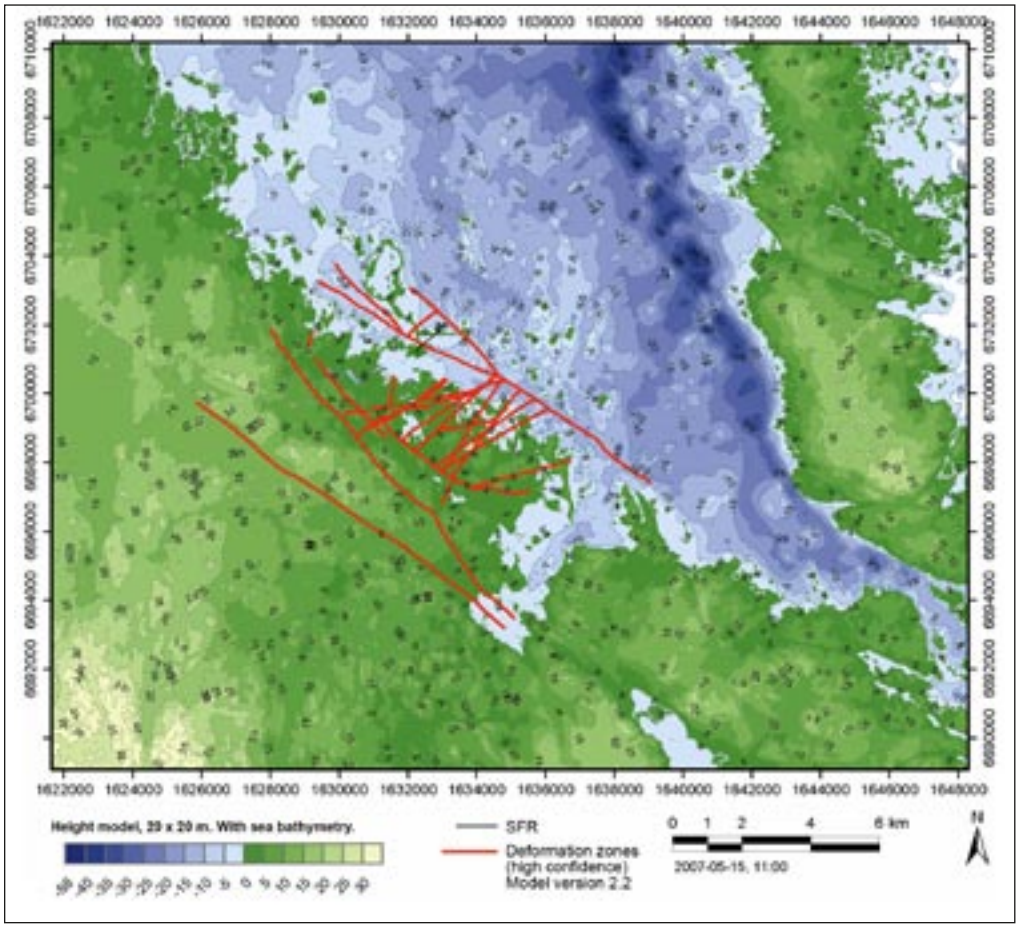

Figure 3-2. *Local topography of the SFR region and the high confidence large-scale deformation zones as defined in the site investigation programme.*

The other specified boundary conditions comprised a no-flow condition on all lateral sides and at the bottom. The lateral side beneath the sea is approximately 10 km from the generic coast line and effects of the no-flow boundaries are small. This was confirmed by sensitivity studies of the specification of this lateral boundary changed into specified head conditions instead of no-flow.

The regional topographical gradient used was taken over a large transect in the easterly – westerly direction.

The top boundary conditions were specified as equal to the local topographic height along the defined transect. However, the topography was created with mathematical tools and was a simplification of the real topography at the site. The regional topographical gradient was specified to be 3 metres per kilometre and was taken from a simple regression of the elevation data in a topographical map of Sweden along a transect of 100 km scale. The simplified local topography fringing the generic coast line resembled information in other numerical groundwater flow studies /e.g. Holmén and Stigsson 2001, Holmén et al. 2003, Holmén and Forsman 2004, Hartley et al. 2006/ (cf Figure 3-2).

As a consequence of the boundary conditions adopted along with the fresh water model used, some flow paths just follows the boundaries, a situation that would not be expected in a more realistic setting. Neither would the groundwater flow penetrate as deeply as herein indicated. This excessive penetration is due to the boundary conditions imposed but would also be prevented in reality because of the presence of deeper saline waters and of depth trends in the hydraulic conductivity (cf Section 3.3.6, Figure 3-31).

More realistic deep flow regimes with associated flow paths have been addressed in regional groundwater flow studies that have incorporated saline water as well as more realistic definitions of the boundary conditions /e.g. Holmén et al. 2003, Hartley et al. 2006/.

3.2.4 Model domain and measurement localities

In order to investigate the differences between, and changes in, mass fluxes in the geosphere four pre-defined measurement volumes were established. Two of these pre-defined volumes were used to represent the SFR in terms of their depth below ground surface. These two volumes, labelled SFR 1 and SFR 2, are located beneath a recharge and a discharge area, respectively. The third and fourth measurement volumes, DEEP 1 and DEEP 2, were located at 500 metres beneath ground surface directly below SFR 1 and SFR 2.

3.2.5 Hydrogeological properties

For the base cases, the hydraulic conductivity was assigned a single homogeneous value.

The assigned hydraulic conductivity of $3 \cdot 10^{-8}$ m/s is based on the value used in Holmén and /Stigsson 2001/. The assigned value is assumed to represent the effective hydraulic conductivity for the bedrock surrounding SFR at a regional scale.

The main factor causing a difference between the regional values and the lower local values is the presence of major fracture zones. Hence a variation of the bedrock characteristics has been tested, in which the measurement volumes (SFR 1 and SFR 2) have been caged-off by three major fracture zones. The DEEP locations coincide with the fracture zone comprising the lower boundary of the hydraulic cage.

The typical contrast, of assigned hydraulic conductivity, between the large scale deformation zones and the rock mass in-between is in the order of 2–5 orders of magnitude.

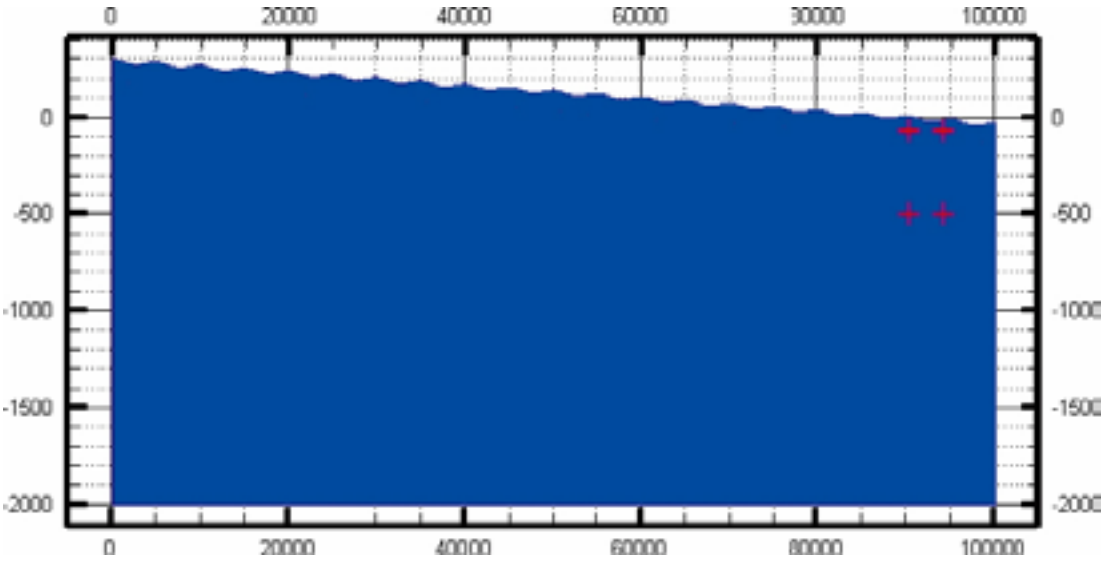

Figure 3-3. *Location of the four pre-defined measurement volumes (SFR 1, SFR 2, DEEP 1, and DEEP 2).*

3.2.6 Case descriptions

Herein the chosen base cases are presented.

Common to all base cases are no-flow boundary conditions on the lateral (side) boundaries and at the bottom.

The model is a fresh water model.

The upper boundary is a spatially distributed specified pressure boundary assessed for the different surface conditions (climate domains).

All simulations are steady-state.

All assigned hydrogeological properties are homogeneous within their specified model domains (see illustration below):

- Unfrozen bedrock [3] (deep bedrock) has a hydraulic conductivity of $3 \cdot 10^{-8}$ m/s.
- Frozen bedrock [2] (permafrost) has a hydraulic conductivity of $3 \cdot 10^{-14}$ m/s.
- An active layer [1], if present, has a hydraulic conductivity of $3 \cdot 10^{-4}$ m/s.

Temperate (reference case, R1)

The assigned generic topography defines the pressure on the top boundary.

A variant of the hydraulic conductivity field has been tested. This includes a hydraulic cage of fracture zones, as illustrated below. The fracture zones each have a width of 20 metres. For the base cases the fracture zones are approximately five orders of magnitude more permeable than the bedrock.

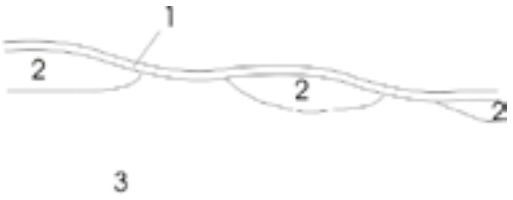

Figure 3-4. *Conceptual illustration of permafrost (2), unfrozen regions and taliks (3), and active layer (1).*

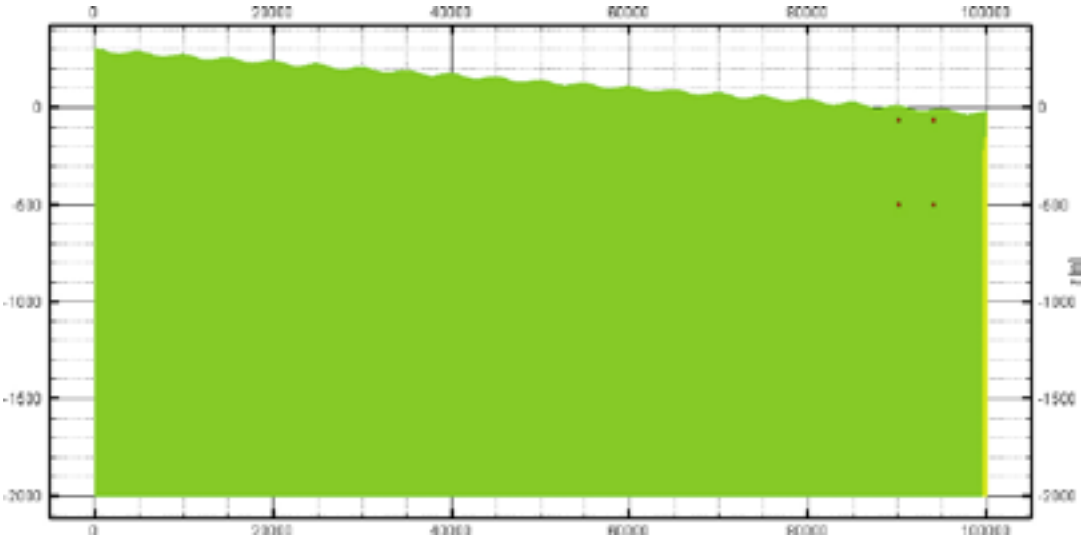

Figure 3-5. *Conceptual framework for the temperate case.*

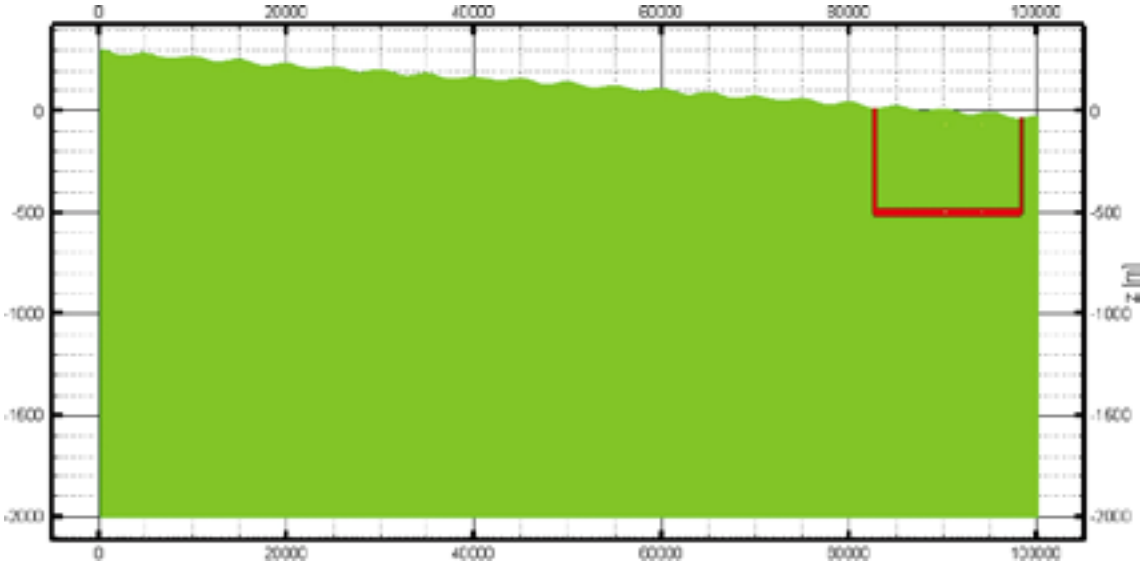

Figure 3-6. *Conceptual framework for the variant temperate case including a caging fracture zone configuration.*

Sporadic permafrost

The sporadic permafrost case is illustrated below. The maximum depth of permafrost is 100 metres. The chosen maximum permafrost depth is used since it is adequate for illustration purposes. The maximum infiltration scenario includes all of the hydraulic conductivity types described above (unfrozen bedrock, frozen bedrock and an active layer). The limited infiltration scenario has no active layer.

As in the temperate case, a variant of the hydraulic conductivity field has been tested in which fracture zones constitute a hydraulic cage.

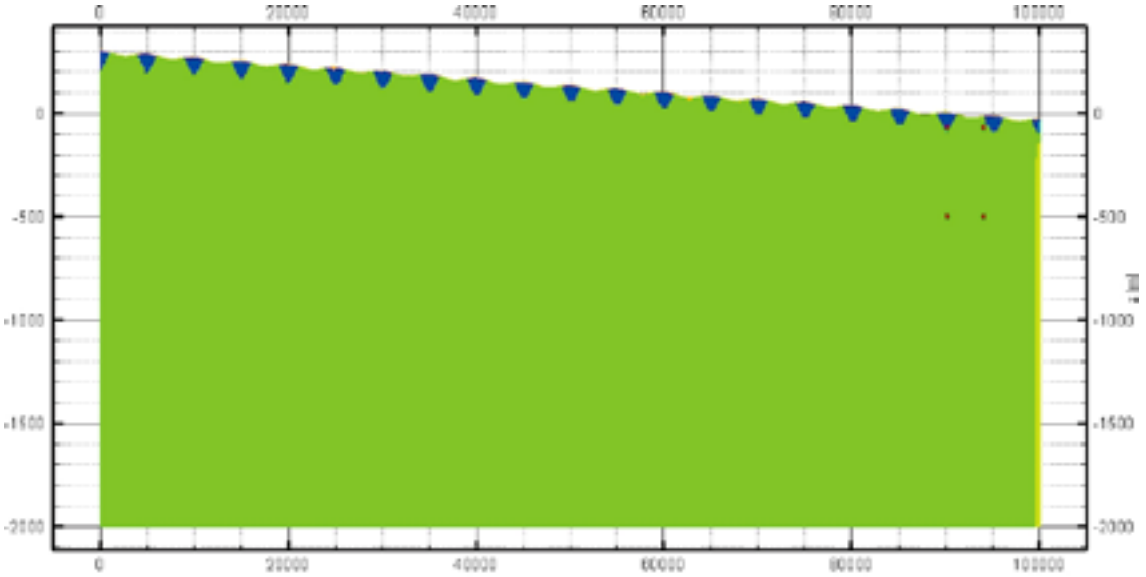

Figure 3-7. *Conceptual framework for the sporadic permafrost case.*

Continuous permafrost with taliks

The continuous permafrost case is illustrated below. The maximum depth of permafrost is 100 metres. The chosen maximum permafrost depth is used since it is adequate for illustration purposes. The maximum infiltration scenario includes all of the hydraulic conductivity types described above (unfrozen bedrock, frozen bedrock and an active layer). The limited infiltration scenario has no active layer. Open taliks are located between the extensive areas of permafrost.

As in the temperate case, a variant of the hydraulic conductivity field has been tested in which fracture zones constitute a hydraulic cage.

Ice sheet

The ice sheet case combines topographically defined pressure beyond the margins of the ice sheet with a pressure beneath the ice sheet defined by an empirical relationship /Paterson 1994/:

$$z_{ice} = 3.4 \cdot \sqrt{x_{margin} - x_{dist}} \,,$$

where z_{ice} is the elevation of the ice sheet and is assumed identical to the required pressure, x_{margin} is the position of the ice margin (from a reference datum), and x_{dist} is the point of interest beneath the ice sheet.

The empirical relationship yields a specified pressure as illustrated below, where the three different ice sheet shapes illustrates three different locations of the ice sheet front.

As in the temperate case, a variant of the hydraulic conductivity field has been tested in which fracture zones constitute a hydraulic cage.

Ice sheet overriding continuous permafrost

This base case combines the two cases.

It includes the hydraulic conductivity characteristics of the continuous permafrost case and the specified pressure of the ice sheet case.

Beneath the ice sheet, at five kilometres or more from the ice margin, the permafrost is assumed to be completely melted. At locations closer to the ice sheet margin the permafrost remains un-melted as in the base case for permafrost.

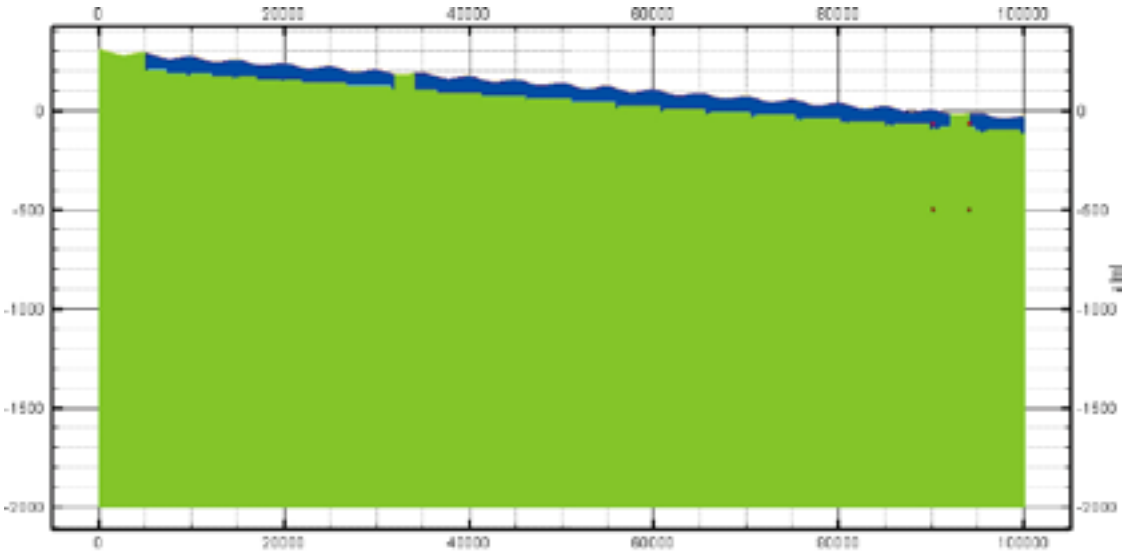

Figure 3-8. *Conceptual framework for the continuous permafrost case incorporating taliks.*

Figure 3-9. *Conceptual illustration of ice sheet (shape) with an ice margin located at three different positions in relation to the conceptual illustration of permafrost.*

3.3 Model results

3.3.1 Temperate

This situation is used as the reference case. Hence, all other base case simulations are compared with these results.

These results are considered to be a representation of the previously modelled situation for present-day conditions /Holmén and Stigsson 2001/. However, the simulations are a simplification in terms of conceptual model as well as flow dimensions and hydrogeological properties. Hence, a comparison with earlier model results is not straightforward.

For simulations of the reference case, the hydraulic conductivity was specified as a homogeneous value of $3 \cdot 10^{-8}$ m/s. The upper boundary has a set pressure at ground surface, which mimics a case of maximum infiltration (groundwater recharge). The regional topographic gradient is 3 metres per kilometre, but applies in combination with a more local gradient created by a sinusoidal surface with a wavelength of 5 kilometres and amplitude of 10 metres. Further, the groundwater throughout the domain is taken to be fresh water.

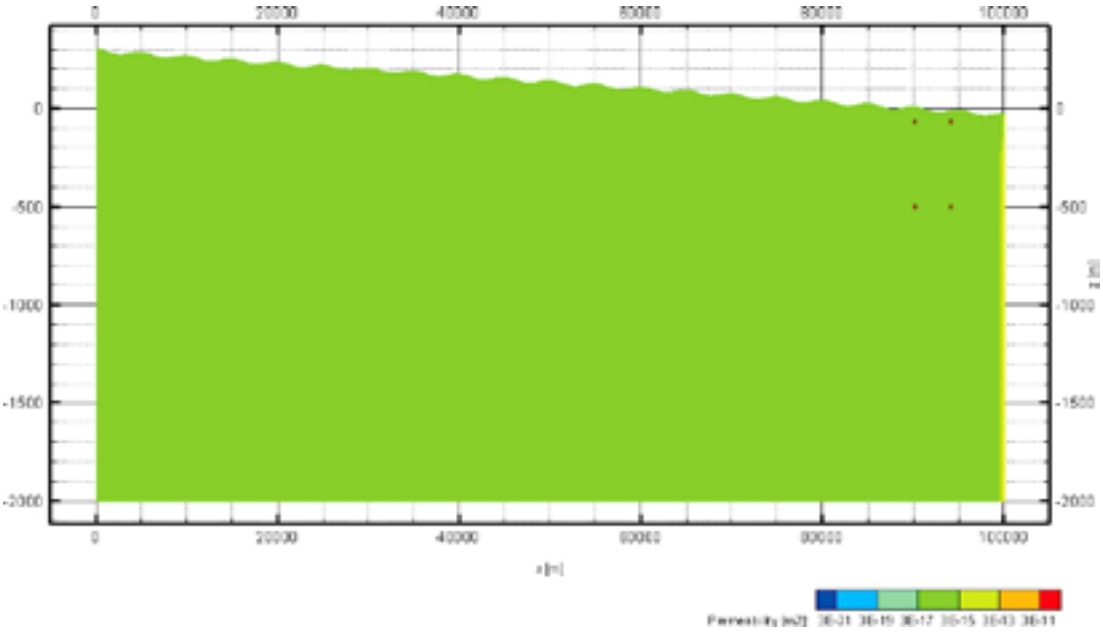

Figure 3-10. *Permeability structure of the reference case.*

Figure 3-11 presents the fresh water head of the steady-state solution of the reference case. The head situation along with the illustrative streamlines indicates the strong influence of the local topographic gradient. However, these results are strongly dependent on the shape of the local topography; for a case with only a regional gradient the flow also is regional with discharge only in the sea. A smaller local topographic variation yields more regional flow as compared with the reference case. These effects also affect the magnitude of the flux and were hence the subject of the sensitivity study presented below.

It should be noted that regions located beneath sea elevation (zero metre altitude) all have a fresh water head of zero independent of where the sea bottom is located.

Table 3-1 presents the mass fluxes through the two pre-defined volumes of principal interest. In the table, three entities are presented: the mass flux through a vertical surface (horizontal flow), the mass flux through a horizontal surface (vertical flow), and the total flux through the pre-defined volume (10 by 100 by 1 m, where the nominal thickness of the 2D model is taken as 1 m). For the flux through the surfaces, information on flow direction is presented, along with the equivalent Darcy velocities.

These results are determined by the properties and boundary conditions used in the simulations. The sensitivity to the upper boundary condition is reported below. The sensitivity to deep bedrock properties was also examined. The results indicate that a change of hydraulic conductivity by one order of magnitude also changes the mass flux by one order of magnitude.

Table 3-1. Mass flux, Darcy velocities, and flow directions for two pre-defined volumes.

	Horizontal surface 10 m²			Vertical surface 100 m²			Total
	Mass flux [kg/s]	Darcy velocity [m/s]	Flow direction	Mass flux [kg/s]	Darcy velocity [m/s]	Flow direction	Mass flux [kg/s]
SFR 1	$1.14 \cdot 10^{-6}$	$1.14 \cdot 10^{-10}$	→	$-1.58 \cdot 10^{-5}$	$1.58 \cdot 10^{-10}$	↓	$1.67 \cdot 10^{-5}$
SFR 2	$3.37 \cdot 10^{-9}$	$3.37 \cdot 10^{-13}$	→	$7.56 \cdot 10^{-7}$	$7.56 \cdot 10^{-12}$	↑	$7.59 \cdot 10^{-7}$

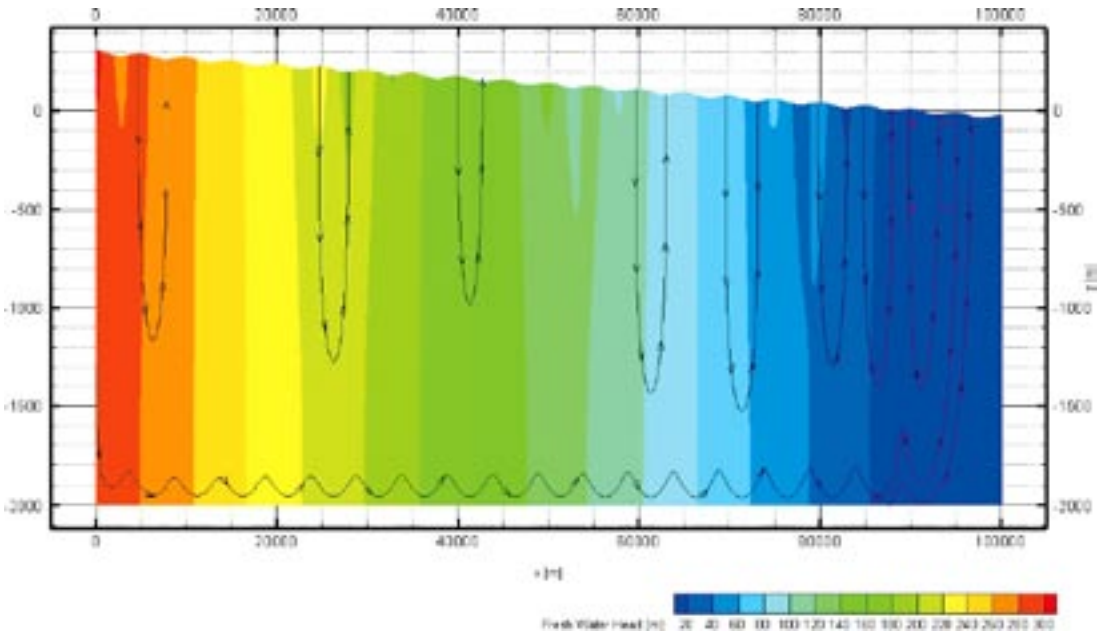

Figure 3-11. *Fresh water heads of the steady-state solution of the reference case.*

Sensitivity to upper boundary

Since this study was designed to support the safety assessment SFR1 SAR-08, it is of interest to evaluate what uncertainties the imposed upper boundary conditions introduce into the results. In order to address this issue, a series of sensitivity studies varying the upper boundary condition was conducted.

The upper boundary is herein a simplified mathematical surface. The regional gradient is expressed as a highest value e.g. 300 metres elevation at X = 0, and a lowest value e.g. –30 metres at X = 100,000 m. The local gradient is expressed using a sinusoidal curve with amplitude of e.g. 10 metres and a wavelength – distance between two peaks – of e.g. 5,000 metres. The reference values used to characterise elevation are those given above.

Figure 3-12 to Figure 3-18 present the fresh water head of the steady-state solution of the reference case (R1) and six sensitivity cases (S1 to S6). The spatial distribution of pressure head values along with the form of the illustrative streamlines indicate the strong influence of both the regional and local topographic gradients.

As a general comment to the illustrations, it is worth noticing that some of the illustrative streamlines that "flow" mainly horizontally show oscillations along their paths. These oscillations are not due to instabilities in the numerical results of DarcyTools; as verified by numerical sensitivity runs. The oscillations could possibly result from instabilities in the post-processing tool within the visualisation programme and the oscillations coincide with regions were the un-structured grid of DarcyTool is significantly changing cell size over a small distance.

Table 3-3 presents the mass flux through a horizontal and through a vertical surface at two pre-defined volumes ($10 \cdot 100 \cdot 1$ m^3). Along with the flux through the surfaces, information on the flow direction is presented along with relative magnitude of mass flux values to those in the reference case (R1). The table presents the sensitivity cases as relative values for each of the investigated volumes. Comparisons are related to the same location, that is SFR1 is always compared with SFR1 and vice versa for SFR2. In order to compare the different locations, values must be normalised via the reference case.

Comparing the reference case (R1) with sensitivity cases (S4) and (S1) indicates that a less pronounced regional topographic gradient yields larger fluxes at a hypothetical repository located in discharge areas. However, such effect is thought to be created by the influence of "shoreline displacement" that induces a groundwater flow from a "small" island to the right of the SFR 2 location; the island "emerges" from the sea for these sensitivity cases but is beneath the sea-level in the reference case. This effect is plausibly much more important than the overall change in regional gradient and general conclusions on the effects of changes in regional gradient are hence difficult to establish.

The effect on mass fluxes beneath recharge areas due to changed regional topographic gradients (decreased) are smaller and can result in smaller mass fluxes.

Comparing the two sensitivity cases (S3) and (S2) indicates that mass fluxes will increase as well as change flow direction at our hypothetical discharge location due to the process of shoreline displacement (land rise). As SFR at the present-day is at a discharge location these results are in agreement with the earlier model results by /Holmén and Stigsson 2001/. This type of process was not intended to be investigated in this study, but it is confidence building that the simplified model set-up adopted captures the same flow characteristics as the more detailed flow model used in the SFR-SAFE assessment.

The sensitivity cases (S5) and (S6) and the reference case (R1) indicate the effect of the local topographic gradient. A decreased local topographic gradient yields smaller mass fluxes in both horizontal and vertical flow directions.

Table 3-2. Definition of top boundary specifications used as sensitivity cases. The information within brackets are as exemplified in the full description "the regional gradient is expressed as a highest value e.g. 300 metres elevation at X = 0, and a lowest value e.g. –30 metres at X = 100,000 metres. The local gradient is expressed using a sinusoidal curve with amplitude of e.g. 10 metres and a wavelength of e.g. 5,000 metres.

	Case description
R1	Regional topography (300, –30), undulating (105,000)
S1	No regional topography, undulating (105,000)
S2	Regional topography (100, –1), no undulation
S3	Regional topography (100, –10), no undulation
S4	Regional topography (100, –10), undulating (105,000)
S5	Regional topography (300, –30), no undulation
S6	Regional topography (300, –30), undulating (55,000)

Table 3-3. Mass fluxes, flow directions, and mass fluxes relative to the reference case (R1). Comparisons are related to the same location that is SFR1 is always compared with SFR1 and vice versa for SFR2. In order to compare the different locations values must be normalised as regard of the reference case.

		Horizontal surface 10 m²			Vertical surface 100 m²		
		Mass flux [kg/s]	Flow direction	Relative [–]	Mass flux [kg/s]	Flow direction	Relative [–]
R1	SFR 1	$1.14 \cdot 10^{-6}$	→	1	$-1.58 \cdot 10^{-5}$	↓	1
	SFR 2	$3.37 \cdot 10^{-9}$	→	1	$7.56 \cdot 10^{-7}$	↑	1
S1	SFR 1	$3.52 \cdot 10^{-7}$	→	0.3	$-1.51 \cdot 10^{-5}$	↓	1.0
	SFR 2	$-1.60 \cdot 10^{-6}$	←	–476.0	$2.09 \cdot 10^{-6}$	↑	2.8
S2	SFR 1	$7.87 \cdot 10^{-7}$	→	0.7	$-3.22 \cdot 10^{-6}$	↓	0.2
	SFR 2	$3.12 \cdot 10^{-7}$	→	92.7	$-2.61 \cdot 10^{-6}$	↓	–3.5
S3	SFR 1	$3.35 \cdot 10^{-7}$	→	0.3	$2.21 \cdot 10^{-6}$	↑	–0.1
	SFR 2	$7.21 \cdot 10^{-10}$	→	0.2	$1.41 \cdot 10^{-7}$	↑	0.2
S4	SFR 1	$6.58 \cdot 10^{-7}$	→	0.6	$-1.53 \cdot 10^{-5}$	↓	1.0
	SFR 2	$-1.02 \cdot 10^{-6}$	←	–303.6	$1.01 \cdot 10^{-5}$	↑	13.3
S5	SFR 1	$5.42 \cdot 10^{-7}$	→	0.5	$2.21 \cdot 10^{-6}$	↑	–0.1
	SFR 2	$1.79 \cdot 10^{-9}$	→	0.5	$3.43 \cdot 10^{-7}$	↑	0.5
S6	SFR 1	$9.10 \cdot 10^{-7}$	→	0.8	$-7.36 \cdot 10^{-6}$	↓	0.5
	SFR 2	$2.68 \cdot 10^{-9}$	→	0.8	$5.45 \cdot 10^{-7}$	↑	0.7

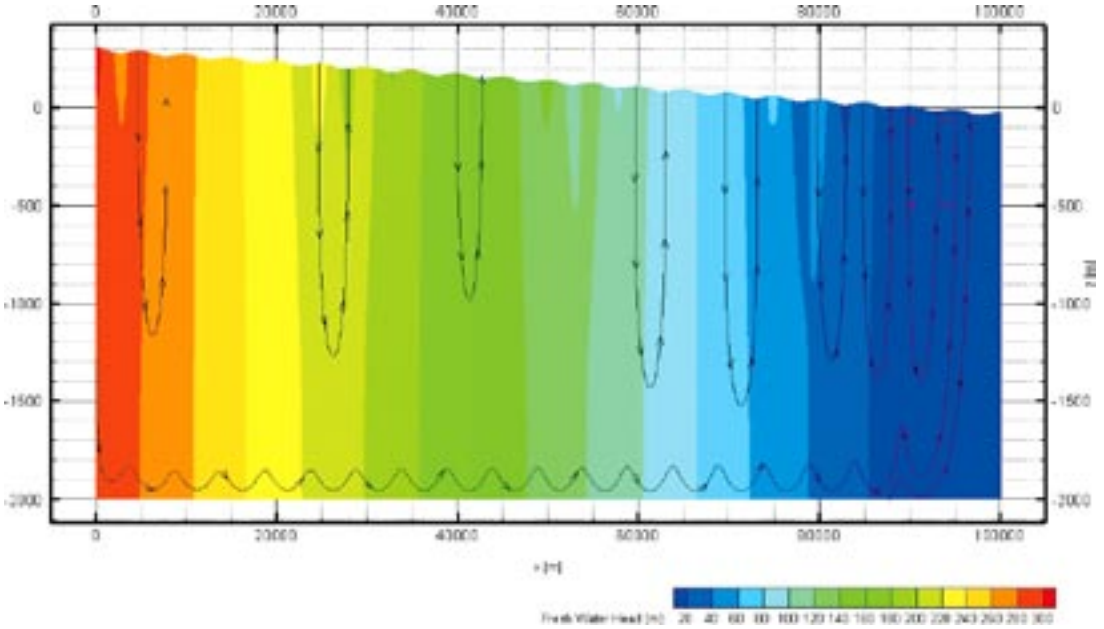

Figure 3-12. *Reference case (R1). The regional topographic gradient is approximately 3 metres per kilometre and local topographic variation is simulated with an undulation with amplitude of ten metres and a wavelength of five kilometres. The hypothetical repository is located beneath an elevation of approximately 0 metres (shoreline). Illustrative streamlines created using the visualisation code show plausible flow paths (same as Figure 3-11).*

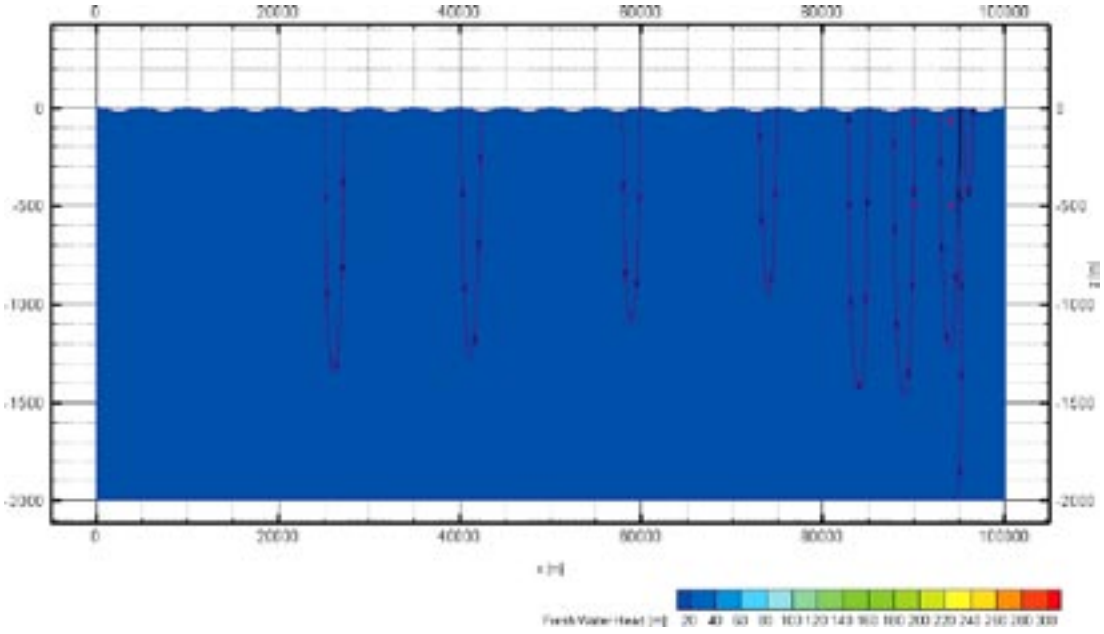

Figure 3-13. *Sensitivity case (S1). The regional topographic gradient is 0 metre per kilometre and local topography is simulated with an undulation with amplitude of ten metres and wavelength of five kilometres. The hypothetical repository is located beneath an elevation of approximately 0 metre (shoreline). Illustrative streamlines created using the visualisation code show plausible flow paths.*

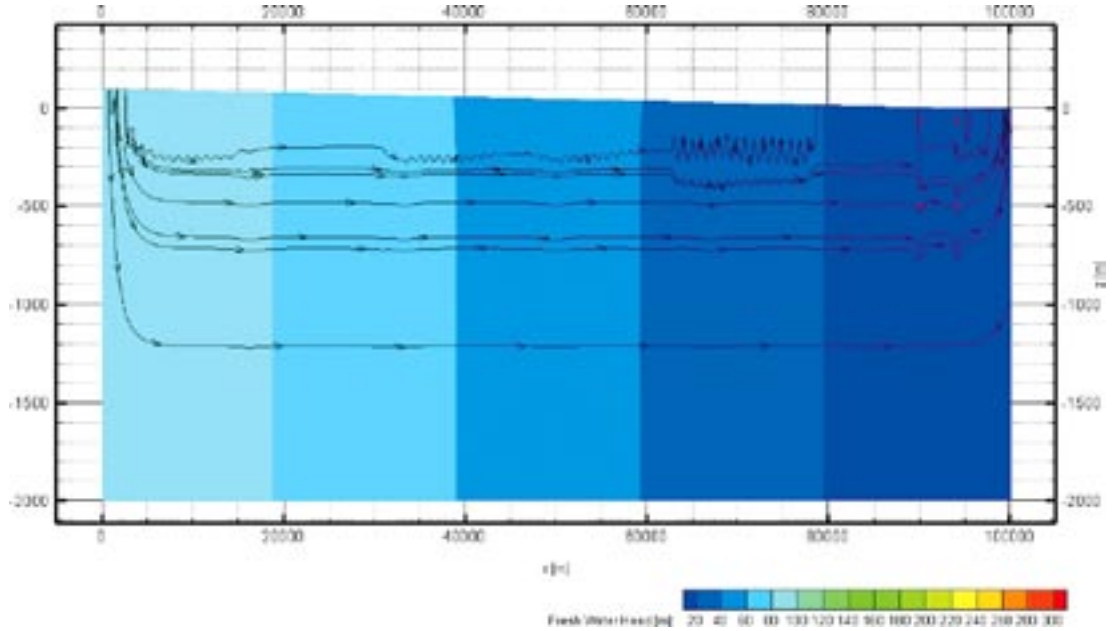

Figure 3-14. *Sensitivity case (S2). The regional topographic gradient is approximately 1 metre per kilometre. The hypothetical repository is located beneath an elevation of approximately 10 metres. Illustrative streamlines created using the visualisation code show plausible flow paths.*

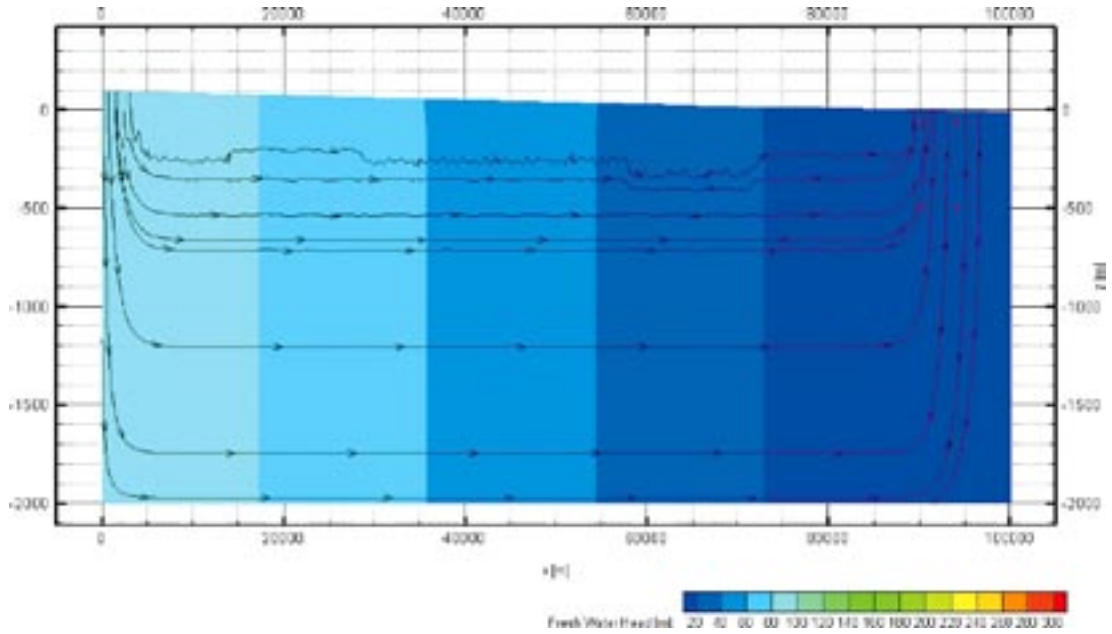

Figure 3-15. *Sensitivity case (S3). The regional topographic gradient is approximately 1 metre per kilometre. The hypothetical repository is located beneath an elevation of approximately 0 metres (shoreline). Illustrative streamlines created using the visualisation code show plausible flow paths.*

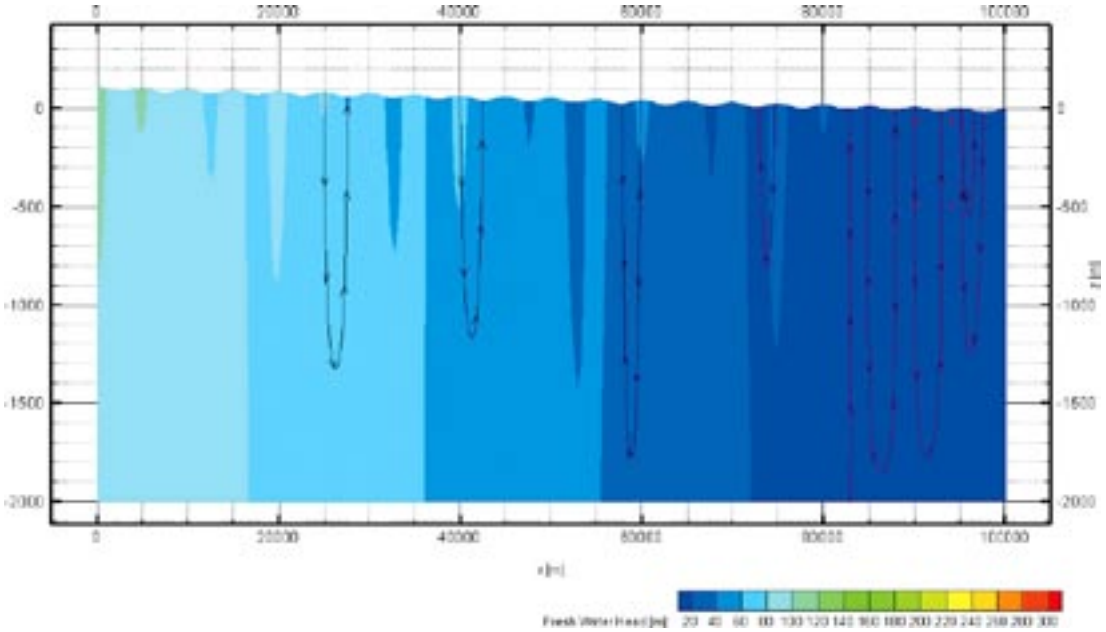

Figure 3-16. *Sensitivity case (S4). The regional topographic gradient is approximately 1 metre per kilometre and the local topography is simulated with an undulation with amplitude ten metres and wavelength of five kilometres. The hypothetical repository is located beneath an elevation of approximately 0 metres (shoreline). Illustrative streamlines created using the visualisation code show plausible flow paths.*

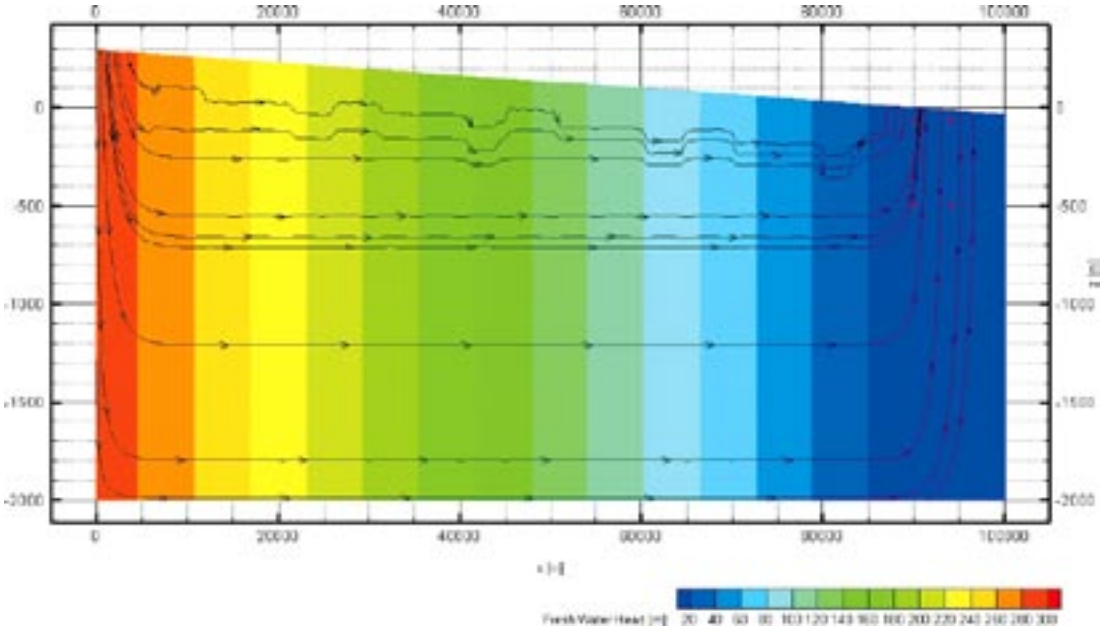

Figure 3-17. *Sensitivity case (S5). The regional topographic gradient is approximately 3 metres per kilometre. The hypothetical repository is located beneath an elevation of approximately 0 metres (shoreline). Illustrative streamlines created using the visualisation code show plausible flow paths.*

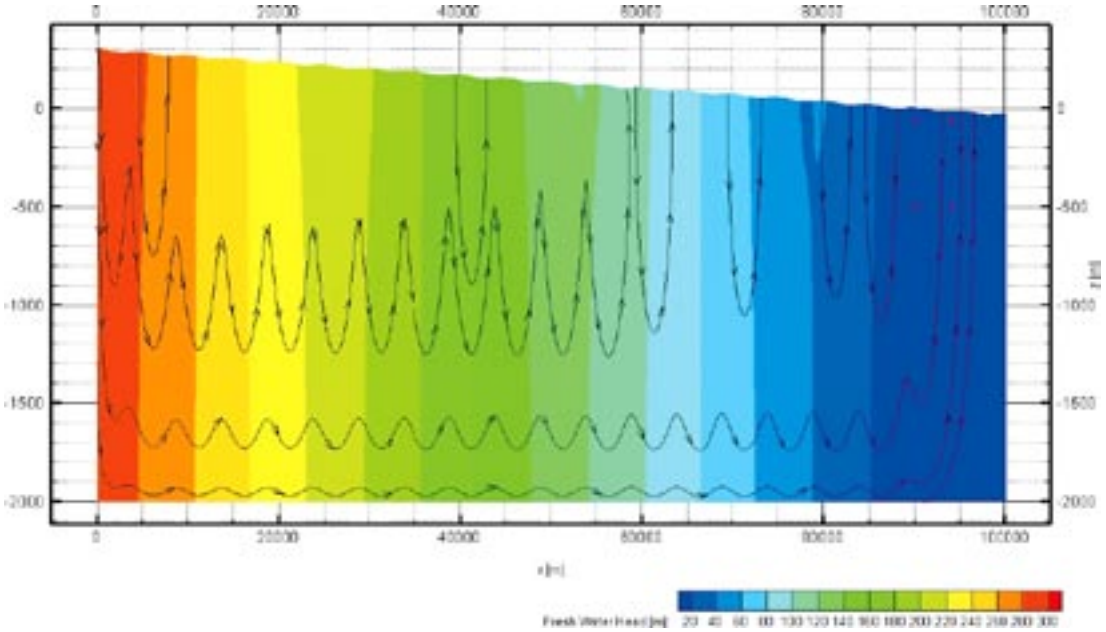

Figure 3-18. *Sensitivity case (S6). The regional topographic gradient is approximately 3 metres per kilometre and a local topography is simulated with an undulation with amplitude of five metres and wavelength of five kilometres. The hypothetical repository is located beneath an elevation of approximately 0 metres (shoreline). Illustrative streamlines created using the visualisation code show plausible flow paths.*

Fracture zone

As a variant, conducted on most simulated cases, a hydraulic cage concept was represented.

In Figure 3-19 the location of a system of highly permeable fracture zones is shown. The simulated fracture zones comprise three individual fracture zones, two vertical structures of twenty metres width and one horizontal also of twenty metres width. The latter fracture zone crosses two of the pre-defined volumes (DEEP 1 and DEEP 2).

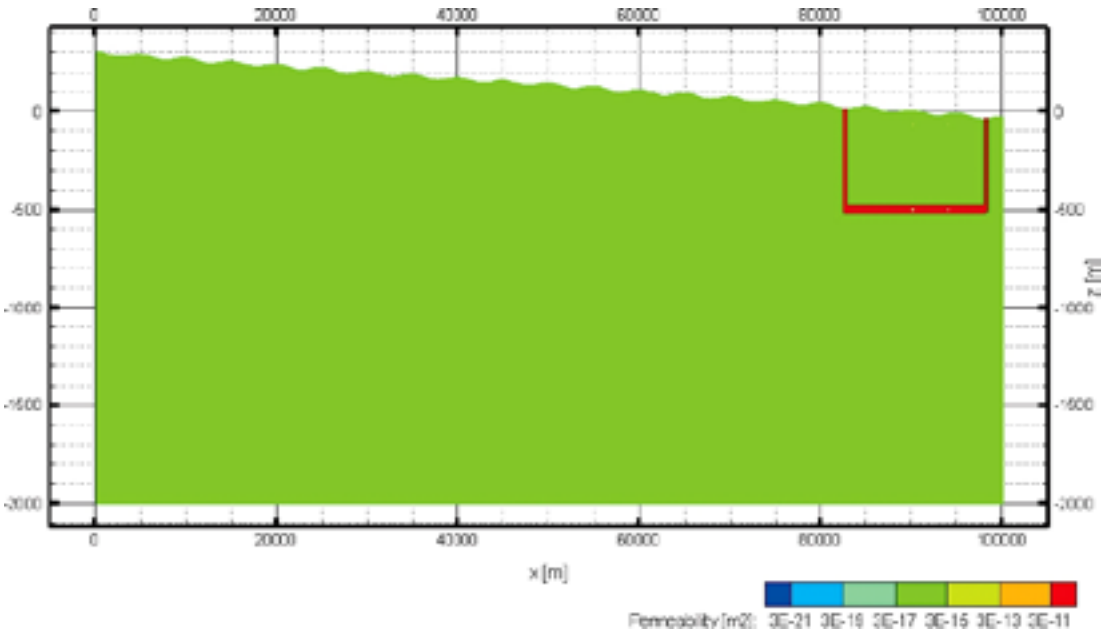

Figure 3-19. *Permeability structure of the reference case including the fracture zones that comprise a hydraulic cage.*

Figure 3-20 presents the fresh water head of the steady-state solution of the reference case with fracture zones present. The head situation, along with the illustrative streamlines, indicates the strong influence of the local topographical gradient as well as capturing the effects of the fracture zones on the flow distribution.

Table 3-4 presents the mass fluxes through all four pre-defined volumes. In the table, two measures are again presented: the mass flux through a vertical surface (horizontal flow) and the mass flux through a horizontal surface (vertical flow). For the fluxes through the surfaces, information on the magnitude of the mass flux values relative to the reference case is presented along with the equivalent Darcy velocities.

The results indicate that the local mass flux is not only dependent on the hydraulic cage effect but to a large degree also on the local topography. For a repository located beneath a local summit, the presence of the fracture zones yields a decrease in mass flux but the opposite result arises in regions of local discharge.

The pre-defined volumes located within the fracture zones experience a large mass flux and both the numerical values of the mass flux as well as the streamlines indicate that the fracture zones pull water into themselves.

Table 3-4. Mass fluxes, Darcy velocities, and mass fluxes relative to the reference case for two pre-defined volumes. The DEEP measurement locations are located within the fracture zones.

	Horizontal surface 10 m²			Vertical surface 100 m²		
	Mass flux [kg/s]	Darcy velocity [m/s]	Relative	Mass flux [kg/s]	Darcy velocity [m/s]	Relative
SFR 1	$5.83 \cdot 10^{-7}$	$5.83 \cdot 10^{-11}$	0.5	$-1.05 \cdot 10^{-5}$	$1.05 \cdot 10^{-10}$	0.7
SFR 2	$1.34 \cdot 10^{-8}$	$1.34 \cdot 10^{-12}$	4.0	$1.10 \cdot 10^{-5}$	$1.10 \cdot 10^{-10}$	14.6
DEEP 1	$4.28 \cdot 10^{-2}$	$4.28 \cdot 10^{-6}$	within FZ	$5.96 \cdot 10^{-3}$	$5.96 \cdot 10^{-8}$	within FZ
DEEP 2	$2.23 \cdot 10^{-2}$	$2.23 \cdot 10^{-6}$	within FZ	$-4.87 \cdot 10^{-3}$	$4.87 \cdot 10^{-8}$	within FZ

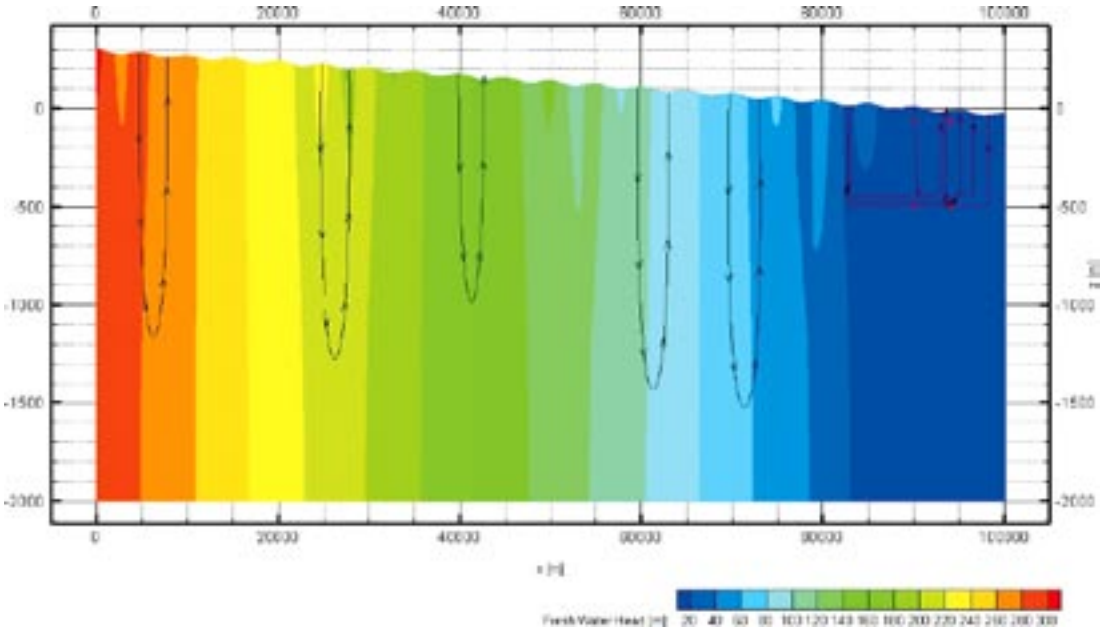

Figure 3-20. *Fresh water heads of the steady-state solution of the reference case including a caging fracture zone system.*

The simulations also indicate the cage effect that the fracture zones have on the flow distribution. Streamlines outside the fracture zones stays outside, whereas flow within the cage is trapped within the local system.

The sensitivity to the chosen hydraulic conductivity contrast between the fracture zone and the deep bedrock was investigated and results are presented in Table 3-5. The results indicate that a contrast of two orders of magnitude produce significant changes in the flux within the caged-off rock volume.

3.3.2 Sporadic permafrost

The situation described as sporadic permafrost has a hydraulic conductivity structure as in Figure 3-21. In the top 3 metres, a highly permeable layer exists connecting over the entire domain. Beneath all of the local summits permafrost prevails down to a maximum depth of 100 metres; all other parts of the model domain have the deep bedrock characteristics of the reference case described above.

Table 3-5. Relative mass fluxes in relation to the reference case for two pre-defined volumes.

Hydraulic conductivity contrast	SFR 1		SFR 2	
More permeable fracture zones	Horizontal Relative	Vertical Relative	Horizontal Relative	Vertical Relative
$1.70 \cdot 10^5$ (same as case in Table 3-4)	0.5	0.7	4.0	14.6
$1.70 \cdot 10^4$	0.5	0.7	4.0	14.0
$1.70 \cdot 10^3$	0.5	0.3	5.8	5.5
$1.70 \cdot 10^2$	0.5	1.1	2.0	3.1
No fracture zones	1	1	1	1

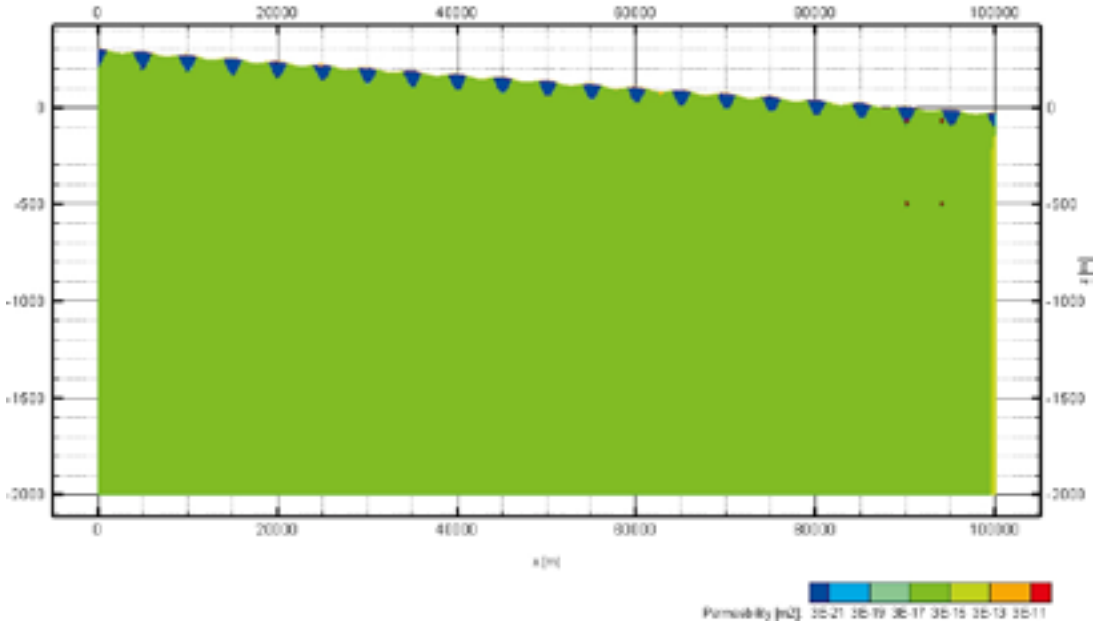

Figure 3-21. Permeability structure of the sporadic permafrost case.

Within the sporadic permafrost case, two variants have been simulated. The first represents a scenario with much available water denoted “maximum infiltration” and the second variant represents a dryer scenario with less available water denoted “limited infiltration”.

Maximum infiltration scenario

Figure 3-22 presents the fresh water head of the steady-state solution of the maximum infiltration case of sporadic permafrost. The head situation along with the illustrative streamlines indicates the strong influence of the local topographic gradient. However, since much of the recharge area on the summits is frozen, the local topography driven flow is not as deep and it seems that the regional flow may be more important in the case of occurrence of sporadic permafrost.

Table 3-6 presents the mass fluxes through the two pre-defined volumes of principal interest and related quantities, as described previously.

Table 3-6. Mass fluxes, Darcy velocities, and mass fluxes relative to the reference case for two pre-defined volumes. A negative value in the relative column indicates a changed flow direction.

	Horizontal surface 10 m²			Vertical surface 100 m²		
	Mass flux [kg/s]	Darcy velocity [m/s]	Relative	Mass flux [kg/s]	Darcy velocity [m/s]	Relative
SFR 1	No flux	No flow	frozen	No flux	No flow	frozen
SFR 2	$-2.50 \cdot 10^{-8}$	$2.5 \cdot 10^{-12}$	–7.41	$1.01 \cdot 10^{-7}$	$1.01 \cdot 10^{-11}$	0.1

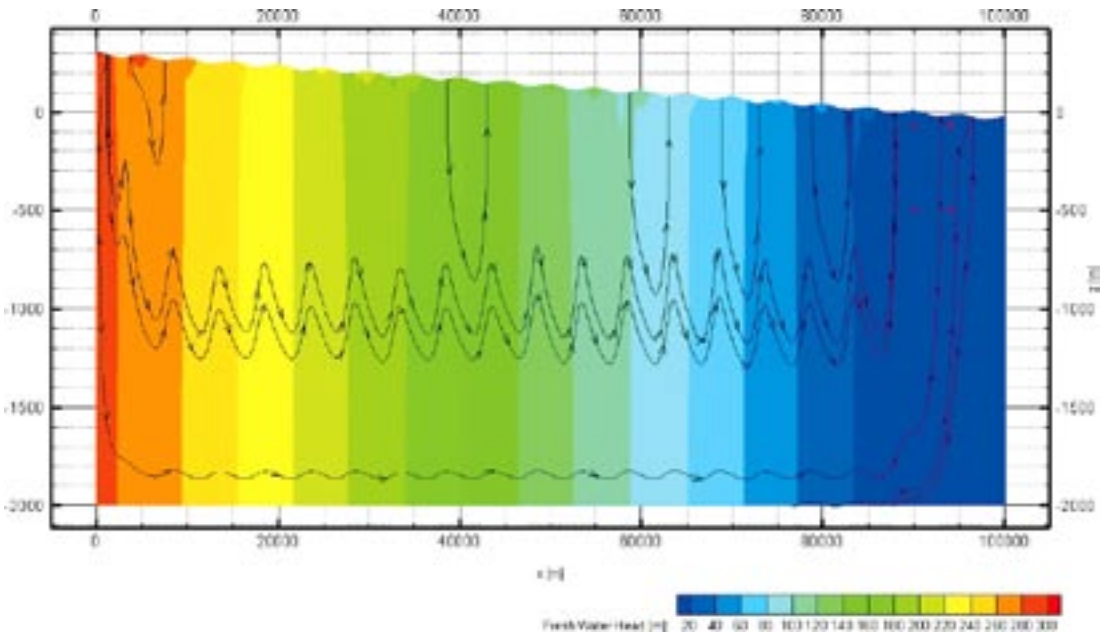

Figure 3-22. *Fresh water heads of the steady state solution of the sporadic permafrost case.*

The increase and change of flow direction for horizontal flow at SFR 2 is plausible due to a re-direction of flow along the bottom of the permafrost in association with a concentration of flow within the talik.

However, these results are strongly dependent on the shape of the local topography. This factor also affects the magnitude of the flux and are hence was the subject of a sensitivity study. Table 3-7 presents the results from this sensitivity study on different topographical settings for the case of sporadic permafrost.

The sensitivity of the results obtained to deep bedrock properties was also tested. The results indicate that a change of hydraulic conductivity by one order of magnitude also changes the mass flux by one order of magnitude.

The sensitivity to the hydraulic conductivity assumed for the frozen rock has been investigated. The results are presented in Table 3-8.

Table 3-7. Sensitivity to different regional and local topographical settings. Relative mass fluxes in relation to the base case of sporadic permafrost for one pre-defined volume. A negative value in the relative column indicates a changed flow direction as compared with the reference case. SFR 1 is frozen. For explanations of values see Section 3.3.1, Sensitivity to upper boundary.

		Horizontal Relative [–]	Vertical Relative [–]
No regional topography, undulating (105,000)	SFR 2	–0.7	–4.3
Regional topography (100, –1), no undulation	SFR 2	–8.5	–3.5
Regional topography (100, –10), no undulation	SFR 2	0.7	0.7
Regional topography (100, –10), undulating (105,000)	SFR 2	0.5	0.2
Regional topography (300, –30), no undulation	SFR 2	1.7	1.8
Regional topography (300, –30), undulating (55,000)	SFR 2	1.3	1.4
Regional topography (300, –30), undulating (105,000) *	SFR 2	1	1

* Base case for sporadic permafrost.

Table 3-8. Test of sensitivity to the chosen hydraulic conductivity on the frozen rock.

	SFR 1				SFR 2			
Frozen rock hydraulic conductivity	Horizontal mass flux	Relative	Vertical mass flux	Relative	Horizontal mass flux	Relative	Vertical mass flux	Relative
$3.00 \cdot 10^{-14}$ *	No flux	frozen	No flux	frozen	$-2.50 \cdot 10^{-8}$	–7.9	$1.01 \cdot 10^{-7}$	0.1
$3.00 \cdot 10^{-11}$	$3.13 \cdot 10^{-8}$	0.03	$-3.24 \cdot 10^{-8}$	$2 \cdot 10^{-3}$	$-2.51 \cdot 10^{-8}$	–8.0	$9.92 \cdot 10^{-8}$	0.1
$3.00 \cdot 10^{-9}$	$2.93 \cdot 10^{-7}$	0.3	$-7.78 \cdot 10^{-6}$	0.5	$-2.01 \cdot 10^{-8}$	–6.4	$4.98 \cdot 10^{-7}$	0.7
$3.00 \cdot 10^{-8}$ **	$1.14 \cdot 10^{-6}$	1	$-1.59 \cdot 10^{-5}$	1	$3.15 \cdot 10^{-9}$	1	$7.53 \cdot 10^{-7}$	1

* Base case for sporadic permafrost.

** No permafrost within the bedrock, equivalent to a case of soil on top of unfrozen bedrock.

Fracture zone

As a variant, conducted on most simulated cases, a hydraulic cage concept was studied.

Table 3-9 presents the mass fluxes through the two pre-defined volumes of principal interest and related quantities.

This situation results in a large increase in flow at the SFR 2 location and it seems that the fracture zones enhance the effect of the re-direction and flow concentration. The result was rather unexpected and further investigation may be needed in order to understand the effect.

Limited infiltration scenario

The method used to simulate reduced infiltration (less available water) was to decrease the hydraulic conductivity of the surface layer (remove the active layer). As a comparison, the specified boundary pressure was lowered by 2 metres of fresh water head. For the case of sporadic permafrost, neither of these methods produced a significant change in the mass flux through the two pre-defined volumes of principal interest.

In order to test whether and when a change in the surface layer hydraulic conductivity would affect the mass flux in the SFR 2 location, a sensitivity study with altered hydraulic conductivity values was undertaken. Table 3-10 indicates that for the base case of sporadic permafrost the hydraulic conductivity of the surface layer needs to be less than that of the deeper bedrock in order for a significant change in mass flux to occur. Also, even in these cases, only the discharge area is affected.

Table 3-9. Mass fluxes, Darcy velocities, and mass fluxes relative to the base case of sporadic permafrost for two pre-defined volumes.

	Horizontal surface 10 m²			Vertical surface 100 m²		
	Mass flux [kg/s]	Darcy velocity [m/s]	Relative	Mass flux [kg/s]	Darcy velocity [m/s]	Relative
SFR 1	No flux	No flow	frozen	No flux	No flow	frozen
SFR 2	$-5.50 \cdot 10^{-7}$	$5.5 \cdot 10^{-11}$	22	$2.56 \cdot 10^{-6}$	$2.56 \cdot 10^{-11}$	2

Table 3-10. Test of sensitivity to the hydraulic conductivity of the surface layer. Mass fluxes are relative to the base case of sporadic permafrost. SFR 1 is frozen.

Active layer hydralic conductivity	SFR 2 Horizontal Relative	Vertical Relative
$3 \cdot 10^{-4}$ *	1	1
$3 \cdot 10^{-5}$	1.0	1.0
$3 \cdot 10^{-6}$	1.0	1.0
$3 \cdot 10^{-7}$	1.0	1.0
$3 \cdot 10^{-8}$	1.0	1.0
$3 \cdot 10^{-9}$	0.9	0.9
$3 \cdot 10^{-10}$	0.7	0.8

* Base case for sporadic permafrost.

3.3.3 Continuous permafrost with taliks

The situation considered as continuous permafrost has a hydraulic conductivity structure as in Figure 3-23. In the top 3 metres, a highly permeable layer exists that is connected over the entire domain. Beneath this layer, large areas of continuous permafrost exist. The permafrost prevails down to a depth of 100 metres and is continuous across both topographic highs and lows. However, at three specified locations open taliks exist that connect the deep bedrock with the surface layer The SFR 1 measurement volume is located within the permafrost, whereas the SFR 2 measurement volume is located on the down-gradient side of the open talik. The hydraulic conductivity in all other parts of the model domain has the deep bedrock characteristics from the reference case described above.

As for the sporadic permafrost case, two variants were simulated for the continuous permafrost case. The first represents a scenario with much available water denoted “maximum infiltration” and the second variant represents a dryer scenario with less available water denoted “limited infiltration”.

Maximum infiltration scenario

Figure 3-24 presents the fresh water head of the steady-state solution of the maximum infiltration case for continuous permafrost. The head situation along with the illustrative streamlines indicates the strong influence of the open taliks and of the regional topographical gradient. The flow is from one open talik toward the next, downstream, open talik. The results further indicate that a talik located along the regional gradient acts as a discharge location but also, at the same time, recharges water into the system.

Table 3-11 presents the mass fluxes through the two pre-defined volumes of principal interest and related quantities.

The increase and change of flow direction for horizontal flow at SFR 2 is plausible. It arises from a re-direction of flow along the bottom of the permafrost in association with a concentration of flow within the talik.

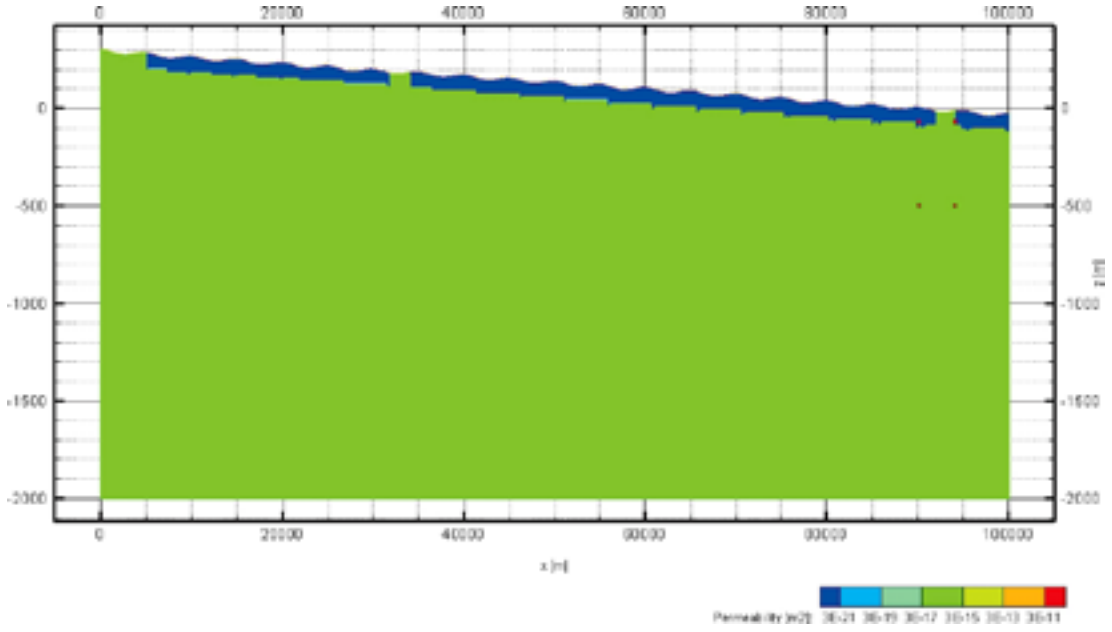

Figure 3-23. *Permeability structure of the continuous permafrost case.*

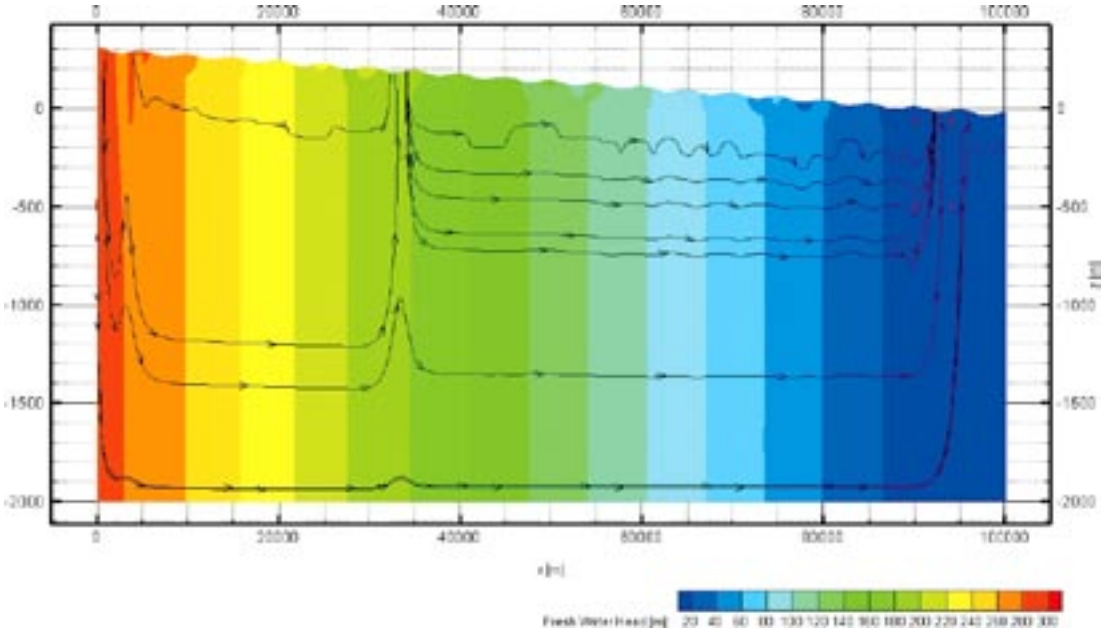

Figure 3-24. *Fresh water heads of the steady-state solution for the continuous permafrost case.*

Table 3-11. Mass fluxes, Darcy velocities, and mass fluxes relative to the reference case for two pre-defined volumes. A negative value in the relative column indicates a changed flow direction.

	Horizontal surface 10 m²			Vertical surface 100 m²		
	Mass flux [kg/s]	Darcy velocity [m/s]	Relative	Mass flux [kg/s]	Darcy velocity [m/s]	Relative
SFR 1	No flux	No flow	frozen	No flux	No flow	frozen
SFR 2	$-1.57 \cdot 10^{-8}$	$1.57 \cdot 10^{-12}$	–4.7	$2.90 \cdot 10^{-6}$	$2.90 \cdot 10^{-11}$	3.8

However, these results are dependent on both the regional and local topography. These factors affect both the flow direction and magnitude of the fluxes. A sensitivity study was conducted to investigate these factors and results are presented in Table 3-12.

Further as indicated by the illustrative streamlines, the results are dependent on the siting of the hypothetical repository within the open talik. This effect has been investigated by choosing three additional locations of SFR 2 within the open talik. The location in the reference case is on the down-stream side relative to the regional topographic gradient, but not as low as possible within the local topography. The three additional locations are: one located on the up-stream side relative to the regional gradient; one located beneath the lowest elevation within the talik, and one in-between the latter and the reference location (see Figure 3-25).

The total flow through a SFR 2 volume was found to be largest on the up-stream side, with values that exceeded the reference case total flow by a factor 8. The smallest increase found was by a factor 3, on the down-stream side.

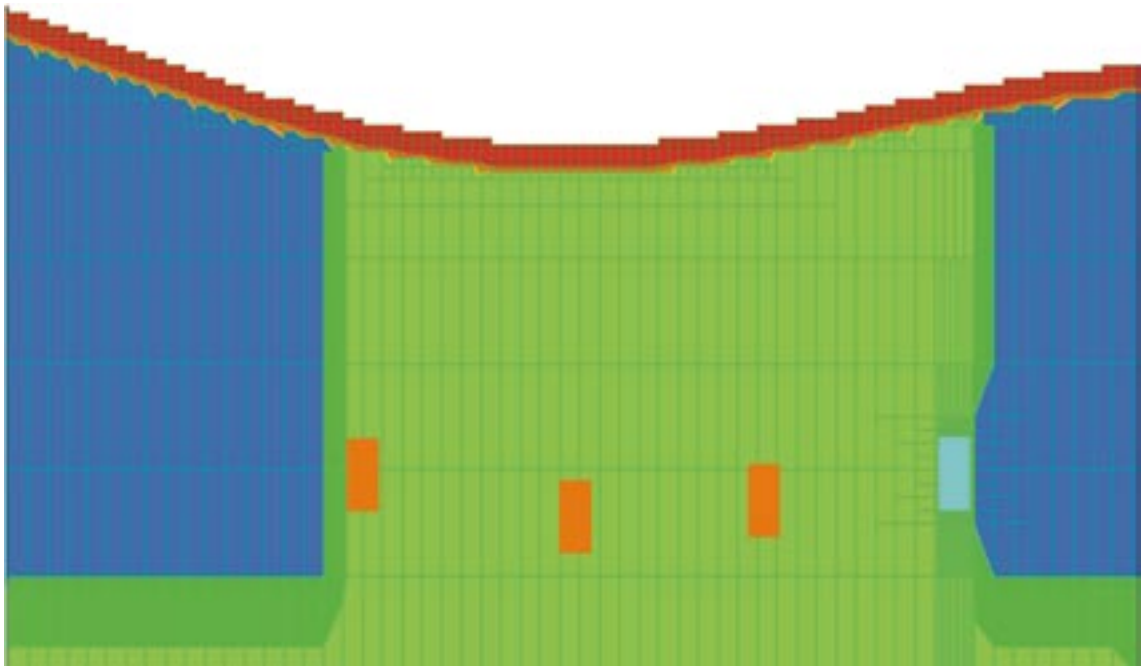

Figure 3-25. *Illustration of tested locations of SFR 2 within the open talik. The three orange coloured blocks illustrate the alternative locations tested.*

Table 3-12. Sensitivity to different regional and local topographical settings. Relative mass fluxes in relation to the base case of continuous permafrost for one pre-defined volume. A negative value in the relative column indicates a changed flow direction as compared with the base case of continuous permafrost. SFR 1 is frozen. For explanations of values see Section 3.3.1, Sensitivity to upper boundary.

		Horizontal Relative [–]	Vertical Relative [–]
No regional topography, undulating (105,000)	SFR 2	3.2	–4.1
Regional topography (100, –1), no undulation	SFR 2	–4.0	–0.7
Regional topography (100, –10), no undulation	SFR 2	0.3	0.3
Regional topography (100, –10), undulating (105,000)	SFR 2	0.6	0.6
Regional topography (300, –30), no undulation	SFR 2	1.0	1.0
Regional topography (300, –30), undulating (55,000)	SFR 2	1.0	1.0
Regional topography (300, –30), undulating (105,000) *	SFR 2	1	1

* Base case of continuous permafrost.

Sensitivity to the chosen upper boundary

The sensitivity to the chosen representation of frozen rock was tested by specifying all permafrost parts as no-flow cells. That is these cells became non-active during the simulations.

This alternative methodology did not affect the calculated values of mass flux for the chosen measurement volumes.

Fracture zone

As a variant on most of the simulated cases, a hydraulic cage concept was adopted.

Table 3-13 presents the mass fluxes through the two pre-defined volumes of principal interest.

This situation creates an increase in flow at the SFR 2 location. However, the effect of the fracture zones does not enhance the effect of the re-direction and flow concentration as much as in other cases in which the effects of a hydraulic cage were studied. As in the sporadic permafrost case discussed above, this increase in flow was un-expected and further investigation is needed in order to understand the effect.

Limited infiltration scenario

The method used to simulate less infiltration (less available water) was to decrease the hydraulic conductivity of the surface (removed active layer). As an alternative approach, the specified pressure was lowered by 2 metres of fresh water head. For the case of continuous permafrost, the latter method produced no significant change in the mass flux through the pre-defined volumes. However, the former method produced some changes, as discussed below.

Table 3-14 presents the results of the limited infiltration scenario for the approach based on a decreased hydraulic conductivity of the surface layer. These results indicate that a limited infiltration variant of continuous permafrost gives mass fluxes somewhat lower than those in the reference case.

Table 3-13. Mass fluxes, Darcy velocities, and mass fluxes relative to the base case of continuous permafrost for two pre-defined volumes (effected by a hydraulic cage). A negative value in the relative column indicates a changed flow direction.

	Horizontal surface 10 m²			Vertical surface 100 m²		
	Mass flux [kg/s]	Darcy velocity [m/s]	Relative	Mass flux [kg/s]	Darcy velocity [m/s]	Relative
SFR 1	No flux	No flow	frozen	No flux	No flow	frozen
SFR 2	$-8.4\cdot10^{-8}$	$8.42\cdot10^{-12}$	5.5	$1.7\cdot10^{-5}$	$1.7\cdot10^{-10}$	6

Table 3-14. Mass fluxes, Darcy velocities, and mass fluxes relative to the base case of continuous permafrost for two pre-defined volumes for the limited infiltration scenario. A negative value in the relative column indicates a changed flow direction.

	Horizontal surface 10 m²			Vertical surface 100 m²		
	Mass flux [kg/s]	Darcy velocity [m/s]	Relative	Mass flux [kg/s]	Darcy velocity [m/s]	Relative
SFR 1	No flux	No flow	frozen	No flux	No flow	frozen
SFR 2	$-1.6\cdot10^{-9}$	$1.6\cdot10^{-13}$	0.1	$2.9\cdot10^{-7}$	$2.9\cdot10^{-12}$	0.1

3.3.4 Ice sheet

For simulations of the ice sheet case, the hydraulic conductivity values were as specified for the reference case.

The regional topographical gradient is 3 metres per kilometre superimposed on a more local gradient created by a sinusoidal surface with a wavelength of 5 kilometres and amplitude of 10 metres. The ice sheet overlies this topography.

Figure 3-26 to Figure 3-28 present the fresh water head of the steady-state solution of the ice sheet case. In Figure 3-26, the ice sheet margin is at X = 41,000 metres and is still far from the pre-defined volumes. The illustrative streamlines indicate the strong influence of the ice sheet and also how rapidly beyond the front of the ice sheet this effect disappears. In Table 3-15, the situation presented in Figure 3-26 is denoted "X = 41,000 metres" and there is no significant change of the mass fluxes as compared with the reference case.

Figure 3-27 and Figure 3-28 present the situation when the front is at X = 92,000 metres and X = 98,000 metres, respectively. In the first of these two situations, the SFR 1 volume is overridden but the SFR 2 volume is still beyond the margin of the ice sheet. In the situation presented in Figure 3-28 all pre-defined volumes have been over-ridden by the ice. Table 3-15 presents the mass fluxes through two pre-defined volumes and associated quantities.

The extreme values are primarily the horizontal fluxes when the ice sheet has extended beyond SFR 1 and SFR 2. For the location SFR 2, the temperate simulation results in very little horizontal flow. However, beneath the ice sheet "only" horizontal flow towards the ice sheet margin is possible. Hence the extreme increase for these values.

Table 3-15. Mass fluxes, Darcy velocities, and flows for two pre-defined volumes for different locations of the ice sheet front.

		Horizontal surface 10 m²			Vertical surface 100 m²		
		Mass flux [kg/s]	Darcy velocity [m/s]	Flow direction	Mass flux [kg/s]	Darcy velocity [m/s]	Flow direction
X = 41,000 metres	SFR 1	$1.1 \cdot 10^{-6}$	$1.1 \cdot 10^{-10}$	→	$-1.6 \cdot 10^{-5}$	$-1.6 \cdot 10^{-10}$	↓
	SFR 2	$3.4 \cdot 10^{-9}$	$3.4 \cdot 10^{-13}$	→	$7.5 \cdot 10^{-7}$	$7.5 \cdot 10^{-12}$	↑
X = 92,000 metres	SFR 1	$9.9 \cdot 10^{-6}$	$9.9 \cdot 10^{-10}$	→	$-3.1 \cdot 10^{-5}$	$-3.1 \cdot 10^{-10}$	↓
	SFR 2	$8.4 \cdot 10^{-8}$	$8.4 \cdot 10^{-12}$	→	$1.8 \cdot 10^{-5}$	$1.8 \cdot 10^{-10}$	↑
X = 98,000 metres	SFR 1	$4.7 \cdot 10^{-6}$	$4.7 \cdot 10^{-10}$	→	$-5.5 \cdot 10^{-6}$	$-5.5 \cdot 10^{-11}$	↓
	SFR 2	$4.2 \cdot 10^{-6}$	$4.2 \cdot 10^{-10}$	→	$-1.2 \cdot 10^{-5}$	$-1.2 \cdot 10^{-10}$	↓

Table 3-16. Mass fluxes relative to the reference case for two pre-defined volumes for different locations of the ice sheet front.

		Horizontal Relative	Vertical Relative
X = 41,000 metres	SFR 1	1.0	1.0
	SFR 2	1.0	1.0
X = 92,000 metres	SFR 1	8.6	2.0
	SFR 2	25.1	24.2
X = 98,000 metres	SFR 1	4.1	0.3
	SFR 2	1,248.1	–15.2

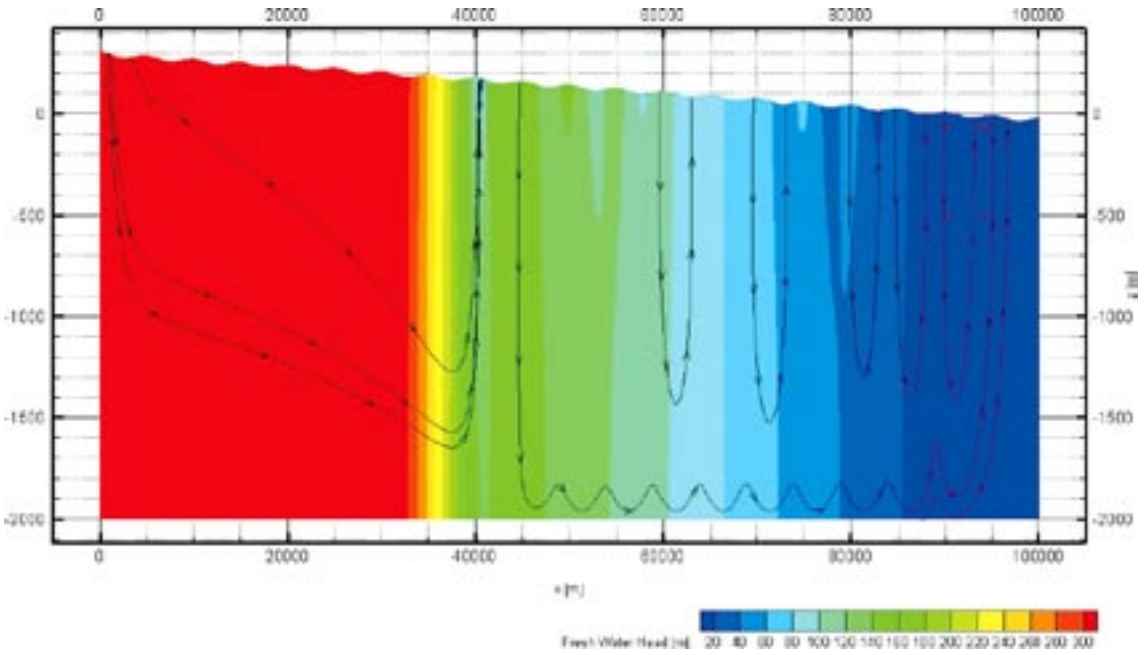

Figure 3-26. *Fresh water heads of the steady-state solution for the case of an ice sheet with its front at X = 41,000 metres.*

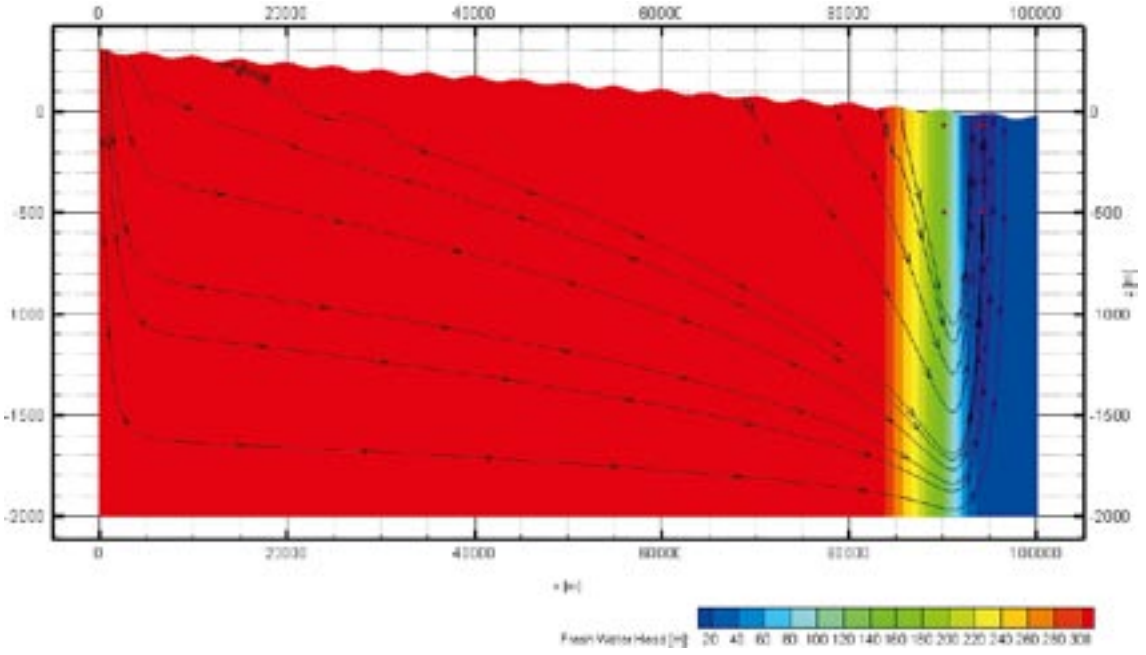

Figure 3-27. *Fresh water heads of the steady state solution for the case of an ice sheet with its front at X = 92,000 metres.*

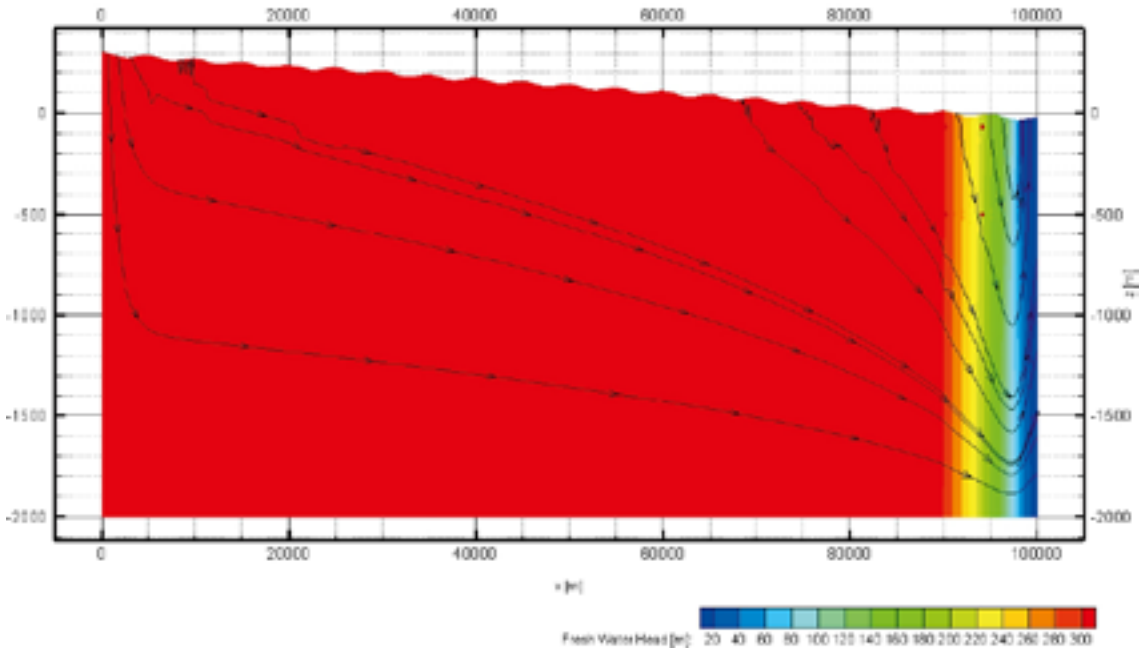

Figure 3-28. *Fresh water heads of the steady state solution for the case of an ice sheet with its front at X = 98,000 metres. The results are not significantly affected by the chosen down-stream boundary condition beneath the sea (cf Section 3.3.6).*

The development of the horizontal and vertical mass flux when the ice sheet margin passes over the area was investigated through a series of "snapshots". Table 3-17 presents the mass flux values along with values relative to the distant ice sheet situation (X = 41,000 metres) for the two pre-defined SFR measurement volumes. The maximum values for the SFR 2 volume are encountered when the ice front is receding and is located immediately above the test volume. Thus, the magnitude of the total mass flux for this position, with X = 94,000 metres is 183 times the mass flux in the reference case.

Table 3-17. Test of sensitivity to the ice sheet location. Values relative to those with the ice sheet front at the 41,000 metres position.

	SFR 1				SFR 2			
Ice sheet location	Horizontal mass flux	Relative	Vertical mass flux	Relative	Horizontal mass flux	Relative	Vertical mass flux	Relative
41,000	$1.1 \cdot 10^{-6}$		$-1.6 \cdot 10^{-5}$		$3.4 \cdot 10^{-9}$		$7.5 \cdot 10^{-7}$	
89,000	$1.8 \cdot 10^{-6}$	1.6	$2.3 \cdot 10^{-5}$	–1.4	$1.0 \cdot 0^{-8}$	3.0	$2.4 \cdot 10^{-6}$	3.1
90,000	$7.0 \cdot 10^{-6}$	6.2	$1.7 \cdot 10^{-4}$	–10.9	$1.8 \cdot 10^{-8}$	5.3	$4.1 \cdot 10^{-6}$	5.5
91,000	$1.4 \cdot 10^{-5}$	12.7	$-4.7 \cdot 10^{-5}$	2.9	$3.6 \cdot 10^{-8}$	10.6	$8.2 \cdot 10^{-6}$	10.8
92,000	$9.9 \cdot 10^{-6}$	8.6	$-3.1 \cdot 10^{-5}$	2.0	$8.4 \cdot 10^{-8}$	25.2	$1.8 \cdot 10^{-5}$	24.3
93,000	$7.9 \cdot 10^{-6}$	6.9	$-2.2 \cdot 10^{-5}$	1.4	$2.9 \cdot 10^{-7}$	87.7	$4.7 \cdot 10^{-5}$	62.5
94,000	$6.8 \cdot 10^{-6}$	6.0	$-1.6 \cdot 10^{-5}$	1.0	$2.0 \cdot 10^{-5}$	6,017.0	$1.2 \cdot 10^{-4}$	156.8
98,000	$4.7 \cdot 10^{-6}$	4.1	$-5.5 \cdot 10^{-6}$	0.3	$4.2 \cdot 10^{-6}$	1,253.5	$-1.2 \cdot 10^{-5}$	–15.2

Fracture zone

As a variant of most simulated cases, a hydraulic cage concept was studied. Table 3-18 presents the mass fluxes and associated quantities for the two pre-defined volumes of principal interest.

The most interesting change in Table 3-18 is the increase by more than an order of magnitude for the vertical flow at the SFR 2 location due to the presence of the fracture zones. Since the fracture zone system discharges in front of the ice sheet it is plausible that the fracture zone system is a low pressure system and that the gradient acting at the location at this time is more downward.

3.3.5 Ice sheet and continuous permafrost with taliks

The situation considered as continuous permafrost has a hydraulic conductivity structure as in Figure 3-23 except that permafrost at X < 34,000 metres has disappeared. In the top 3 metres, a highly permeable layer exists that is connected over the entire domain. Beneath this, large areas continuous permafrost exist. The permafrost prevails down to a depth of 100 metres and extends across both topographic highs and lows; at one pre-defined location (SFR2) an open talik exists that connects the deep bedrock with the surface layer. The hydraulic conductivity in all other parts of the model domain has the deep bedrock characteristics from the reference case described above.

An ice sheet has developed over the model domain with a front located at X = 41,000 metres. Between X = 34,000 and X = 41,000 metres the ice sheet overrides a frozen region but separated from the permafrost by the permeable surface layer of 3 metres thickness.

Figure 3-29 presents the fresh water head of the steady-state solution of the case of ice sheet overriding continuous permafrost. The head situation along with the illustrative streamlines indicates the strong influence of the open taliks and of the ice sheet. The flow is mainly from beneath the ice sheet toward the next downstream open talik. However, the results indicate that some of the deep recharge from beneath the ice sheet is discharged through the surface layer between the ice and the frozen ground. Table 3-18 presents the mass fluxes and related quantities through the pre-defined SFR 2 volume (SFR 1 is frozen).

Table 3-18. Mass fluxes, Darcy velocities, and mass fluxes relative to the base case of an ice sheet present for two pre-defined volumes. The comparison is between a hydraulic cage present and absent. A negative value in the relative column indicates a changed flow direction.

		Horizontal surface 10 m²			Vertical surface 100 m²		
		Mass flux [kg/s]	Darcy velocity [m/s]	Relative	Mass flux [kg/s]	Darcy velocity [m/s]	Relative
X = 41,000 metres	SFR 1	$6.0 \cdot 10^{-7}$	$6.0 \cdot 10^{-11}$	0.5	$-5.2 \cdot 10^{-6}$	$5.2 \cdot 10^{-11}$	0.3
	SFR 2	$2.1 \cdot 10^{-8}$	$2.1 \cdot 10^{-12}$	6.1	$6.2 \cdot 10^{-6}$	$6.2 \cdot 10^{-11}$	8.2
X = 92,000 metres	SFR 1	$5.2 \cdot 10^{-6}$	$5.2 \cdot 10^{-10}$	0.5	$-2.1 \cdot 10^{-4}$	$2.1 \cdot 10^{-9}$	6.8
	SFR 2	$1.2 \cdot 10^{-7}$	$1.2 \cdot 10^{-11}$	1.5	$6.8 \cdot 10^{-5}$	$6.8 \cdot 10^{-10}$	3.8
X = 98,000 metres	SFR 1	$2.7 \cdot 10^{-6}$	$2.7 \cdot 10^{-10}$	0.6	$-4.6 \cdot 10^{-4}$	$4.6 \cdot 10^{-9}$	83.6
	SFR 2	$4.1 \cdot 10^{-6}$	$4.1 \cdot 10^{-10}$	1	$-4.1 \cdot 10^{-4}$	$4.1 \cdot 10^{-9}$	34.2

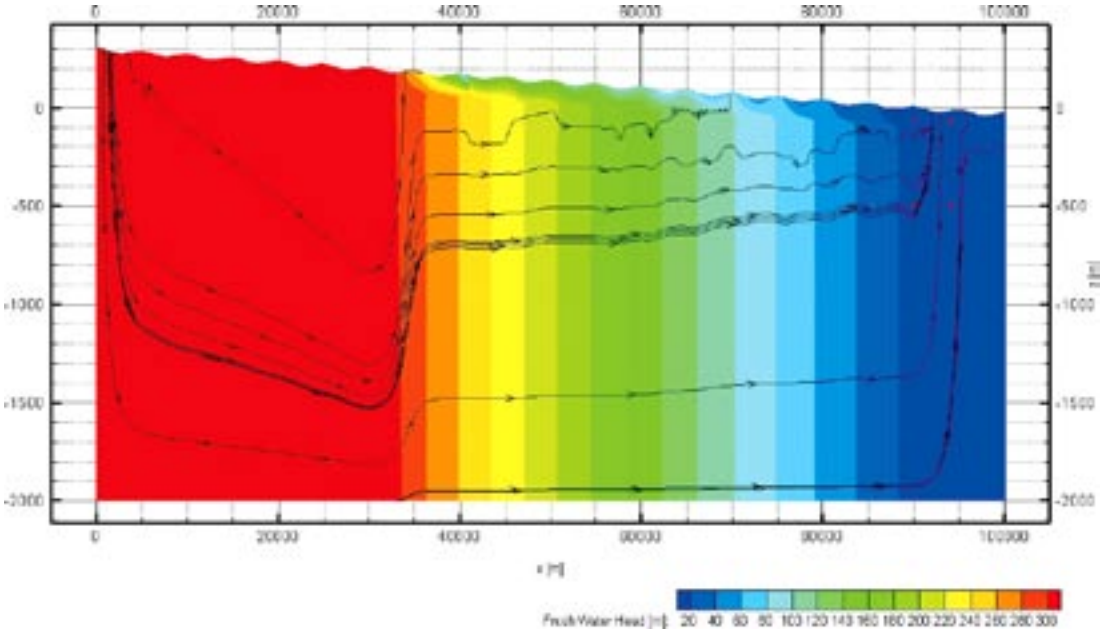

Figure 3-29. *Fresh water heads of the steady-state solution of the case of an ice sheet overriding continuous permafrost.*

Table 3-19. Mass fluxes, Darcy velocities, and mass fluxes relative to the reference case for the SFR 2 volume for the case of an ice sheet and continuous permafrost with taliks. SFR 1 is frozen.

	SFR 2 Horizontal			Vertical		
	Mass flux [kg/s]	Darcy velocity [m/s]	Relative	Mass flux [kg/s]	Darcy velocity [m/s]	Relative
Maximum infiltration scenario	$-2.2 \cdot 10^{-8}$	$2.2 \cdot 10^{-12}$	0.9	$4.0 \cdot 10^{-6}$	$4.0 \cdot 10^{-11}$	40.0
Limited infiltration scenario	$-1.7 \cdot 10^{-8}$	$1.7 \cdot 10^{-12}$	0.7	$3.0 \cdot 10^{-6}$	$3.0 \cdot 10^{-11}$	29.7

3.3.6 Comparisons

A comparison of the total mass flux over the pre-defined volumes has been made

Table 3-20 presents the relative changes in the total flux due to the different imposed upper boundary conditions. Table 3-21 presents a comparison of the effects of hydrological caging by fracture zones for the different upper boundary conditions.

Table 3-20. Comparison between the different base cases. Relative total mass flux through the pre-defined volumes (10·100·1 m^3).

Case	SFR 1	SFR 2
Temperate	1	1
Sporadic permafrost	no flow	0.2
Continuous permafrost	no flow	3.9
Ice sheet, at X = 41,000 metres	1.0	1.0
Ice sheet, at X = 92,000 metres	2.4	24.2
Ice sheet, at X = 98,000 metres	0.6	20.8

Table 3-21. Comparison between the different base cases. Relative values between scenario with and without fracture zones (value with fracture zone/ value without fracture zone). A relative number > 1 indicate a larger mass flux with fracture zones than without fracture zones.

Case	SFR 1		SFR 2	
	Horizontal	Vertical	Horizontal	Vertical
Temporate	0.5	0.7	4.0	14.6
Sporadic permafrost	0.3	0.4	22.0	25.5
Continuous permafrost	0.6	0.6	5.4	5.9
Ice sheet, at X = 41,000 metres	0.5	0.3	6.1	8.2
Ice sheet, at X = 92,000 metres	0.5	6.8	1.4	3.7
Ice sheet, at X = 98,000 metres	0.6	83.4	1.0	35.6

Sensitivity to lateral boundary

The sensitivity to the chosen no-flow boundary was tested by changing the boundary beneath the sea to a hydrostatic boundary condition. Figure 3-30 illustrate the flow situation for an ice sheet at X = 92,000 metres.

Sensitivity simulations of the chosen boundary condition have been conducted for all cases and the Darcy flow velocities are not affected by the chosen boundary condition. For the case were the ice sheet front is located at X = 98,000 metres, that is about 2 kilometres from the boundary a minor change in the mass flux was found, but this was not significant.

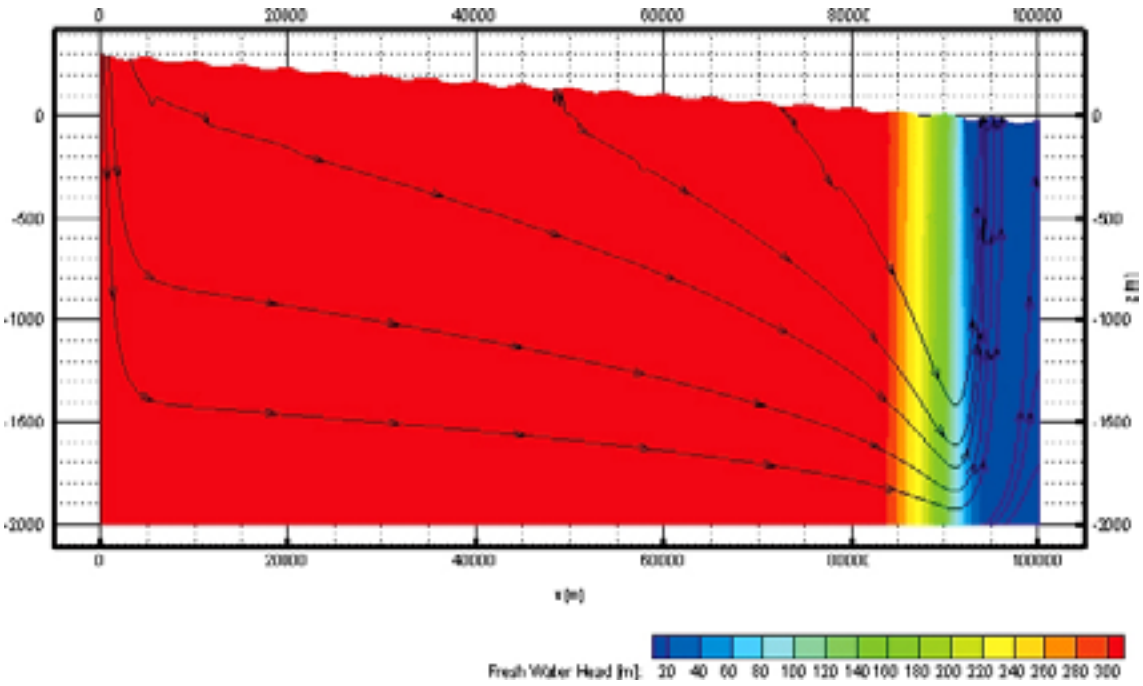

Figure 3-30. *Fresh water heads of the steady state solution for the case of an ice sheet with its front at X = 92,000 metres. Same as Figure 3-27 but for the lateral boundary beneath the sea, which here is replaced by a hydrostatic boundary condition.*

Sensitivity to depth trend

The sensitivity to the specified hydraulic conductivity was tested by applying a depth trend in the hydraulic conductivity distribution in the bedrock /e.g. Hartley et al. 2006/ also see chart below.

Depth [m.b.s.l.]	Hydraulic conductivity depth trend
–20 metres	$K = 5 \cdot 10^{-3} \cdot 10^{-depth/3}$; $K_{min} = 1 \cdot 10^{-6}$
20–350 metres	$K = 5 \cdot 10^{-8} \cdot 10^{-1.7 \cdot (depth-20)/330}$
350–metres	$K = 5 \cdot 10^{-11}$

Figure 3-31 illustrate the flow situation for an ice sheet at X = 92,000 metres.

Sensitivity simulations with the assigned depth trend have been conducted for all cases and the Darcy flow velocities are significantly affected. However, the relationships between the cases simulated were unaltered.

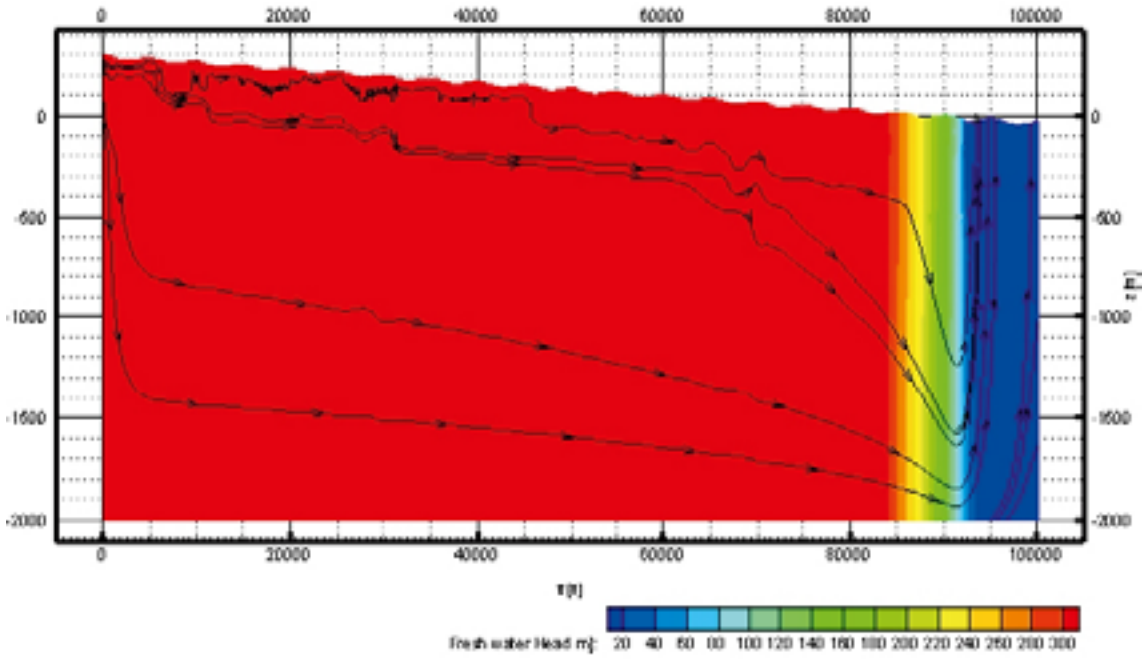

Figure 3-31. *Fresh water heads of the steady state solution for the case of an ice sheet with its front at X = 92,000 metres. Same as Figure 3-27 but for an assigned depth trend in hydraulic conductivity and the lateral boundary beneath the sea, which here is replaced by a hydrostatic boundary condition.*

4 Discussion

The numerical results of the groundwater flow study indicate a significant influence of the climatic upper boundary condition on the flow situation in the selected measurement volumes.

However, the results are also significantly affected by differences in the adopted "natural" surface conditions, such as local and regional topographical characteristics. The possibility of drawing general conclusions on the climatic effects is limited by the fact that the imposed influences of the highly stylised "natural" characteristics are different for different climatic conditions.

Boundary conditions

The "natural" surface conditions adopted are simplified and the gradients used within the local topographic conditions are realistic for local characteristics of the area around the SFR /Holmén and Forsman 2004/. For the transect that was adopted, the regional topographical gradient is plausible at the 100 km scale. The reference case may, therefore, be taken as representative of present-day conditions; however, the simplified hydrogeological properties and the adopted flow-dimensions (2D) makes direct comparison of results and uncertainty ranges between these results and earlier model results complicated.

Even though direct comparisons are complicated, it is reassuring that the reference case used in this study shows the same general behaviour as the model results obtained by /Holmén and Stigsson 2001/. This helps to justify the use of these model results within the SFR1 SAR-08 assessment.

Another important consideration identified when analysing these model results was the significant differences found in the results associated with a local recharge or discharge area. Based on the present-day topographical characteristics of the SFR area, it is plausible to assume that the discharge location is the most realistic measurement volume to use in the SFR1 SAR-08 assessment due to its location on the shoreline just beneath the sea. However, with time the shoreline displacement lifts SFR above the sea. Hence the former discharge area slowly transforms into a recharge area.

Bedrock properties

The results of the various simulation studies undertaken were found to be significantly affected by the assumed bedrock properties, both regarding quantitative estimates of flow and spatial characteristics of the flow regime. In a two-dimensional model, it is difficult to represent the characteristics of fractured bedrock and the results obtained are significantly affected by the fracture statistics. A fracture network is by nature three-dimensional and in two dimensions the representation of the connectivity of such a network may be totally erroneous. The sensitivity cases simulated in this study have tested a couple of simple variations in the bedrock characteristics.

The sensitivity to the specified hydraulic conductivity of the bedrock has been addressed and regarding the deep bedrock hydraulic conductivity (overall) the resulting mass flux is found to change by the same amount as the hydraulic conductivity is changed. This sensitivity test has been conducted both in the reference case and in the permafrost case, and the same conclusion could be drawn from both studies. These results are in no way surprising and may simplify the safety analysis.

The hydraulic conductivity value used the deep bedrock is valid at a regional scale. However, with decreasing scale, local bedrock volumes may deviate significantly from this general value.

The extreme variation in hydrogeological properties in bedrock makes detailed predictions associated with large uncertainties. The plausible character of a more local bedrock volume is generally assessed as being less permeable than the regional value herein used /Holmén and Forsman 2004/ assessed a bedrock hydraulic conductivity of this area of approximately $5 \cdot 10^{-9}$ m/s), hence the assessed bedrock properties plausibly over-estimate the mass fluxes within local bedrock regions of interest.

The main factor causing a difference between the regional values and the less permeable local values is the presence of major fracture zones. Hence a variation of the bedrock characteristics has been tested, in which the measurement volumes have been caged-off by three major fracture zones. If all other model settings are kept unchanged from the reference case, introduction of the caging fractures results in a general decrease in mass fluxes at recharge areas; however at discharge areas the mass fluxes increase. This is likely due to the fact that the flow is trapped within the local volume. The results indicate that local flow for the reference case may be changed by one order of magnitude due to the presence of local major fracture zones. However the results are not fully understood and further investigations may be needed in order to determine the reason for these changes.

In developing recommendations, the cases without the fracture zones have mainly been used, since these are believed to yield results more similar to those obtained in earlier studies. However, a further consideration was that the extreme cage effect modelled in this study is not applicable to the SFR; even though SFR is surrounded by large scale deformation zones (cf Figure 3-2). In part, this is because these fracture zones are not expected to show large hydraulic conductivity contrasts relative to the overall rock mass see /e.g. SKB 2005/.

Permafrost issues

Two different groundwater flow scenarios involving the presence of permafrost have been studied. These are; i) a sporadic permafrost distribution, in which the groundwater within local topographic highs is frozen, and ii) a continuous permafrost distribution, in which extensive permafrost exist all over the model domain, only locally by-passed by open taliks (i.e. un-frozen regions in the permafrost).

The sporadic permafrost produces a situation where the regional groundwater flow becomes more important and the flow driven by local topographical differences becomes less important. This yields a smaller total flow for the sporadic permafrost scenario as compared with the reference case. This decrease is, however, possibly counteracted by the presence of caging fracture zones, which increase the flow in the discharge region as compared with the reference case.

The continuous permafrost case yields an increase in the water flux all over a talik where discharge of water is occurring; a situation where a talik contain regions of both recharge and discharge is possible according to the conceptual model used, but is more likely to occur in upstream locations than at the location of SFR. However, after emerging from the sea by shoreline displacement, when permafrost first is encountered, the location of SFR will be on a hill side. The location is more on the shaded side and hence it is possible for it to have early permafrost development. Hence the location may become frozen relatively early. However, the location of the shoreline when the first permafrost arrives is not well determined, and for a situation in which the SFR is still beneath water at that time, a talik could be formed above it. A sensitivity test of the location of the measurement volume within a talik indicates that a continuous permafrost situation could enhance the water flux through the facility by up to one order of magnitude.

The continuous permafrost situation may have a smaller impact, if the amount of available water is small, an effect different from that found in the sporadic permafrost case. However, the decrease in a dry scenario is not so large that it counteracts the effect of a talik in increasing the flow.

In relation to permafrost cases, it should be noted that most simulated episodes of possible future permafrost have reached a depth exceeding that of the SFR repository. If the ground surrounding the repository is frozen, the groundwater flow becomes negligible, but other problems arise, such as possible failures of the buffer material.

Ice sheet issues

One scenario of an ice sheet overriding the continuous permafrost has been simulated. The results indicate a significant increase of groundwater flow through the open talik included in the model. The increase in the water flux when the ice sheet is very distant is approximately 40 times, and it is anticipated that this increase will be significant larger when the ice sheet is closer. However, it should be noted that the conceptual understanding of ice sheet hydraulics is limited and subjected to great uncertainties /e.g. Jansson et al. 2007/. Also worth noticing is that the simulated talik is located in order to create maximum effect at the measurement volume. It could be argued that the adopted methodology overestimates the effects of an ice sheet, and this is plausible for the case in which an ice sheet has completely overrun the site, since the applied pressure boundary is thought to over-estimate groundwater recharge. For the case of an ice sheet overriding permafrost, overestimation is not so easily argued. The case of an ice sheet over permafrost may, therefore, be the most critical scenario to assess.

The simulated ice sheet scenarios are by far the climate scenario that yield the largest impact on water fluxes. For the scenario situation where the ice sheet margin advances over SFR located beneath a discharge area, the results indicate an increase of the mass flux by two to three orders of magnitude. If this groundwater flow scenario were to happen, then, based on ice sheet development during the last glaciation (Weichselian), it would occur over a few years. In this case, the discharge would be extremely localised in front of the ice sheet, with a large amount of discharged melt water.

The results in relation to the climate variants

Up to this point, the time aspect of the climate scenarios has been omitted from the discussion. In order to include the time aspect, a simplification of the climate domain sequences for the three climate variants (Base, Greenhouse, Permafrost) described above is presented below.

Base variant

The first change that occurs for all variants is the change in flow regime due to shoreline displacement. The effect of this climate-related process is more thoroughly described in /Holmén and Stigsson 2001/, but the simulated sensitivity cases indicate an increase in mass flux as the elevation rises.

Of the changed situations investigated herein, the first that occurs is the Permafrost case. Permafrost development starts with sporadic permafrost and it is not possible to conclude when sporadic permafrost develops into continuous permafrost. For the Base and Greenhouse variants, it is plausible that the first episode of permafrost never advances beyond sporadic permafrost in the Forsmark region; the same is probably true for the “extreme” climate variant. However, since the sporadic permafrost results is a decrease in water flux, it may, for safety assessment purposes, be cautious but reasonable to assume that all these events rapidly develops into continuous permafrost and that SFR is located within an open talik.

In the climate Base variant, the first permafrost occurs in about 8,000 years and remains for a couple of thousands of years (Figure 2-10). Temperate conditions then prevail for approximately 10,000 years before a extensive period of permafrost occurs, persisting until the first ice sheet advances over the permafrost in about 60,000 years. Hence, for the climate Base variant, the first order of magnitude change arise after approximately 8,000 years and the first likely two or three orders of magnitude change arises after approximately 60,000 years. After the deglaciation

of the ice sheet, an episode of high sea levels prevails for about 10,000 years (Figure 2-10). This episode is postulated to have little impact on the flow around the SFR repository since the site experiences a period with little or no topographic gradient and hence the only possible flow is due to differences in density of the sea water and the groundwater beneath. This scenario is studied in /Vidstrand et al. 2006/. The climate Base variant includes a change from permafrost to a warm-based ice sheet after approximately 90,000 years (Figure 2-10). The latter situation may be close to the simulated ice sheet cases. Also during the ice sheet retreat, even though the melt water is being discharged into the sea, the situation is close to that simulated in the ice sheet cases.

Greenhouse variant

In the Greenhouse variant, 50,000 years of temperate climate conditions have been inserted prior to the onset of a climate development identical to that in the Base variant (Figure 2-12). Hence the first order of magnitude of change in mass flux occurs after approximately 60,000 years and the first likely two or three orders of magnitude change occurs after approximately 110,000 years.

Permafrost variant

The permafrost variant described above does not include ice sheet development. Instead most of the 120,000 years is dominated by permafrost conditions. The first episode of permafrost occurs in some hundreds of years. This episode is short and the permafrost does not develop deep, and continuous permafrost is not likely to develop for this episode. However, after approximately 6,000 years continuous permafrost prevails and most likely prevails also for most of the following 100,000 years.

Overall, it is important to emphasise that the studies that have been conducted include a large degree of uncertainty due to the simplified settings. However, since the assumptions used in many aspects of the work would result in overestimates of the groundwater flow, it is believed that the results can be used as a good indicator of likely differences in hydrogeology arising under the different surface conditions that prevail for the climate variants herein adopted.

5 Recommendations

5.1 Justification for the SFR issue

A generic two-dimensional model study may seem to have little site-specific relevance. However, in this case, the specified boundary conditions and hydrogeological properties are based on site-specific information relevant to the SFR location.

The model results, as shown below, have the same general characteristics as the more detailed model results /Holmén and Stigsson 2001/ adopted in the SFR-SAFE assessment.

The objective of the study is further to support the safety analysis and hence by adopting conservative parameters and boundary conditions the results may be used, with an appropriate degree of caution, as a basis for site-specific evaluations and decisions.

5.2 Recommeded time sequence and scaling factors

Based on the results of this investigation, recommendations for scaling factors for the flux values to be applied when assessing the selected climatic scenarios have been established for the SFR site. These scaling factors are presented below in three tables, one for each climate variant.

The scaling factors are mainly based on the results obtained under the different climatic boundary conditions simulated. The bedrock was assumed to be homogeneous in the base cases adopted for the different climatic boundary conditions. The basis for using these specific conditions has been presented in the above discussion. However, some scaling factors are based not on quantitative results but on reasoning in the discussion section above. These values are marked as *italic* in the tables.

The low scaling factor presented for permafrost cases (*0.0001*) represents frozen bedrock regions and hence a no-flow situation. The low value of *0.01* for submerged conditions is representative for situations in which no, or only small, driving forces are present. For the submerged situation, this applies for all offshore locations. However, for situations close to the shoreline, the scaling factor is likely to be similar to the one in the temperate case.

The temperate case is representative for present-day conditions. In order to account for the effects of shore-level changes application of the results of /Holmén and Stigsson 2001/ is recommended.

For the ice sheet advance and retreat situation, “point values” of the scaling factor are specified. It should be kept in mind that these values apply on a time scale of 1–2 years and that they are not, as are the other values in the tables below, representative on the one-thousand year scale. Scaling factors in the tables have been adjusted to be in an order of magnitude scale rather than being specific values from the simulations. The recommendations are found in Table 5-1 to Table 5-3.

Table 5-1. Recommendations for scaling factors of flow for the Base variant. Negative values imply change of flow direction. The small value of 0.0001 implies no flow and applies to frozen regions of the bedrock. The small value of 0.01 implies very small flow beneath the sea. Values for ice sheet advance/retreat are relevant on a time scale of 1–2 years.

Climate domain	Time [kyears]	SFR 1	SFR 2
Temperate	0–8	1	1
Sporadic permafrost (frozen/talik)	8–10	0.0001/*0.5*	*0.0001*/0.2
Temperate	10–23	1	1
Continuous permafrost (frozen/talik)	23–56	0.0001/*10*	*0.0001*/5
Ice sheet advance	56	–10	150
Ice sheet covered	56–66	0.5	–0.5
Ice sheet retreat	66	–10	150
Submerged	66–75	0.01	0.01
Continuous permafrost (frozen/talik)	75–91	0.0001/*10*	*0.0001*/5
Ice sheet advance	91	–10	150
Ice sheet covered	91–109	0.5	–0.5
Ice sheet retreat	109	–10	150
Submerged	109–120	0.01	0.01

Table 5-2. Recommendations for scaling factors of flow for the Greenhouse variant. Negative values imply change of flow direction. The small value of 0.0001 imply no flow and applies to frozen regions of the bedrock. The small value of 0.01 imply very small flow beneath the sea. Values for ice sheet advance/retreat are relevant on a time scale of 1–2 years.

Climate domain	Time [kyears]	SFR 1	SFR 2
Temperate	0–58	1	1
Sporadic permafrost (frozen/talik)	58–60	0.0001/*0.5*	*0.0001*/0.2
Temperate	60–73	1	1
Continuous permafrost (frozen/talik)	73–106	0.0001/*10*	*0.0001*/5
Ice sheet advance	106	–10	150
Ice sheet covered	106–116	0.5	–0.5
Ice sheet retreat	116	–10	150
Submerged	116–120	0.01	0.01

Table 5-3. Recommendations for scaling factors of flow for the Permafrost variant. The small value of 0.0001 implies no flow and applies to frozen regions of the bedrock.

Climate domain	Time [kyears]	SFR 1	SFR 2
Temperate	0–4	1	1
Sporadic permafrost (frozen/talik)	4–5	0.0001/*0.5*	*0.0001*/0.2
Temperate	5–8	1	1
Continuous permafrost (frozen/talik)	8–15	0.0001/*10*	*0.0001*/5
Temperate	15–20	1	1
Continuous permafrost (frozen/talik)	20–37	0.0001/*10*	*0.0001*/5
Temperate	37–41	1	1
Continuous permafrost (frozen/talik)	41–108	0.0001/*10*	*0.0001*/5
Temperate	108–120	1	1

6 Conclusions

In the earlier modelling for SFR-SAFE it was concluded that the groundwater flow would increase with time along with the shoreline displacement. Even though the numerical results are different the same conclusion is drawn after this study.

General conclusions from the present study are that:

- The upper boundary conditions have a significant impact on the groundwater flow in the geosphere.
- The characteristic of the surface in regards of being a recharge or discharge area affects the results.
- In general, a discharge area will experience an increase in groundwater flow under changed conditions.
- The presence of caging fracture zones affects the results, and, for the tested un-frozen SFR situation, the resulting effect is an increase in groundwater flow.

Specific conclusions regarding the relative change of groundwater flow due to different surface conditions are that:

- The permafrost scenarios, along with the development from sporadic permafrost to continuous permafrost, yield increased groundwater flows in unfrozen parts of the domain. The increase is one order of magnitude or less. In the permafrost, the flow is negligible.
- The ice sheet scenarios yield situations with significantly increased groundwater flow. The results indicate an increase by two to three orders of magnitude. These increased values, however, apply only for short duration intervals. It is possible that such intervals may be only a couple of years.
- In the selected climate Base variant, repeating the conditions for the last glacial cycle, permafrost conditions occur after 8,000 years. In the climate variant affected by increased greenhouse warming, permafrost conditions do not occur until after more than 50,000 years.
- In the chosen climate variants, ice sheets reach the Forsmark area and cause significantly increased groundwater flow, after ~60,000 years or more.

7 References

Balling N, 1995. Heat flow and thermal structure of lithosphere across the Baltic Shield and northern Tornquist Zone. Tectonophysics, Vol 244, pp 13–50.

Berger A, 1978. Long-term variations of daily insolation and Quaternary climatic changes. Journal of Atmospheric Science 35:2, 362–2,367.

Berger A, Loutre M F, 2002. An exceptionally long interglacial ahead? Science 297:1, 287–1,288.

BIOCLIM, 2003. Continuous climate evolution scenarios over western Europe (1,000 km scale), Deliverable D7. Work package 2: Simulation of the future evolution of the biosphere system using the hierarchical strategy. 88 p.

Boulton G S, Kautsky U, Morén L, Wallroth T, 2001. Impact of long-term climate change on a deep geological repository for spent nuclear waste. SKB TR-99-05, Svensk Kärnbränslehantering AB.

Burn C R, 2002. Tundra lakes and permafrost, Richards Island, western Arctic coast, Canada. Canadian Journal of Earth Sciences, Vol. 39, pp. 1,281–1,298.

Chan T, Christiansson R, Boulton G S, Ericsson L O, Hartikainen J, Jensen M R, Mas Ivars D, Stanchell F W, Vidstrand P, Wallroth T, 2005. DECOVALEX III, BMT3/BENCHPAR WP4. Report of BMT3/WP4 – the thermo-hydro-mechanical responses to a glacial cycle and their potential implications for a deep geological disposal of nuclear fuel waste in a fractured crystalline rock mass. SKI report 2005:28, Swedish Nuclear Power Inspectorate, Stockholm, 2005, See CD-ROM attachment entitled, DECOVALEX III, BMT3/BENCHPAR WP4: The THM conditions during the dynamics of a glaciation cycle: a synthetic case based mainly on simplified data from the Whiteshell site.

French H M, 1996. The Periglacial Environment. Second edition; Addison Wesley Longman Limited.

Hartikainen J, Mikkola M, 1997. Thermomechanical model of freezing soil by use of the theory of mixtures. In: Proceedings of the Sixth Finnish Mechanics Days, Oulu, Finland, September 5–6 1997, pp. 1–26.

Hartikainen J, 2004. Permafrost modelling in DECOVALEX III for BMT3. In Eloranta, E ed., DECOVALEX III 1999–2003. An international project for modelling of coupled thermo-hydro-mechanical processes for spent nuclear fuel disposal. Finnish national contributions. STUK-YTO-TR 209, Helsinki, Finland.

Hartley L, Hoch A, Jackson P, Joyce S, McCarthy R, Rodwell W, Swift B, Marsic N, 2006. Groundwater flow and transport modelling during the temperate period for the SR-Can assessment. Forsmark area – version 1.2. SKB R-06-98, Svensk Kärnbränslehantering AB.

Holmén J G, Stigsson M, 2001. Modelling the future hydrogeological conditions at SFR, SKB R-01-02, Svensk Kärnbränslehantering AB.

Holmén J G, Forsman J, 2004. Flow of groundwater from great depths into the near surface deposits – modelling of a local domain in northeast Uppland. SKB R-04-31, Svensk Kärnbränslehantering AB.

Holmén J G, Stigsson M, Marsic N, Gylling B, 2003. Modelling of groundwater flow and flow paths for a large regional domain in northeast Uppland. SKB R-03-24, Svensk Kärnbränslehantering AB.

IPCC, 2001. Climate Change 2001: The Scientific Basis. Contributions of the Working Group I to the Third Assessment Report of the Intergovermental Panel on Climate Change. Houghton et al. (eds). Cambridge University Press, New York.

IPCC, 2007. The Scientific Basis. Contributions of the Working Group I to the Fourth Assessment Report of the Intergovermental Panel on Climate Change. Reports can be downloaded from the IPCC web site, http://www.ipcc.ch.

Jansson P, Näslund J O, Rodhe L, 2007. Glacial hydrology and eskers. A review of ice sheet hydrology. SKB TR-06-34, Svensk Kärnbränslehantering AB.

Lindborg T (ed), 2005. Description of surface systems Preliminary site description Forsmark area – version 1.2. SKB R-05-03, Svensk Kärnbränslehantering AB.

Paterson W S B, 1994. The Physics of Glaciers. 3rd Edition. Elsevier Science Ltd.

Rhén I, Follin S, Hermansson J, 2003. Hydrogeological Site Descriptive Model – a strategy for its development during Site Investigations. SKB R-03-08, Svensk Kärnbränslehantering AB.

SKB, 2005. Preliminary Site Description. Forsmark area – version 1.2. SKB R-05-18, Svensk Kärnbränslehantering AB.

SKB, 2006a. Climate and climate-related issues for the safety assessment SR-Can. SKB TR-06-23, Svensk Kärnbränslehantering AB.

SKB, 2006b. Long-term safety for KBS-3 repositories at Forsmark and Laxemar – a first evaluation: Main Report of the SR-Can project. SKB TR-06-09, Svensk Kärnbränslehantering AB.

SKB, 2006c. SFR Final repository for radioactive operational waste. Svensk Kärnbränslehantering AB.

Stigsson M, Follin S, Andersson J, 1998. On the simulation of variable density flow at SFR, Sweden. SKB R-98-08, Svensk Kärnbränslehantering AB.

Svensson U, Kuylenstierna HO, Ferry M, 2004. DarcyTools Version 2.1. Concepts, methods, equations and demo simulations. SKB R-04-19, Svensk Kärnbränslehantering AB.

Vidstrand P, Svensson U, Follin S, 2006. Simulations of hydrodynamic effects of salt rejection due to permafrost. SKB R-06-101, Svensk Kärnbränslehantering AB.

Yershov E D, 1998. General Geocryology. Cambridge University Press.